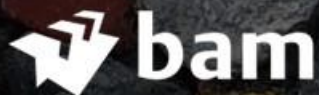


Application of XblocPlus on Breakwater Roundheads

J. van Oorschot 4923936

Faculty of Civil Engineering and Geosciences
MSc Civil Engineering
Master Thesis

Delft University of Technology



Application of XblocPlus on Breakwater Roundheads

By

J. van Oorschot

in partial fulfilment of the requirements for the degree of

Master of Science
in Civil Engineering

at the Delft University of Technology,
to be defended publicly on Wednesday July the 3rd, 2024 at 10:00.

Supervisor:	Prof. dr. ir. M.R.A. van Gent	TU Delft
Thesis committee:	Dr. ir. P. Mares Nasarre, Ir. B. Reedijk, Ir. T. Ruwiel,	TU Delft BAM Infraconsult BAM Infraconsult

An electronic version of this thesis is available at <http://repository.tudelft.nl/>.

Preface

Before you lies the Master Thesis “Application of XblocPlus on Breakwater Roundheads”. I wrote this thesis in partial fulfilment of the requirements for the degree of Master of Science in Civil Engineering, specialized in Hydraulic and Offshore Structures, entailing the end of my academic journey at Delft University of Technology. I was engaged in researching and writing this thesis from February to June 2024.

During my thesis, I had the honour and pleasure to collaborate with the coastal engineering section of BAM Infraconsult, located in Gouda, The Netherlands. Among the activities my thesis entailed was physical model testing in a wave flume. This allowed me to employ the theoretical knowledge obtained in the past two years and expand my expertise in hydraulic engineering, an experience I value deeply. Additionally, BAM and its people showed me the passion and thirst for constant innovation of a commercially oriented company.

I would like to express my gratitude to the people who helped me realize this thesis. Firstly, my colleagues at BAM Infraconsult: Ir. Bas Reedijk for granting me this opportunity, Ir. Pieter Bakker for his support and profound interest in the research, and everyone regularly present at the laboratory for the advice and insights provided. Furthermore, I would like to express my appreciation for the never-ending feedback and guidance of Ir. Tim Ruwiel. Secondly, I would like to thank the committee from the TU Delft, Prof. dr. ir. Marcel van Gent and Dr. ir. Patricia Mares Nasarre, for the insightful sessions and constructive feedback. Lastly, I want to express my appreciation to my girlfriend and family for always supporting me and showing sincere interest in my field of study.

*J. van Oorschot
Delft, June 2024*

Abstract

Twenty years after the introduction of Xbloc, DMC, which is a member of Royal BAM Group, introduced a uniformly placed and interlocking concrete armour unit named XblocPlus, which is suitable for straight to mildly curved breakwater sections, whereas Xbloc is currently applied on roundheads. Therefore, this study investigates modifications to the design or placement configuration of XblocPlus to enable its application on roundheads. Two concepts were tested on a $H/V = 4/3$ roundhead slope for hydraulic stability in DMC's wave flume. The first configuration consisted of regular XblocPlus combined with XP-Curve, a variant adjusted for narrowing radii, and XP-Base, a legged XblocPlus originally devised for bottom row applications. Tests with normative 0.02 wave steepness yielded a stability number ($H_s/\Delta D_n$) ranging from 2.72 to 3.09 due to uplift-related damage. The second configuration, featuring solely XP-Base and XP-Curve, resulted in a hydraulic stability number of 1.96 due to significantly less interlocking. No improvements were observed with respect to hydraulic stability compared to previous research. However, these designs notably reduced rotation-induced failure and enhanced applicability by enabling transition to the trunk and increasing maximum construction height. Additionally, this thesis investigated the validity of testing a three-dimensional structure in a 2D configuration, a method employed to maintain consistency with previous research. Wave heights in front of the structure were measured using parallel gauge sets, allowing the determination of the average disparity. This disparity was found to be within the acceptable margins for the principal test configuration. However, further research is needed to assess test conservativeness. In conclusion, this thesis provides recommendations aimed at improving the applicability and stability of XblocPlus on breakwater roundheads.

Keywords: rubble mound breakwater, roundheads, hydraulic stability, concrete armour, regular placement, XblocPlus

Contents

1.	Introduction	1
1.1.	Problem definition	1
1.2.	Objectives	2
1.3.	Methodology	3
1.4.	Thesis outline.....	3
2.	Theoretical Framework.....	4
2.1.	Breakwaters.....	4
2.2.	Armour.....	6
2.3.	XblocPlus.....	10
2.4.	XP-Curve	13
2.5.	Scaling.....	15
2.6.	Roundhead configuration	15
2.7.	Limitations.....	17
3.	Design.....	18
3.1.	Preliminary design	18
3.2.	Proposed design.....	24
4.	Physical model	30
4.1.	Flume dimensions.....	30
4.2.	Test configuration.....	30
4.3.	Models	35
4.4.	Armour units	38
5.	Test programme	42
5.1.	Waves.....	42
5.2.	Water depth	44
5.3.	Measurement equipment	47
5.4.	Damage description	48
5.5.	Test procedure	50
6.	Results.....	52
6.1.	Model 0.....	54
6.2.	Model 1.....	56
6.3.	Model 2.....	63
6.4.	Xbloc.....	67
6.5.	Reflection analysis.....	70
7.	Discussion.....	74
7.1.	Design comparison and analysis.....	74
7.2.	Analysis of test influences.....	78
7.3.	Performance in context of previous research	82

8. Conclusions and recommendations.....	84
8.1. Conclusions	84
8.2. Recommendations	87
References.....	90
A. Theoretical Background	94
A.1. Wave Theory	94
A.2. Breakwater design.....	98
A.3. Dimensionless numbers in fluid mechanics	99
A.4. Fluid-structure interaction	100
B. Armour units	102
B.1. Production	102
B.2. Mass, volume and density	104
C. Wave climate	108
D. Visual documentation of test series.....	112
D.1. Model 0	112
D.2. Model 1	114
D.3. Model 2	127
D.4. Xbloc.....	136

1. Introduction

20 years ago, Delta Marine Consultants (DMC), which is a member of Royal BAM Group, introduced its first breakwater armour unit named Xbloc, of which over 500,000 blocks have been successfully placed around the world (*Xbloc*, n.d.). The Xbloc is robust and durable, has low concrete consumption and CO₂ footprint compared to other armour units and is adaptable to various site conditions. Most single layer blocks, including the Xbloc, necessitate random unit orientations, which requires the crane operator to assess the orientation of each individual unit during placement (Donnelly et al., 2020). As a result, fifteen years after the introduction of Xbloc, DMC introduced a new interlocking breakwater unit called XblocPlus, which is placed with uniform block orientations. In 2018, Rijkswaterstaat (executive agency of the Dutch government) commissioned the consortium Levvel, which includes DMC, to prepare the design of the Afsluitdijk, including reinforcement of the armour layers and wave overtopping reduction (Van de Koppel et al., 2023). Due to requirements by Rijkswaterstaat, Xbloc was deemed not suitable for the Afsluitdijk due to its random orientation and XblocPlus was applied for the first time. Thereafter, additional applications of XblocPlus followed in Poland and La Reunion.

1.1. Problem definition

The applicability of XblocPlus ranges from straight to mildly curved breakwater sections where the advantages of the unit can be used to its full extent (Xbloc, 2023). An alternative unit named XP-Wing is applied in combination with XblocPlus for medium curved sections. However, XblocPlus is not yet applicable on strongly curved sections or roundheads where regular Xbloc units are applied as shown in Figure 1.1, allowing flexible placement on curved surfaces. To simplify the placement process and improve aesthetic appearance, application of XblocPlus or a variant across the entire breakwater would be favourable (*Introduction of the New XblocPlus*, 2018).

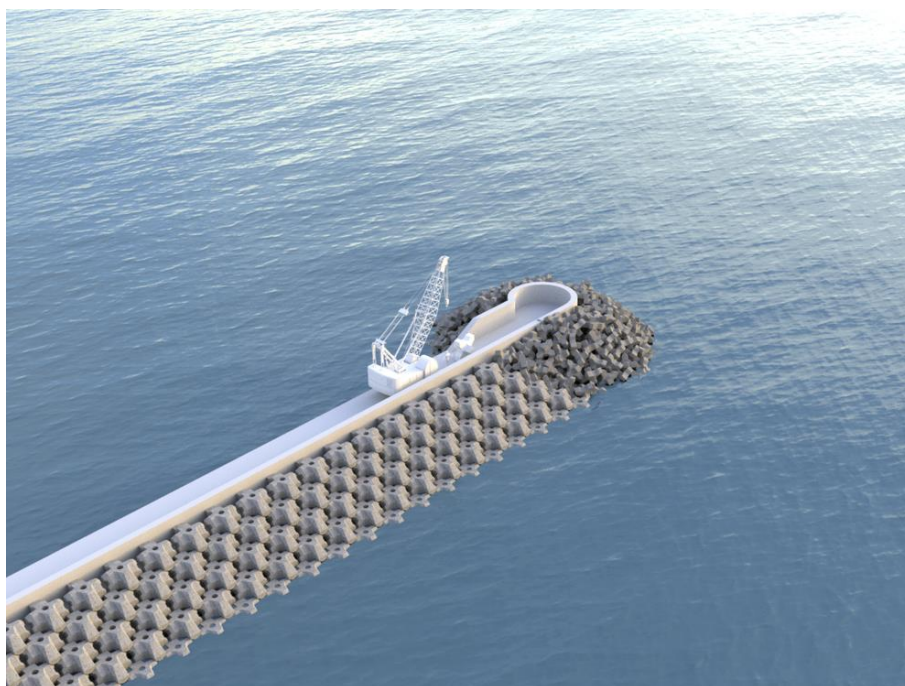


Figure 1.1. Application of Xbloc and XblocPlus on a breakwater (DMC, 2018).

Recently, multiple studies have been conducted on the instructions of BAM Infraconsult to devise a variant of XblocPlus which is applicable on breakwater roundheads. Currently, the most promising development is the so-called XP-Curve. This concrete armour unit is derived from the XblocPlus and shows alterations at the top- and backside. XP-curve has been tested in different configurations. Wiersma (2021) researched XP-curve as a transition between consecutive rows of XblocPlus, enabling applicability of XblocPlus on a smaller radius. Similar tests were executed by De Raad (2021), with an additional configuration consisting solely of XP-Curve. However, none of the structures proved sufficient hydraulic stability. Therefore, the objective of this research project is to provide an alternative or redesign of the XblocPlus to accommodate this concrete armour unit on roundheads of breakwaters while ensuring sufficient stability.

1.2. Objectives

There are many different possible redesigns and configurations of the XblocPlus which could prove stable. Furthermore, stability can be tested in different types of wave flumes. In this research, the focus will be to devise a redesign of the XblocPlus which is applicable and stable on a breakwater roundhead. XP-Curve serves as a potential starting point as applicability on roundheads has already been studied and considered as potentially suitable. As mentioned in the previous section, the XP-Curve has been tested as a transition between consecutive rows of XblocPlus, as well as the sole element on the roundhead. The mesh in which the redesign will be tested depends on the characteristics of the to be designed unit. The units will be subjected to two-dimensional physical model tests, executed in the wave flume of DMC, located in Gouda, the Netherlands. The results will be compared to Wiersma (2021) and De Raad (2021), as the same test facility and set-up were used.

In this report, an answer to the following research question will be sought:

How could XblocPlus be redesigned to provide sufficient applicability and stability on breakwater roundheads?

To address this overarching question, the following sub-questions will be examined:

1. What is the XblocPlus and which mechanisms contribute to its stability?
 - a. How do the applicability and stability of XblocPlus differ between the breakwater head and trunk?
 - b. What factors limited stability of XblocPlus on a roundhead in previous tests?
2. How can stability of XblocPlus on a roundhead be assessed from wave flume tests?
 - a. How can XblocPlus be downscaled to model stability in a wave flume?
 - b. How can a 3D structure be assessed when subjected to testing within a 2D configuration?
 - c. What are the limitations of testing in a 2D configuration?
3. What adaptations can be made to XblocPlus to enable its application on roundheads and enhance resistance against observed failure mechanisms?
 - a. How can the adaptations be implemented in the shape of XblocPlus?

Each sub-question is designed to delve into aspects of the redesign process, ultimately contributing to understanding the challenges and opportunities associated with enhancing the XblocPlus for roundhead applications. The hierarchy of the sub-questions consists of a main question which is answered through the consecutive sub-questions.

1.3. Methodology

To determine or estimate the stability of concrete armour units, several methods can be used, of which two will be discussed here. Firstly, a numerical model can be applied to probe the complexity of the interacting physics of systems. For example the combined finite-discrete element method (FEMDEM), which “is a multi-body method ideally suited to model the behaviour of the armour layer system and the stress generated within complex shape units” (Latham et al., 2014). However, Wolters et al. (2009) states that design or model experiences are not straightforwardly transferable, as each coastal structure is designed to local boundary conditions. Additionally, as numerical models are relatively expensive, time consuming to develop and require a high quantity of computational power, physical model tests are used in this research for preliminary validations of the design.

1.4. Thesis outline

To address the main research question, this study is structured around three sub-questions. Sub-questions one and two are theoretically addressed in Chapter 2, leading to the development of a practical design solution outlined in Chapter 3. This chapter details the preliminary design and proposed modifications. Chapter 4 focusses on the physical model used to assess the hydraulic stability of the devised design. Additionally, a description of the models, which will be referred to throughout the thesis, is provided. The wave programme employed in the flume, including design wave characteristics and measurement methods, is described in Chapter 5. In Chapter 6, the test results are objectively presented, including stability assessments and failure mode descriptions. Chapter 7 interprets the results by evaluating the performance of different designs against each other and previous research, while also analysing the test configuration. Finally, Chapter 8 formulates conclusions and offers recommendations for further research and practical applications.

2. Theoretical Framework

This chapter describes theoretical insights required to answer sub-questions one and two and provide a framework for sub-question three.

2.1. Breakwaters

Breakwaters are structures widely used throughout the world and are primarily designed for the protection of vessels harboured within ports and of port facilities from wave action. Furthermore, breakwaters can be applied to protect beaches from erosion or to protect valuable habitats that are threatened by the destructive forces of the sea (Van den Bos & Verhagen, 2017). For a description of the most important design parameters, see Appendix A.

2.1.1. Types of breakwaters

Many different types of breakwaters exist which are divided into categories depending on their structural features. The distinction is made based upon the ratio between load and strength, i.e. wave height (H) and the dimensions and relative density of the elements (Δd). The different types of breakwaters, in descending order of $H/(\Delta d)$, are: sandy beach, gravel beach, rock slope, berm breakwater, (stable) rubble mound breakwater and caisson (Van den Bos & Verhagen, 2017). This study will focus on a rubble mound protected by a cover layer of concrete armour units, of which a schematic overview is shown in Figure 2.1.

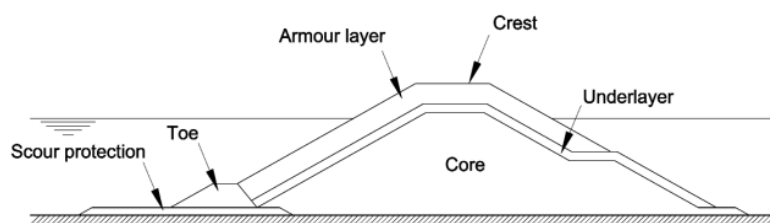


Figure 2.1. Cross-section of a typical rubble mound breakwater (CIRIA et al., 2007/2012).

2.1.2. Failure mechanisms

In the majority of cases, the most important function of breakwaters is protection against wave penetration into the harbour (Van den Bos & Verhagen, 2017). Failure of the structure is defined as the condition in which the specified functionality is lost. The distinction is made between a serviceability limit state or an ultimate limit state. To assess the behaviour and reliability of the structure under design conditions, an overview of the potential failure mechanisms is required. The possible failure modes for a rubble mound breakwater, as visualized by Burcharth (1992), are shown in Figure 2.2.

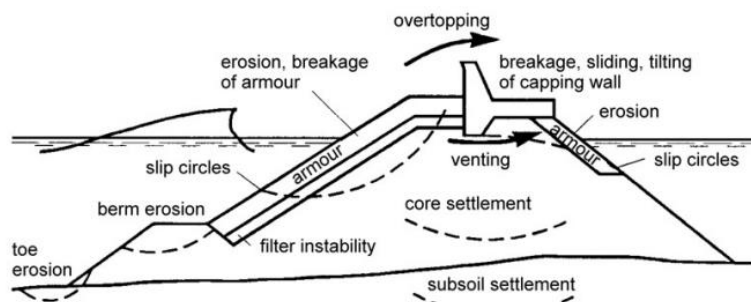


Figure 2.2. Failure modes for a rubble mound breakwater (Burcharth, 1992).

2.1.3. Roundhead

Figure 2.2 depicts common failure modes of the trunk of a breakwater, analysing the stability of the bidimensional section. However, breakwaters can be subdivided into separate regions, namely the breakwater head and trunk. The seaward end of a shore-connected rubble mound breakwater, or both ends of an offshore breakwater, is termed the roundhead and is circular in plan (CIRIA et al., 2007/2012). Special consideration is needed when the armour size on a roundhead is selected as both diffracted waves and overtopping discharges increase exposure. Furthermore, due to the curvature, the armour units are less supported and have less interlocking (Van den Bos & Verhagen, 2017). The head of a breakwater is often reinforced either by: using larger size armour units, reducing the slope and/or increasing the density of the armour units.

The radius and the side slope are the main parameters of a roundhead. The Rock Manual (2007/2012) proposes a selection of the radius as a function of the significant wave height at the design water level. The most severe attack is often at the leeward side of the roundhead, visualized in Figure 2.3.

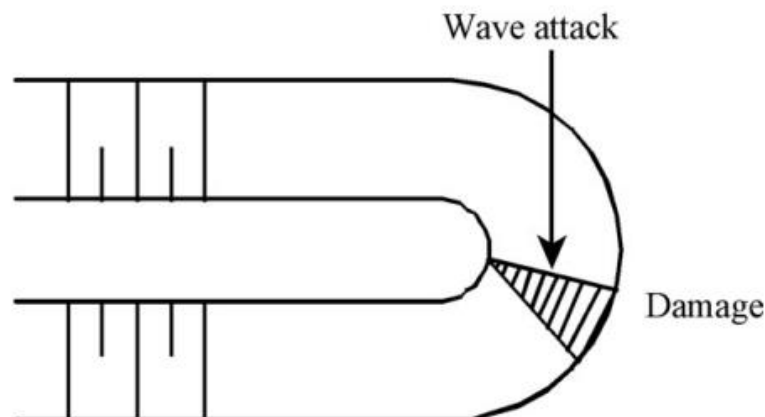


Figure 2.3. Typical damage pattern breakwater head (Van den Bos & Verhagen, 2017).

Breakwater roundheads impose further complications. If the breakwater is likely to be extended in the future, the designers should be aware that units will be lost since dismantling and removal of heavy stones or highly interlocking units is not a straightforward task (CIRIA et al., 2007/2012). Furthermore, careful attention should be paid to the design of the transition between the trunk section and the roundhead.

2.2. Armour

2.2.1. Types of armour

Rubble mound breakwaters are structures built of quarried rock, covered with a protection layer of heavy armour stones or concrete armour units. The availability of large rock is limited but in some cases heavy blocks are required. Therefore, the use of artificial blocks constructed of concrete becomes an interesting alternative. These blocks are not reinforced to prevent corrosion to the steel reinforcement in a saltwater environment. Concrete armour units can be distinguished by the three mechanisms providing stability: weight, interlocking or friction. The units obtaining stability mainly by their weight usually have simple, bulky shapes, while the interlocking units are typically slender. The friction classification consists of pattern placed concrete blocks and columns with maximum design wave heights in the order of 2 to 3 meters, making them less suitable for breakwaters according to Van den Bos & Verhagen (2017).

Concrete armour units can, in addition to stability mechanisms, be distinguished further by the amount of layers, single or double, and the placement method, randomly or uniformly placed (Reedijk & Muttray, 2008). Figure 2.4 provides an overview of a selection of frequently used concrete armour units currently available on the market, divided into different categories. Note, XblocPlus is added to the original figure and positioned in both the interlocking and friction mechanism, in accordance to the conclusions of Vos (2017).

















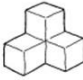


Randomly placed armour units			Uniformly placed armour units	
Double layer placement		Single layer placement		
Stability factor: Own weight	Own weight and interlocking	Interlocking	Friction	
Cube 	Tetrapode France, 1950 	Accropode France, 1980 	Cob UK, 1969 	
Modified Cube USA, 1959 	Akmon NL, 1962 	Core-loc® USA, 1996 	Diahitis Ireland, 1998 	
Antifer Cube France, 1973 	Tribar USA, 1958 	A-Jack USA, 1998 	Seabee Australia, 1978 	
Haro Belgium, 1984 	Stabit UK, 1961 	Xbloc NL, 2003 	Shed UK, 1982 	
Tripod NL, 1962 	Dolos South Africa, 1963 	XblocPlus NL, 2015 		

Figure 2.4. Overview of concrete armour units, after Muttray and Reedijk (2008).

2.2.2. Armour stability

Traditionally, a description of stability is provided by the Hudson formula (Van der Meer, 1998). Originally devised for rock armour, the Hudson formula predicts the size of armour units designed for wave attack. In its most simple form, and amended for concrete armour units, the formula reads:

$$\frac{H_s}{\Delta D_n} = (K_D \cot \alpha)^{\frac{1}{3}} \quad (2.1)$$

K_D is a stability coefficient which, for concrete armour units, is obtained empirically. The general stability of concrete elements is described by the stability number, defined as:

$$N_s = \frac{H_s}{\Delta D_n} \quad (2.2)$$

The expression connects the stability of the armour units to the significant wave height (H_s), the relative reduced unit mass density (Δ) and the nominal diameter D_n . For a formulation of H_s , see Appendix A. Blocks with a higher N_s value have better stability, which means, in principle, they can be smaller and thus more economical. However, numerous practical considerations influence this relationship.

2.2.3. Forcing

As mentioned in Section 2.1, breakwaters are primarily designed to protect against wave impacts. Ultimately, when the waves encounter the slope of the structure, wave breaking will be initiated, leading to the water surging up and down the slope. For a description of wave breaking, see Appendix A. The maximum and minimum levels reached during up- and downrush are termed the runup level (R_u) and rundown level (R_d), respectively (Hald, 1998). The magnitude of up- and downrush depends on the permeability of the structure. Impermeable or less permeable slopes will experience the highest possible velocities as the process only takes place in the outermost porous part of the structure, see Figure 2.5.

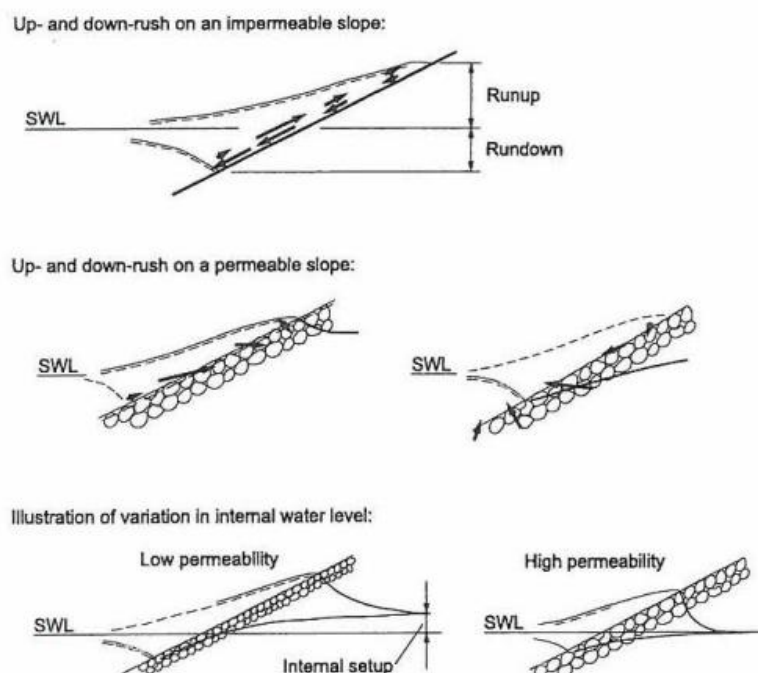


Figure 2.5. Illustration of up- and downrush on a slope (Hald, 1998).

The process illustrated in Figure 2.5 is the driving component of armour forcing. Due to the flow over the slope, all forces, except the gravitational force, may vary in size and direction over time. Depending on the occurring failure mode, different forces will either act stabilizing or destabilizing, demonstrated in Figure 2.6.

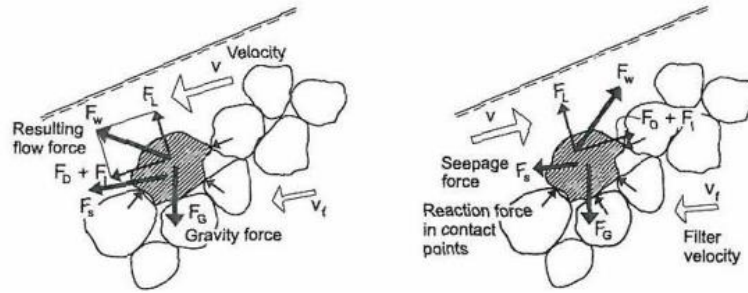


Figure 2.6. Illustration of forces on an armour stone (Hald, 1998).

While the armour is submerged, the buoyancy force remains constant but changes to zero while the free surface passes over. The buoyancy and gravity forces are opposing and when combined result in the following expression of the submerged weight:

$$F'_G = (\rho_m - \rho_w)gD_n^3 \quad (2.3)$$

The up- and downrush result in a wave induced force and can be interpreted as the vectorial sum of a drag force F_D , lift force F_L and inertia force F_I (Hald, 1998), i.e. the external flow forces. Applying the classical Morison equation, the wave induced forces on a single resting armour unit can be expressed as:

$$\vec{F}_w = \vec{F}_D + \vec{F}_L + \vec{F}_I \quad (2.4)$$

In which:

- F_D is a drag force proportional to and in the same direction as the square of the water particle velocity. The force is governed by the armour unit's drag coefficient C_D and cross sectional area.

$$F_D \approx C_D \rho_w A v |v| \quad (2.5)$$

- F_L is a lift force, governed by similar variables as the drag force, which forces the armour unit vertically.

$$F_L \approx C_L \rho_w A v |v| \quad (2.6)$$

- F_I is an inertia force, also termed the virtual mass. The term may be explained as the increase in force caused by an increase of the displaced mass of the fluid when an object is accelerated in a fluid, as compared to acceleration in a vacuum (Woodward-Clyde Consultants, 1980).

$$F_I \approx C_M \rho_w V \frac{dv}{dt} \quad (2.7)$$

The drag, lift and inertia coefficients depend on the armour unit shape, Reynolds number (Re) and Keulegan-Carpenter number (KC). KC , alternatively known as the period number, describes the relative importance of drag forces over inertia forces in an oscillatory flow (Kaneko et al., 2014). For a definition of Reynolds number, see Appendix A.

The second hydrodynamic component forcing armour units on a breakwater are the internal flow forces. This category is caused by the internal water flow out of the structure and is described by the seepage force F_s . The seepage force is composed of two components, namely:

- The force experienced due to build up of hydrostatic pressure, symbolized by F_p .

$$F_p \approx \frac{v}{1-n} \frac{\partial p}{\partial x} \quad (2.8)$$

- As well as the internal flow out of the structure, i.e. F_f . This force is governed by the hydraulic pressure gradient (i) and the porosity of the core material (n).

$$F_f \approx \rho_w g \frac{v}{1-n} i \quad (2.9)$$

$$i = C_a v_f + C_b v_f |v_f| + C_c \frac{\partial v_f}{\partial t} \quad (2.10)$$

The hydraulic pressure gradient is calculated using the extended Forchheimer equation by Polubarinova-Kochina in 1952. The gradient depends on viscous, drag and inertia force coefficients conditional on armour unit shape, size, porosity, Reynolds number and Keulegan-Carpenter number (Van Gent, 1995).

2.2.4. Failure mechanisms

Figure 2.2 illustrates the possible failure mechanisms of a breakwater. Failure could occur due to instabilities in the subsoil, core or filter layer, due to erosion at the toe or outer berm or due to overtopping and subsequently erosion to the inner berm. However, this thesis focusses on the failure modes of armour units, of which two can be distinguished.

Firstly, breakwater armour units are subject to loads in service that induce compression, flexure and shear in the units, which could cause breakage (Smith, 2016). For slender interlocking units a minimum tensile strength, in addition to compressive strength, is specified to prevent flexural failure.

Secondly, erosion of the armour layer by displacement of the units. For armour stones, different types of failure mechanisms are depicted in Figure 2.7, which partly translate to concrete armour units.

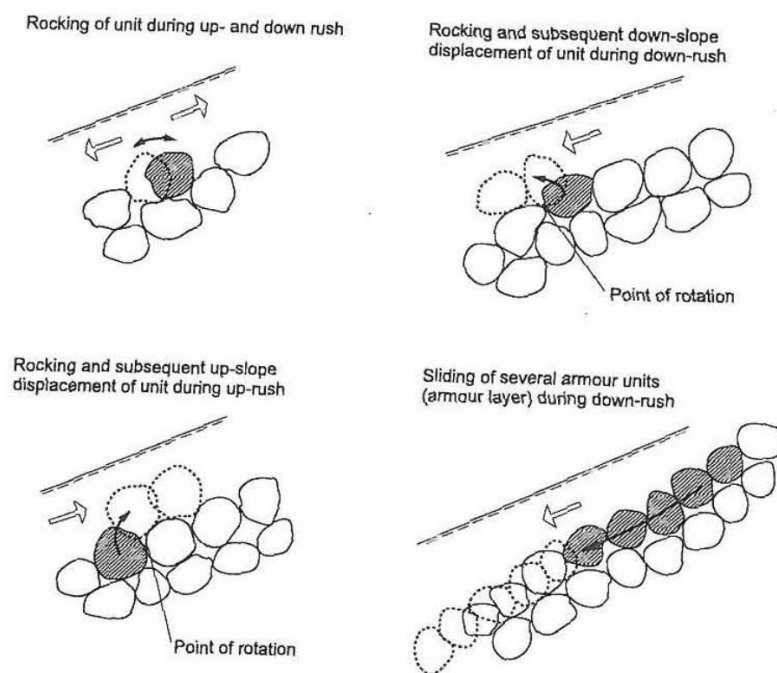


Figure 2.7. Typical armour layer failure modes (Hald, 1998).

According to Iribarren (1938, 1965), sliding of the armour stone is the dominant mode of motion. Hedar (1960) challenged this view and considered rotation to be the dominant mode. However, the same stability criterion was reached during downrush. Hudson (1958) abandoned the Iribarren formulation and developed an equation based on a simple quantitative force ration between driving and resisting forces (Hald, 1998). Neglecting the inertia force,

inserting the expressions for F_D , F_L and F'_G and assuming $v \approx \sqrt{2gH}$, the following criterion was obtained:

$$\frac{F_D + F_L}{F'_G} \approx \frac{\rho_w D_{n50}^2 v^2}{(\rho_m - \rho_w) g D_{n50}^3} K \quad (2.11)$$

The dimensionless function K was found by model tests to depend on the cotangent of α . In this formulation, the direction of the wave induced force is neglected.

2.3. XblocPlus

Xbloc, DMC's pioneering breakwater armour unit, has been a fixture in the market for 20 years, with over 500,000 blocks successfully deployed worldwide since its inception (XBloc, n.d.). With the units' random and interlocking placement system, a hydraulic stability of $K_D = 16$ is achieved. Due to symmetry (see Figure 2.8), Xbloc units interlock on all sides, hence less configuration rules apply compared to similar single layer block solutions.

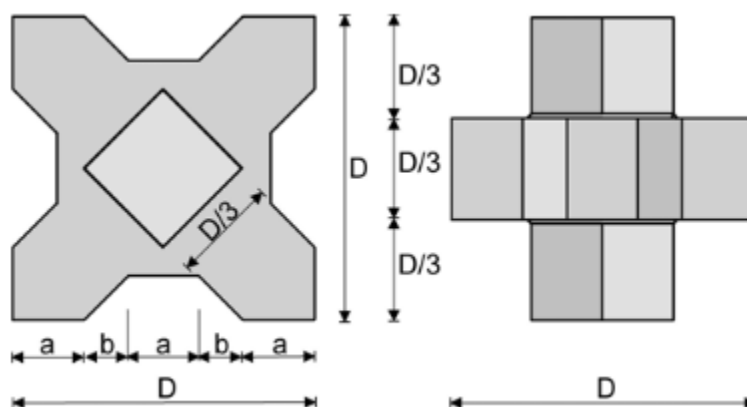


Figure 2.8. Geometry of Xbloc (Muttray et al., 2003).

Today's single layer, interlocking armour units like Xbloc require randomly varying orientation to achieve a properly functioning armour layer (Reedijk et al., 2018). An insufficient variation in the orientation of the armour units will lead to a more uniform appearance of the armour layer. The result is an increase in packing density and concrete usage and a decrease in porosity, possibly leading to larger wave overtopping. Furthermore, preference is given on breakwater construction sites to regular placement of interlocking armour units as less intuition is required and the placement process is sped up. For DMC, this was the main trigger for the development of XblocPlus, innovating on efficient material use, construction speed, construction safety and hydraulic stability (Bakker et al., 2019).

XblocPlus is an interlocking armour unit, placed uniformly on a staggered grid (Figure 2.9). The XblocPlus units rest on the slope of the breakwater and on two units of the next lower row, with stabilization provided by two units of the next higher row. As the placement is uniform, the contact points between units are invariable. Stability of the armour layer is obtained through the weight of the units, friction between neighbouring units and, due to its shape, interlocking (Vos, 2017). The units include a central opening, introduced to prevent water pressure build-up during wave run-up and run-down.



Figure 2.9. XblocPlus placement pattern (left) and side view of unit (right) (Reedijk et al., 2018).

2.3.1. Stability of XblocPlus

The hydraulic performance of XblocPlus is tested extensively in two- and three-dimensional scale model tests on different slope angles (Reedijk et al., 2018). Furthermore, stability under oblique wave attack with wave angles ranging from 0° to 60° was tested in 2017 (Bakker et al., 2019).

Reedijk et al. (2018) describes the results of 2D and 3D stability tests of a rubble mound breakwater with XblocPlus armouring on a gentle 1:2 and a steeper 3:4 slope angle. The relative crest freeboard (R_c/H_s) was 1.27 (3:4 slope) and 1.43 (1:2 slope). The design wave height was based on a stability number of $N_s = 2.5$. Failure of the units was assessed using three different mechanisms, namely: rocking, characterized by repeated back and forth movements of a specific armour unit; displacement, referring to a significant shift or rotation of an armour unit; settlements, relating to a general compaction of the armour layer. In tests with 1:2 slope, no armour unit displacements were observed at overload conditions of 125% H_s . However, a single test with 3:4 slope angle recorded armour unit displacement on the breakwater slope at a wave height of 159% H_s . The observed failure mechanism was rocking. The tests demonstrated that the actual hydraulic stability of XblocPlus exceeds the damage number N_s of 2.5 that is applied for design. Additional conclusions from the model test results include: no indication of influence of wave steepness; no indication of influence of oblique waves on the breakwater trunk; the seabed slope in front of the breakwater has impact on the armour layer stability.

Failure of XblocPlus is described by Vos (2017). During up-rush, the armour units are loaded from below, exerting an upward directed force on the nose and bottom of the unit. Subsequently, the unit is loosened from its stable position. The failing units show developing signs of rocking with increasing wave heights. Ultimately, the unit is tilted with its nose almost vertical, losing contact with the units a row above. The up-rush of a high energy wave group causes the unit to be detached momentarily, after which the down-rush initiates the actual extraction, caused by the combination of a high water level in the core and a through in front of the slope. The process is visualised in Figure 2.10.

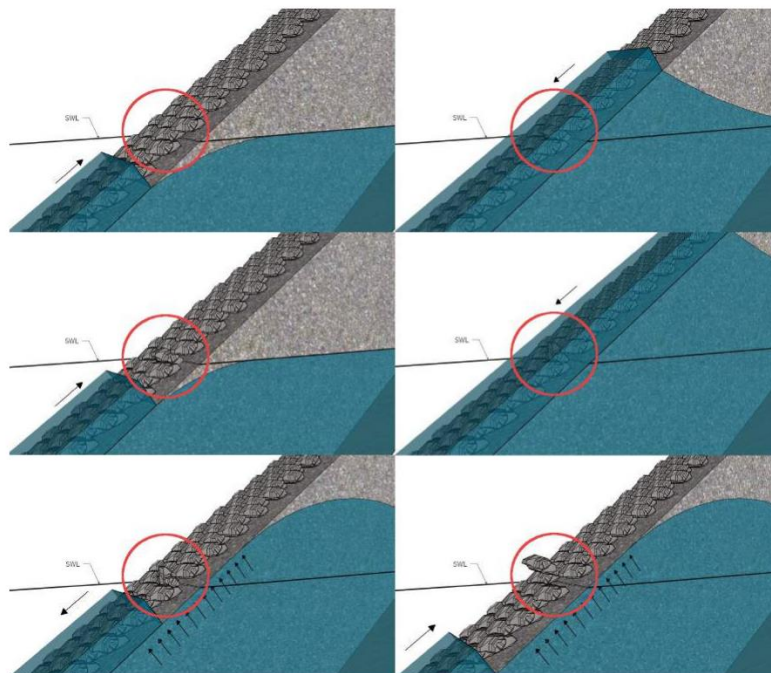


Figure 2.10. Extraction of XblocPlus unit from slope (Vos, 2017).

2.3.2. Applicability of XblocPlus

According to the XblocPlus Design Guidelines (2023), XblocPlus units are used on straight or mildly curved breakwater sections. For medium curved sections so-called XP-Wing, an XblocPlus with reduced width, is applied in combination with XblocPlus. The minimum radius which can be achieved with this arrangement depends on the block size, height of the armour layer and the slope angle. The minimum required radius of the breakwater is reduced with 50% compared to normal XblocPlus when the width of the unit is reduced in 2 steps (10% and 20%). A possible arrangement is shown in Figure 2.11.

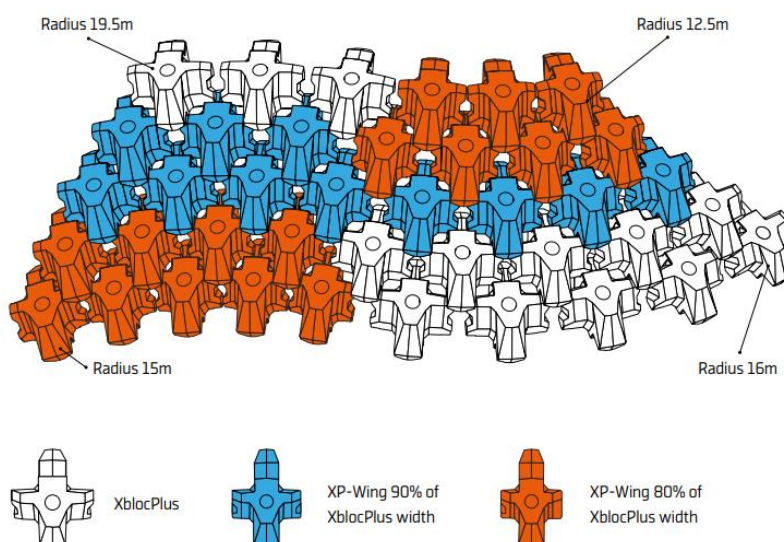


Figure 2.11. Application of XP-Wing with XblocPlus on curved sections (XBloc, 2023).

2.4. XP-Curve

Currently, Xbloc is applied on strongly curved sections or breakwater head. The Xbloc size on a roundhead is designed with a factor of 1.25 compared to the block size on the trunk, as advised by DMC (2023). Subsequently, the weight at the head section is 25% heavier than Xbloc units at the trunk section. The minimum roundhead radius (R) with Xbloc armour is 2.5 times the design H_s taken at design high water level. In case a larger armour unit is applied than based on the advised correction factor of 1.25, R is defined as six times the characteristic height (D) of the Xbloc size.

The horizontal spacing (D_x) between XblocPlus units varies in each row. To enable application of XblocPlus on roundheads, DMC introduced XP-Curve. When D_x is too small for placement of XblocPlus, a row with XP-Curve is placed (Reedijk & Muttray, 2023). In the next row, XblocPlus with normal D_x is placed, see Figure 2.12. The number of rows between XP-Curve rows depend on the radius of the section.

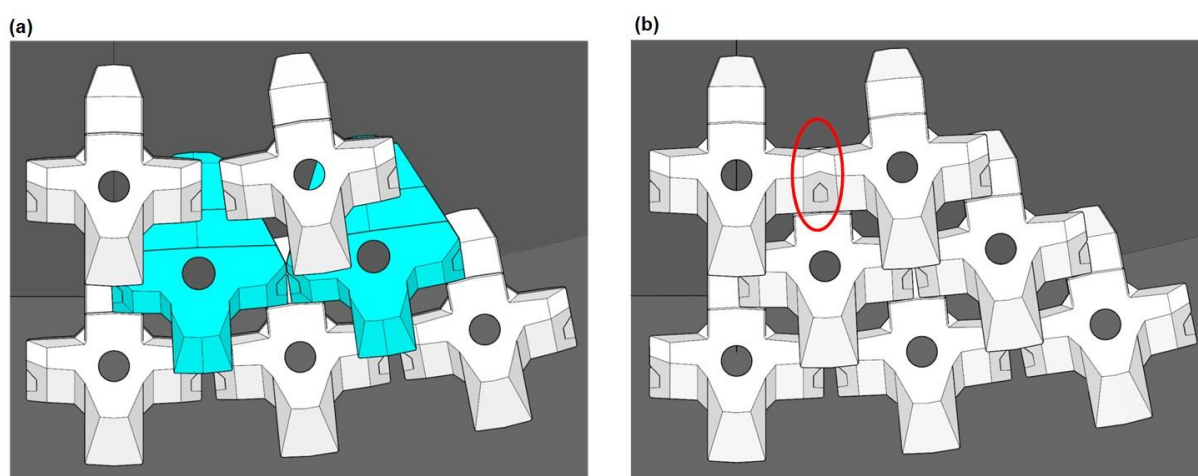


Figure 2.12. Primary function of (a) XP-Curve on breakwater roundheads in comparison to (b) XblocPlus.

XP-Curve shows alterations at the top- and backside with respect to XblocPlus. The rear end of XP-Curve is widened which accommodates placement of XblocPlus on top. However, the interlocking mechanism of the wings is lost due to this modification (de Raad, 2021). Further alterations to the rear end of XP-Curve include an added step to improve underlayer tolerances and allow water to dissipate through the grip hole. A comparison of XP-Curve and XblocPlus is shown in Figure 2.13.

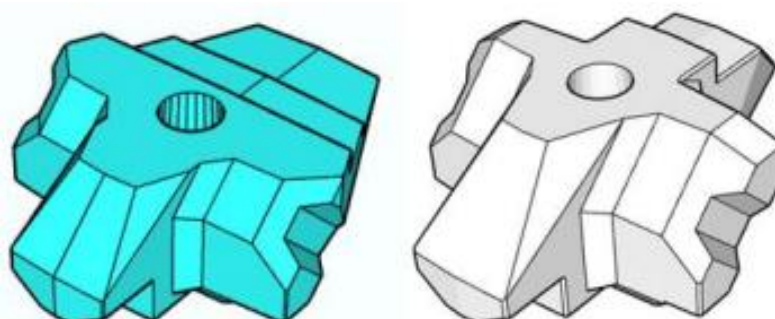


Figure 2.13. XP-Curve (left) and XblocPlus (right) (de Raad, 2021).

2.4.1. Stability of XP-Curve

The stability of XP-Curve has so far been assessed by two 2D test programs. Firstly, Wiersma (2021) tested XP-Curve as a transition between two consecutive rows of XblocPlus. De Raad (2021) executed validation tests on the same configuration and in addition tested a roundhead consisting solely of XP-Curve.

Wiersma (2021) observed failure in two subsequent tests, both with $s_{0,p} = 0.02$. The first test, executed with a water depth at the toe (h_{toe}) of $2.62 H_{s,d}$, was stopped after failure of one XP-Curve unit at $150\% H_{s,d}$. The water depth at the toe is expressed dimensionless in terms of the design significant wave height ($H_{s,d}$) to simplify comparison between studies with different test configurations. The observed failure mechanism is rotation, caused by refraction on the scaled roundhead and turbulence at the leeward side. As the waves approach the roundhead, water depth variations alter the direction and intensity of the waves, leading to rotational movements. The influence of the failed unit on surrounding units was minimal, see Figure 2.14a. The second test run ($h_{toe} = 2.87 H_{s,d}$) of Wiersma (2021) concluded with failure of three units at $130\% H_s$, of which two XblocPlus and one XP-Curve. The failure mode was again identified as rotation, with failure of one XblocPlus unit causing subsequent failure of multiple units. The research concluded with an estimated stability number of $N_s = 3.25$, adjusted with a safety margin to $N_s = 2.5$.

De Raad (2021) validated the observations by Wiersma (2021) and obtained a stability number of $N_s = 2.91$ for the same mesh with XblocPlus and XP-Curve. The failure modes observed are rotation, thus confirming the findings of Wiersma (2021), and uplift. The uplift originated from overpressures underneath the armour layer and depends on the permeability of the core and armour layer. The less favourable wave steepness was determined as $s_{0,p} = 0.02$. The second configuration De Raad (2021) tested consisted solely of XP-Curve. For a wave steepness of $s_{0,p} = 0.02$, this configuration failed at $120\% H_s$, i.e. $N_s = 2.82$. Failure occurred due to rotation and uplift. However, uplift was significantly increased for the configuration of XP-Curve, caused by a higher packing density and subsequently lower permeability.



Figure 2.14. Occurrence of failure in (a) Wiersma (2021) and (b) De Raad (2021).

2.5. Scaling

Wolters et al. (2009) describes the factors that have to be taken into account for scale selection of a hydrodynamic physical model. Generally, the structural dimensions are scaled geometrically, i.e. by $\lambda = \frac{L_p}{L_m}$. Here, λ is a constant scale factor relating dimensions of the prototype (L_p) and model (L_m). Wolters et al. (2009) advises scales which comply with Froude scaling. Furthermore, turbulent flow conditions have to be ensured throughout the primary armour layer to avoid significant Reynolds scaling effects. Increasing the Reynolds number decreasingly influences the drag coefficient in the Morison equation (see Section 2.2.3), corresponding to higher wave run-up. Additionally, the Weber number must be sufficiently large to prevent influence of surface tension in the model. See Appendix A for a description of the Froude, Reynolds and Weber number, and Figure 2.15 for an overview of the scale numbers.

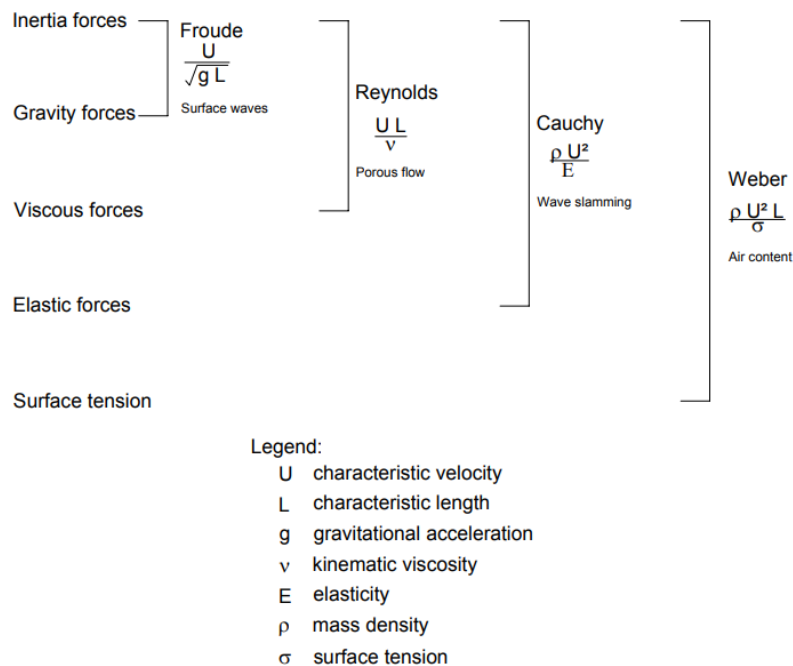


Figure 2.15. Ratios of forces and related scale number (Burcharth & Andersen, 2009).

The aforementioned scale effects result in boundary values for the model size. The water depth should exceed 5 cm, while the wave height is limited to at least 2-3 cm, with 5 cm the lower limit for design wave height. Furthermore, the wave period should represent a realistic wave steepness. Wolters et al. (2009) also proposes lower limits for rock diameter ($> 3 - 5 \text{ mm}$), rock armour ($> 25 \text{ mm}$) and describes the limit of available concrete armour unit size, i.e. $> 30 \text{ mm}$. The scaling of armour materials can be based on permeability- or stability scaling. For toe material and armour layers, the stability number N_s must be the same in model and prototype. For the underlayers and core, geometric scaling may cause viscous scale effects as these layers can become less permeable. Transmission and reflection can be affected by this phenomenon, hence Wolters et al. (2009) suggests careful assessment of permeability scaling. Considering the limits mentioned above, physical breakwater models are commonly scaled ranging from 1:5 to 1:80, with 1:30 – 1:60 for 2D and 1:30 – 1:80 for 3D.

2.6. Roundhead configuration

Ideally, three-dimensional models are used to verify or optimize the roundhead of a breakwater. However, to obtain a reliable comparison of model test results with previous literature, the test set-up, measurement techniques and modelling approach need to be similar (Wolters et al.,

2009). The preceding research by Wiersma (2021) and De Raad (2021) is executed in the two-dimensional DMC wave flume, which will also be used in this research. These tests will not provide definitive measurements of stability, but rather a relative assessment with regards to prior tests. Three-dimensional tests on larger scale will be recommended when the results of the two-dimensional tests are promising.

A scaled breakwater roundhead will be constructed in the wave flume. To model the stability of XblocPlus units on a roundhead, the breakwater is constructed in the direction of the flume. The crest will therefore be build up against the sidewall, while the toe extends to the opposite sidewall. Due to this orientation, the wave attack has an obliquity of 0° with respect to the breakwater and 90° with respect to the roundhead. The orientation of the roundhead with respect to the flume is depicted in Figure 2.16. Note, this figure is indicative and not to scale.



Figure 2.16. Top view of roundhead orientation in flume.

To measure the damage development of the armour layer, several methods can be used. Mares-Nasarre et al. (2021) proposes the use of the Virtual Net method, after Gómez-Martín (2015). The Virtual Net method divides the armour into strips of constant width and length. Subsequently, damage is measured in each strip, considering the porosity evolution in time and space. However, this method is applied to the front slope, crest and rear slope of randomly placed armour layers. For roundheads, strips of constant width and length cannot be achieved due to the curvature. Hence, to measure damage quantitatively, a method similar to de Raad (2021) is proposed, in which the roundhead is divided into sections of equal angles. The damage can subsequently be expressed as the number of displaced units in the reference area divided by the total number of units in that area, obtaining $D_{\%}$ as proposed in USACE (1984). The most exposed sector on a roundhead depends on the relative wave direction and “is located where the wave orthogonal is tangent to the cone and extends somewhat to the lee side of this point” (Jensen, 1984). The proposed method enables the assessment of damage on different sections of the roundhead.

To qualitatively assess the severity of damage on conventional mound breakwaters with single-layer armour, Gómez-Martín (2015) defined three levels of armour damage: ‘Initiation of Damage’ (IDa), i.e. some isolated units are removed from the armour, ‘Initiation of Destruction’ (IDe), i.e. several adjacent units are removed from the armour, and ‘Destruction’ (De). Alternatively, Bakker et al. (2019) applied different descriptions of damage for Xbloc and XblocPlus. For Xbloc, the distinction was made between four states: ‘no damage’, ‘start of damage’, ‘damage, no failure’ and ‘failure’. Regarding XblocPlus, no failure of the armour layer occurred in Bakker et al. (2019), limiting the qualitative damage description to ‘no damage’ and ‘start of damage’. However, both armour units adhered to the same failure criteria, defined for three distinguished wave conditions as described for Xbloc by Ten Oever (2017) and for XblocPlus by Van der Lee (2020):

- Operational conditions (1/1 year condition)
- Design conditions (1/100 year conditions, unless otherwise specified)
- Overload conditions (120% of design condition)

For rocking of units, defined as repeated movement of an individual unit at more than 2% of the waves, failure is defined as exceeding the allowable percentages which, for prototype Xbloc and XblocPlus under 10 m^3 volume, are 1%, 2% and 4% for the three wave conditions respectively. For prototype units exceeding the aforementioned volume, the allowable percentages are 1%, 1% and 2% respectively. Additionally, no dislodgement of a unit from the grid is accepted during the design conditions, whereas 1% is allowed during overload

conditions. No description of the ‘start of damage’ and ‘damage, no failure’ states of the armour layer is provided in Bakker et al. (2019).

2.7. Limitations

Due to the roundhead orientation in the DMC wave flume described in Section 2.6, certain phenomena may provide disturbances in the test results. Figure 2.17 illustrates the relevant wave processes, with further explanations provided in Appendix A.

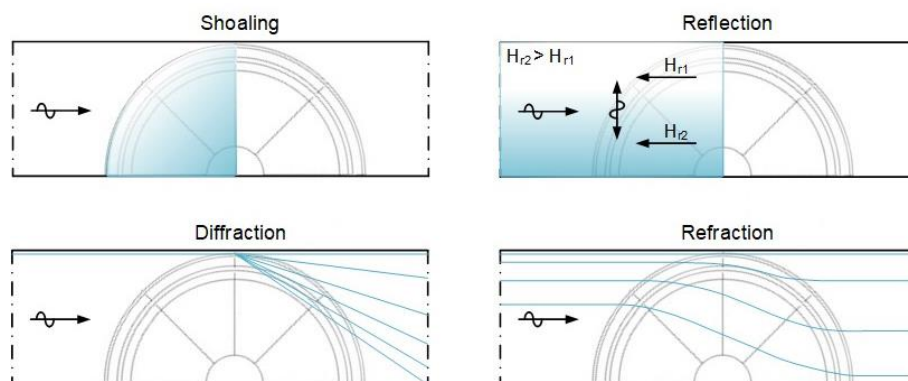


Figure 2.17. Wave processes influencing test results.

The phenomena exemplified in Figure 2.17 can be distinguished and described as follows:

- Shoaling occurs on a sloping bottom due to conservation of energy, increasing the wave amplitude. Due to the nonuniform section of the roundhead in the wave flume, the shoaling coefficient K_{sh} will vary along the width, visualized by the gradient in Figure 2.17 where darker colours correspond to higher shoaling effects. The amplitudes of the wave field will be distorted by shoaling, where higher wave heights are expected towards the crown of the roundhead. Depending on the local Iribarren number, shoaling could initiate wave breaking.
- Waves propagating towards a structure will reflect to some extent, with $K_{refl} = a_r/a_i$ ranging from 0 to 1. Depending on the phase of the reflected waves and the reflection coefficient, amplitudes in the wave field can thus be increased up to a factor of 2 or be completely cancelled out. Similar to shoaling, the roundhead section causes a difference in wave reflection, with lower possible reflection expected at the toe.
- Originating from the Laplace equation of linear wave theory, diffraction describes the variations in amplitude due to the shadowing effect of a breakwater. Due to diffraction, wave rays curve into the shadow area behind the breakwater, contributing to the wave amplitude in this region.
- Harmonic waves approaching a straight coast under oblique incidence will experience refraction, slowly changing the wave direction. Due to depth variation along the wave crest, according to the dispersion relation, the phase speed decreases more in shallower water. However, refraction also applies for regular incidence on structures with varying depth. Figure 2.17 illustrates the direction change of the wave rays due to depth variation along the roundhead. The waves will rotate towards the crown of the roundhead due to decreasing depth, after which the regular incidence is restored due to increasing depth after the roundhead.

3. Design

The design which will be subjected to physical model testing will be discussed in this chapter. A description is provided of the design process of the armour units and how the units are placed in a grid.

3.1. Preliminary design

The initial design, a combination of concepts produced by BAM Infraconsult through an iterative process, consists of three different armour units. Firstly, regular XblocPlus units are applied to compatible rows. However, as mentioned in Section 2.3.2, applicability of XblocPlus is limited on roundheads. Hence, additional concepts are used to accommodate a predefined staggered grid.

3.1.1. XblocPlus

Firstly, regular XblocPlus units are applied. A general description of XblocPlus is previously provided in Section 2.3, including stability and applicability. Additionally, this section will describe the main dimensions.

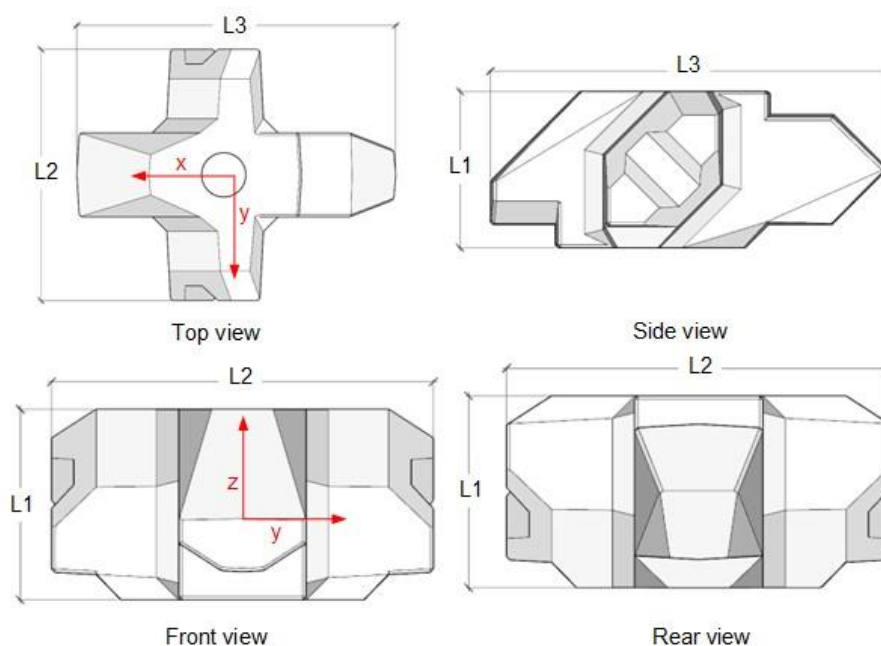


Figure 3.1. Main dimensions of XblocPlus unit with definition of axes indicated.

Figure 3.1 illustrates the faces of an XblocPlus unit with corresponding dimensions L_1 , L_2 and L_3 . The measurements describe the height, width and length, respectively. For units of 2.5 m^3 volume like applied on the Afsluitdijk, this corresponds to 1.12, 2.25 and 2.85 meters respectively (Xbloc, 2023). Units of this proportion are designed for wave heights up to 4.51 meters and weigh 6.0 tonnes. The centre of gravity is located exactly in the middle of the hole to stabilize the unit during placement. XblocPlus or corresponding units should be placed on minimal three contact points: one with the underlayer and at least two on the row below. The latter is achieved by either the nose or the wings of the unit, depending on the rotation around the y-axis, see Figure 3.2.

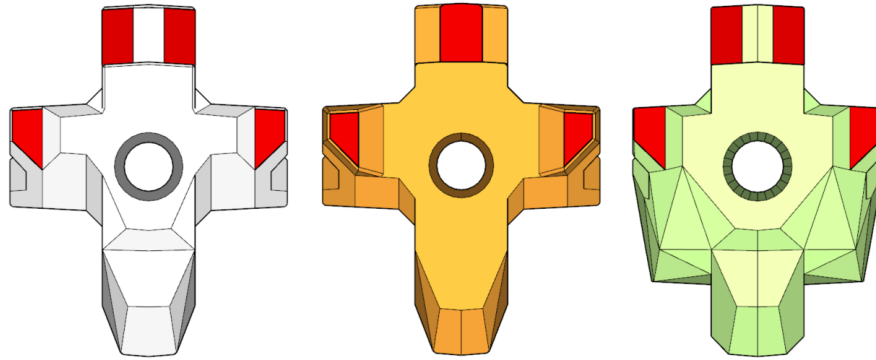


Figure 3.2. Contact surfaces with underlying row of XblocPlus, XP-Base and XP-Curve, respectively.

3.1.2. XP-Base

The second unit considered is a modified version of XblocPlus with similar length and width. However, the bottom is raised and legs are added to the bottom of the wings for several arguments. Firstly, the concept is planned to be applied on the bottom row in a breakwater grid to increase underlayer tolerances, hence named XP-Base. Bakker et al. (2019) concluded that the tolerances in the underlayer for XblocPlus is equal to the tolerances for Xbloc, i.e. $0.5 D_{n50}$. Secondly, the legs should provide more interlocking in shifted rows of the roundhead grid. The unit is depicted in Figure 3.3.

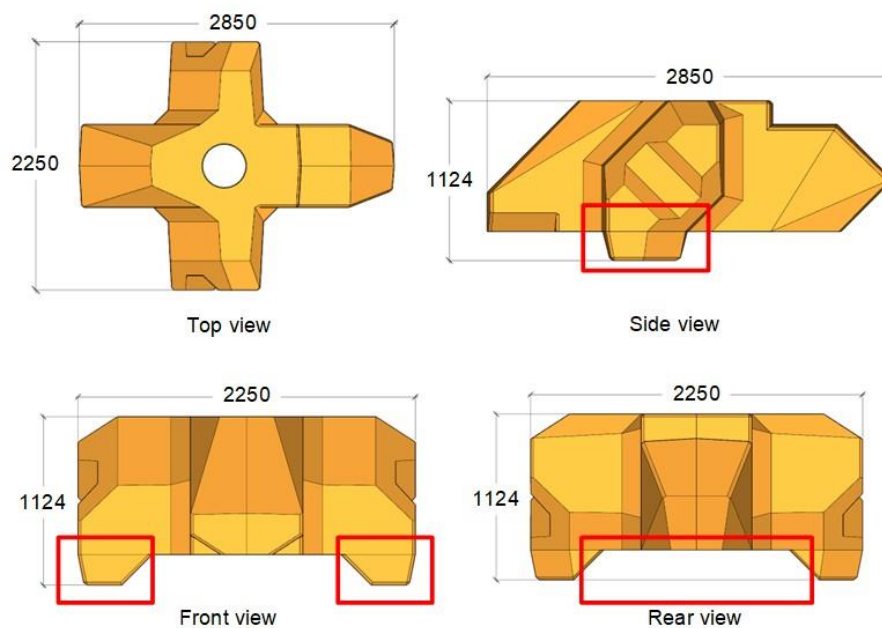


Figure 3.3. Main dimensions of XP-Base unit, modifications with respect to XblocPlus highlighted.

The dimensions correspond to regular XblocPlus units of 2.5 m^3 volume. As aforementioned, the width and length of the units are similar to XblocPlus, i.e. 2.25 and 2.85 meters respectively. However, the height is significantly different as the bottom is raised and legs are added. Due to the alterations, the volume is reduced to 2.29 m^3 .

3.1.3. XP-Curve (version 2)

The third variation is derived from XP-Curve, previously described in Section 2.4. The initial version of the XP-Curve showed alterations at the backside with respect to regular XblocPlus. The tail was widened to accommodate more flexible placement patterns on a roundhead.

However, Wiersma (2021) and De Raad (2021) concluded that the unit lacked sufficient stability due to rotation and uplift. Hence, alterations to XP-Curve are proposed. The modified version will be termed XP-Curve (version 2) in the remainder of this thesis. Section 2.3.2 provides a description of XP-Wing, essentially an XblocPlus with reduced width. Similarly, the width of XP-Curve can be reduced to increase permeability of the armour layer. Higher permeability accommodates more water penetration into the structure during wave run-up which could decrease the forces on the armour units (Van der Meer, 1998). The proposed modifications narrow the XP-Curve by 10 percent. Furthermore, the tail-end is reduced in width and adjustments are made to the contact surface with the row atop to better accommodate XP-Base. Additionally, an inclination in the top surface is added to improve water dissipation from the armour layer. The volume of the unit, placed in a grid with 2.5 m³ XblocPlus, is 2.49 m³. A comparison is depicted in Figure 3.4 and dimensions of the modified version of XP-Curve are shown in Figure 3.5.

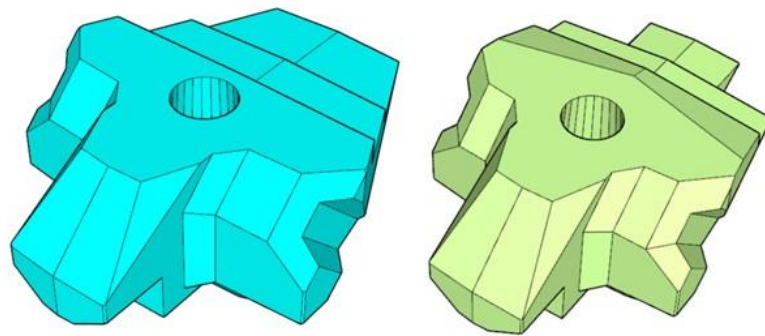


Figure 3.4. Left XP-Curve and right XP-Curve (version 2).

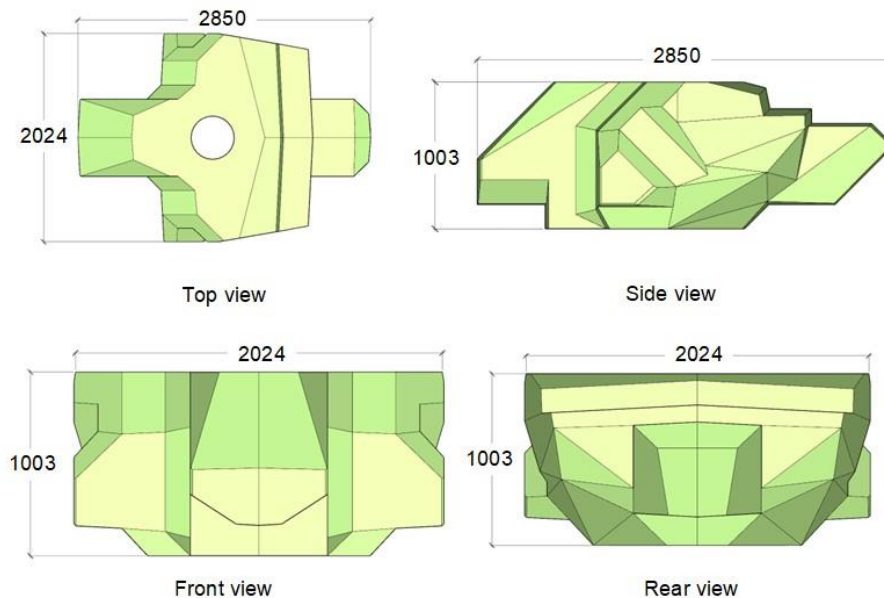


Figure 3.5. Main dimensions of XP-Curve (version 2) unit.

3.1.4. Sequence

The grid in which the aforementioned armour units are placed is explicitly formulated for the specific combination. Multiple views of a roundhead example consisting of 2.5 m³ or equivalent armour units are depicted in Figure 3.6.

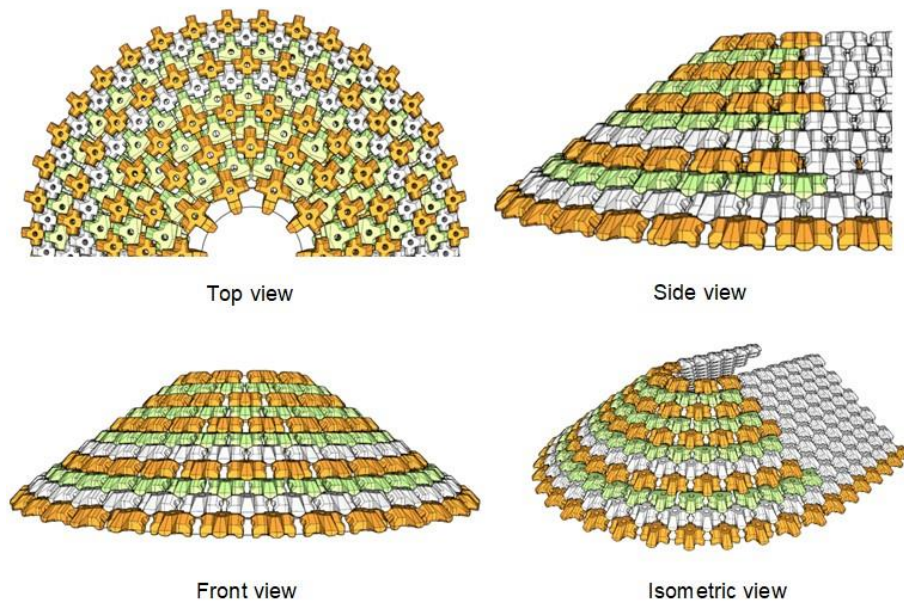


Figure 3.6. Placement grid for XblocPlus, XP-Base and XP-Curve (version 2).

The example in Figure 3.6 illustrates an arbitrary 11-row roundhead constructed of regular XblocPlus, XP-Base and XP-Curve (version 2). The configuration of the rows follows a predefined pattern. Firstly, following the new concept of BAM Infraconsult, the bottom row is constructed of XP-Base to increase underlayer tolerances. Subsequently, rows of regular XblocPlus are placed on top until placement is obstructed by decreased spacing between neighbouring units. The number of consecutive XblocPlus rows depends on the radii as the difference in configuration between straight section and roundhead reduces for increasing curvature radius. The XP-Curve serves as a transition row which enables continuation of the pattern. The next higher row should always contain XP-Base as the legs enable flexible placement and provide additional interlocking. Subsequently, regular XblocPlus can be placed again and the pattern is repeated. Placement of regular XblocPlus will be impeded after a certain number of rows as the radius decreases.

3.1.5. Placement grid

The aforementioned sequence determines the row order of units. Additionally, the placement grid depends on the separation distance at which the units are placed, described by D_x and D_y . D_x refers to the horizontal distance along the curve between the centres of gravity of two subsequent units shown in Figure 3.7a, whereas D_y describes the distance following the slope inclination. For 2.5 m³ XblocPlus units on a straight section, D_x and D_y are defined as 2.47 and 1.42 metres respectively. However, due to the curvature on the roundhead, D_x is subject to variations depending on the design choices. D_y should be approximately equal to D_y for XblocPlus on straight sections to realize the predefined breakwater slope.

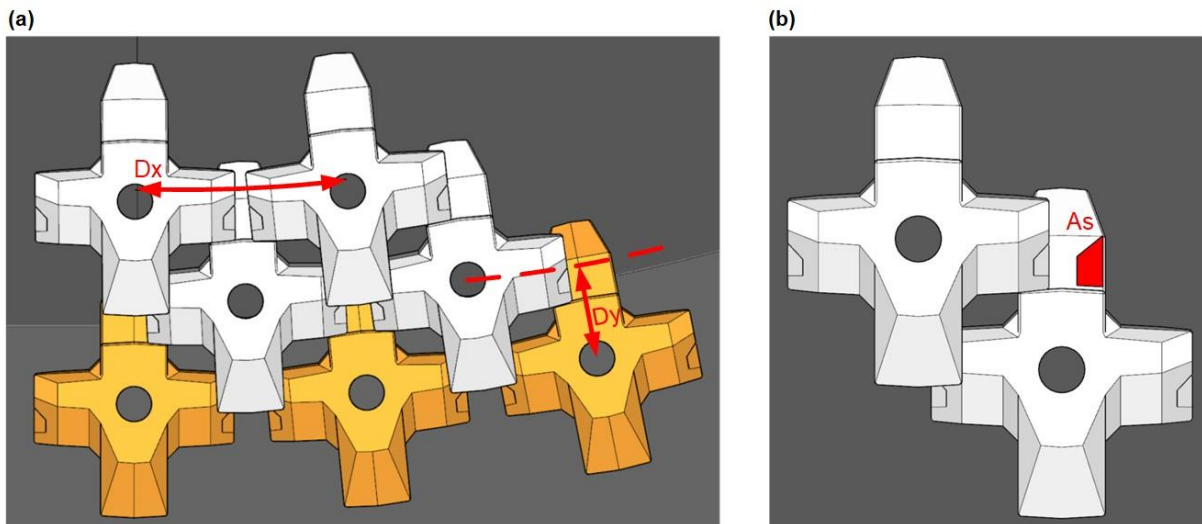


Figure 3.7. Visual description of (a) D_x and D_y and (b) A_s .

D_x depends on the number of units positioned on a certain radius; placement of more units will reduce D_x . The units should be placed on the roundhead in a pattern which enables connection to a straight section. Hence, placement should start at zero distance along the radius for each odd numbered row and at half times D_x for all even numbered rows. Alternatively, the reverse is also feasible. Following the sequence described in Section 3.1.4, positioning of XP-Base is normative as XblocPlus and XP-Curve are regularly placed on top. The distance between subsequent XP-Base units can be defined through several approaches.

Firstly, the space between neighbouring blocks can be bounded by predefined values of D_x along the placement curve. For example, De Raad (2021) applied a minimum spacing of 2% unit width with a maximum D_x of 1.15 unit width, i.e. $1.02 L_2 \leq D_x \leq 1.15 L_2$. This criterion results in a relatively even spacing between XP-Base across the roundhead. However, De Raad (2021) concluded failure due to a too low permeability for an XblocPlus and XP-Curve configuration. Additionally, placement is impeded by the criterion for smaller radii, hence limiting construction height.

Alternatively, positioning can be determined based on the support area of the wing provided by the unit in the previous row, depicted in Figure 3.7b. Applying this approach allows for more flexible placement and possibly higher permeability. The placement is related to the support area of XblocPlus on straight sections, for 2.5 m^3 units equal to 0.081 m^2 , which are positioned with D_x equal to 1.10 times L_2 . Due to block rotation around the z-axis on the roundhead radii, D_x and the support area deviate from this criterion. To provide placement margins, the criterion is posed to approximate the support area of XblocPlus on straight sections with D_x equal to 1.15 times L_2 , equating to 0.055 m^2 , i.e. 68% of the previous criterion. For each row, iterations are executed devising configurations after which the iteration closest to the criterion is selected.

For an arbitrary roundhead, Figure 3.8 depicts a comparison of the spacings between neighbouring XP-Base units.

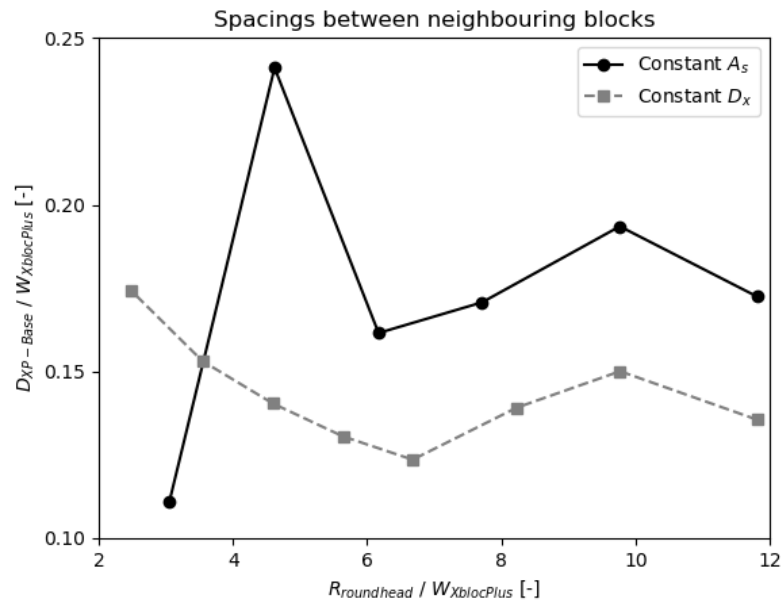


Figure 3.8. Spacings between neighbouring XP-Base units on an arbitrary roundhead.

Figure 3.8 shows relatively larger spacings between subsequent XP-Base units for placement based on constant support area. As the placement pattern is not bound to a range of values for D_x , the units can be placed further apart to accommodate additional rows on top given sufficient A_s . Hence, following the theoretically defined placement pattern, application of this method allows for higher construction height, namely 22 rows for the specific base radius and unit size in comparison to 19 rows for placement based on constant D_x . However, the placement pattern of XP-Base is configurable and the theoretical configuration can be disregarded on higher rows to continue placement. Further differences between methods arise in the sequence in which the units are placed. The roundhead design based on constant D_x disallows the placement of XblocPlus on larger radii than the design based on constant A_s , hence obtaining a difference in number of XblocPlus, XP-Base and XP-Curve. As all three unit volumes are distinct, and the number of units differ per configuration, disparity is expected in packing density and porosity. The packing density is calculated as the total number of units divided by the surface area of the roundhead at the centre of the armour layer. The surface area is calculated assuming a truncated cone with bottom radius, top radius and height as variables. The value is translated to the unit size of the prototype, i.e. 2.5 m^3 . Both the packing density and the porosity relate closely to the values of XblocPlus on a straight section, i.e. a packing density of 28.5 units per 100 m^2 and 60.3% porosity for 2.5 m^3 units. The roundhead design based on constant D_x shows a packing density of 30.1 units per 100 m^2 and 61.0% porosity, while the alternative displays 29.9 $1/100 \text{ m}^2$ and 60.8%, respectively.

3.1.6. Limitations

The aforementioned sequence and placement grids are expected to improve stability of XblocPlus on breakwater roundheads as permeability should be improved and interlocking increased. However, the preliminary design shows difficulties connecting to straight sections due to a difference in the previously explained D_y , see Figure 3.9. On straight sections, 2.5 m^3 XblocPlus is constructed with D_y of 1.42 meters which, on a 3:4 slope, corresponds to a horizontal and vertical distance between rows of 1.133 and 0.850 meters respectively. However, due to decreasing radii on a roundhead, space is lacking for placement of XblocPlus, increasing either component of D_y . For the preliminary design to fit on a roundhead, the horizontal or vertical component should be modified slightly if the complementary is kept constant, hence altering the breakwater slope and complicating transition to the straight section.

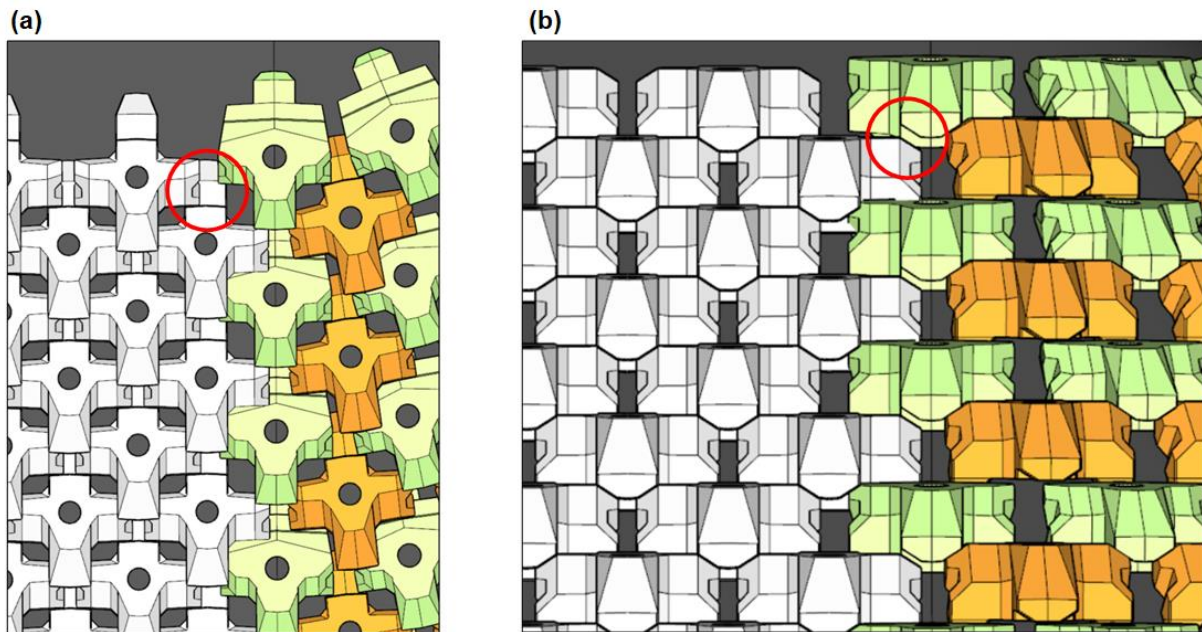


Figure 3.9. (a) Horizontal and (b) vertical differences between roundhead and straight section.

Figure 3.9 depicts the difficulties of applying XblocPlus on a roundhead; due to decreasing radii the unit is lacking space and thus pushes the grid up the slope. Thus, to apply this configuration on a roundhead and retain the original shape of XblocPlus, either XP-Base, XP-Curve or both need to be modified to be able to connect the roundhead to a straight section. Alternatively, the placement sequence can be adjusted.

3.2. Proposed design

The limitations posed in Section 3.1.6 require alterations of the preliminary design to enable connection of the roundhead to straight sections. The modifications proposed in this thesis are twofold.

3.2.1. Modifications

Firstly, adjustments to the shape of the armour units can be made. The alterations should provide an increase in placement space to prevent requirement of corrections as described in Section 3.1.6. The adaptable variables are the tail length of XP-Base and XP-Curve and the size of the support surface of XP-Curve. As previously described in Section 3.1.1, XblocPlus and related units are supported by the slope at the tail and additionally by the wings or nose by the underlying block. By decreasing the length of the tail, i.e. altering L_3 (see Figure 3.1), forward rotation of the units is reduced, hence reducing the difference in the vertical component of D_y with respect to XblocPlus on straight sections. To compensate for differences regarding the horizontal component of D_y , the top support surface of XP-Curve is stretched towards the nose to shift the supported XP-Base forward. Due to the shift, forward rotation around the y-axis of XP-Base is further decreased, contributing to the compensation of the difference in the vertical component of D_y . Additionally, the shift enlarges the radius at which XP-Base is placed and subsequently decreases the difference in horizontal component of D_y .

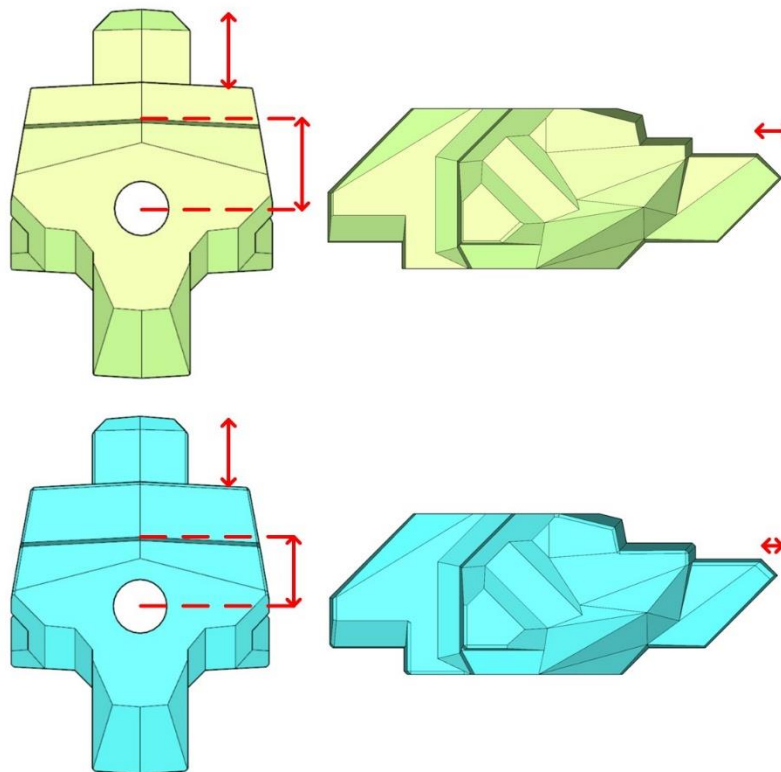
After several iterations comprising alterations of the tail of XP-Base and XP-Curve, as well as variations in the size of the top support surface of XP-Curve, a solution was found which best fitted 3:4 and 1:1.5 roundheads, termed iteration 4 in Table 3.1.

Table 3.1. Iterations of modifications to XP-Base and XP-Curve.

Iteration	XP-Base ΔL_3 [mm]	XP-Curve ΔL_3 [mm]	XP-Curve $\Delta L_{s,top}$ [mm]
1	-150	-150	0
2	-100	-150	+50
3	0	-150	+150
4	0	-100	+150

Note. The iteration selected is marked in bold.

The definitive block modifications comprise a 100 mm (3.5%) decrease in tail length and a 150 mm elongation of the top support surface of XP-Curve (version 2) formerly described in Section 3.1.3, while XP-Base remains unchanged, see Figure 3.10. This modified third version of XP-Curve will be termed XP-Curve (version 3) for the remainder of this thesis. Iteration four resembles iteration three closely regarding unit placement. However, 50 mm tail length was restored to better approximate the ideal forward rotation of the units, which, for XblocPlus on a 3:4 slope, is equal to 2.75 degrees. The placement configuration comprising the aforementioned modified units follows the scheme based on support area described in Section 3.1.5. This design, henceforth labelled Design 1, enables placement of XblocPlus until smaller radii, fitting well with the modified units as shown in Figure 3.11.

**Figure 3.10.** Top and side view comparison of XP-Curve (version 2) and XP-Curve (version 3).

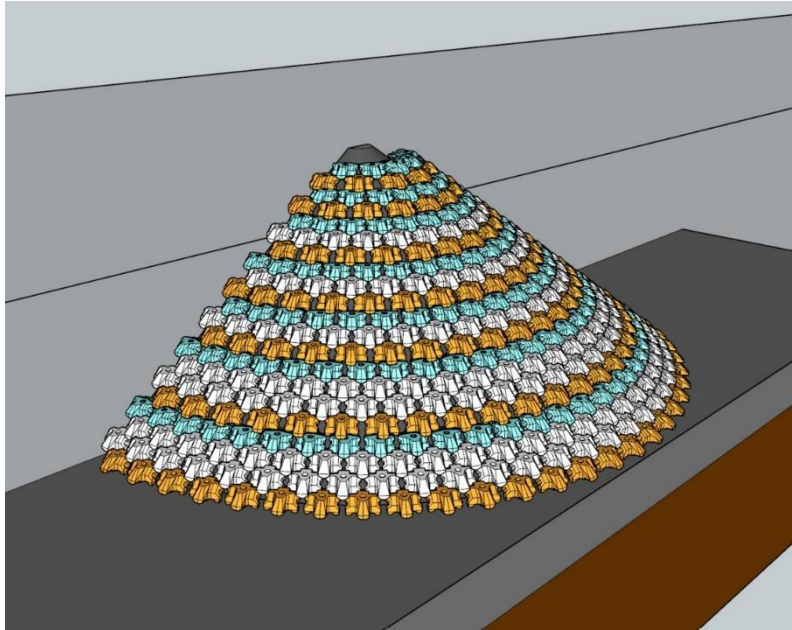


Figure 3.11. Roundhead Design 1, following the design based on A_s with XblocPlus, XP-Base and XP-Curve (version 3).

Secondly and separately, modifications are proposed to the placement sequence. As placement space decreases on a roundhead due to smaller radii, placement of XblocPlus shifts the grid up the slope away from the ideal positioning. However, XP-Base and XP-Curve as described in Sections 3.1.2 and 3.1.3 are designed to fit perfectly on straight sections. Additionally, the width of XP-Curve is reduced by 10% with respect to XP-Base and XblocPlus to always enable placement. Hence, the second design modification proposed in this thesis is a sequence consisting of solely XP-Base and XP-Curve, hereafter termed Design 2. As XP-Base is not required to be positioned in a predefined pattern, packing density of this configuration is highly configurable. Initially, placement of this sequence is based on the D_x criterion posed in Section 3.1.5. However, XP-Base units can be added in certain rows to decrease the intermediate separation between units and increase the support area of the supported XP-Curve. Moreover, separations could be increased to improve permeability if necessary. Additionally, construction is simplified, in production as well as placement, due to a decreased number of unique armour units. The configuration is depicted in Figure 3.12.

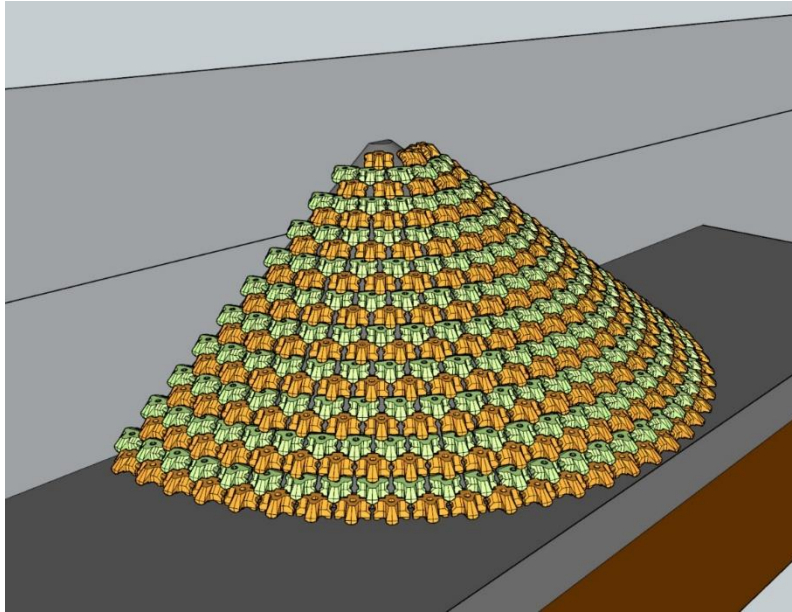


Figure 3.12. Roundhead Design 2, following the design based on D_x with XP-Base and XP-Curve (version 2).

Similarly to Figure 3.8, a comparison can be made between the intermediate unit spacings of the two modified concepts, see Figure 3.13. The normative difference is between XP-Base in both placement schemes as XP-Base establishes the placement pattern for supported units above. In the concept with placement based on A_s , XblocPlus is placed on relatively small radii, accommodated by larger spacings between XP-Base. Meanwhile, due to the lack of XblocPlus in the configuration, placement of XP-Base and thus XP-Curve is configurable in the placement grid based on D_x .

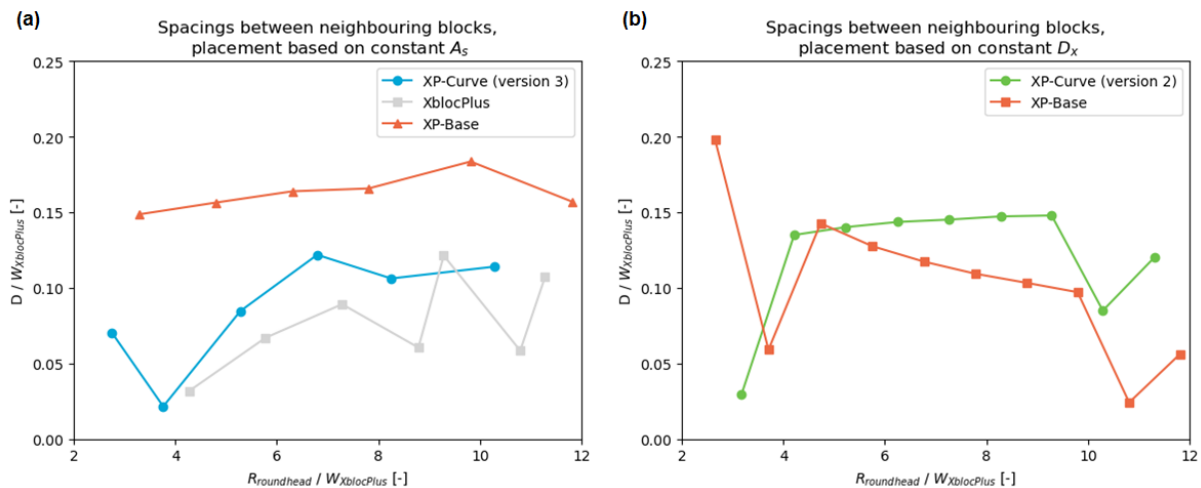


Figure 3.13. Spacings between neighbouring units on an arbitrary roundhead, with placement based on (a) A_s and (b) D_x .

Additionally, the rotation of the units can be compared. As aforementioned, DMC proposes a forward rotation around the y-axis of 2.75 degrees for units on a 3:4 slope to ensure a maximum degree of interlocking. The rotation, here labelled α , depends on the dimensions and sequence of the units and is depicted in Figure 3.14. The configuration of Design 2 shows rotations closer to the value prescribed by DMC.

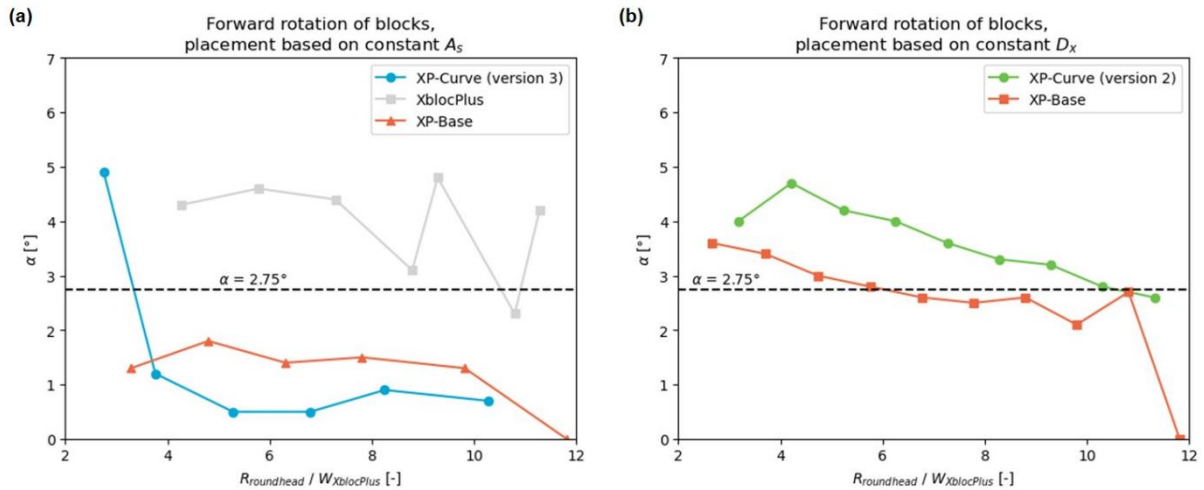


Figure 3.14. Forward rotation of armour units on an arbitrary roundhead, with placement based on (a) A_s and (b) D_x .

3.2.2. Transition

As discussed in Section 3.1.6, the transition of the roundhead to a straight section is a key component of the design. However, due to limitations regarding the test facilities, the transition will not be part of the tested configurations and designs are proposed purely based on digital models. The proposed transitions should be verified in future three-dimensional tests.

A transition is required as for each row of XP-Base one leg coincides with XblocPlus on the straight section. The leg needs to be lifted on top of the XblocPlus unit, inducing rotations to nearby units. Hence, two possible transitions are proposed. Firstly, a transition which compensates the unit rotations in a single column at the edge of the straight section. This concept could initiate a possible weak section at the conversion from straight section to roundhead. However, optimal positioning is further retained on the straight section. Secondly, a transition can be constructed which dissipates the differences in angular rotation and height over a diagonal. In this case, the unit configuration of the roundhead is extended on the straight section over a diagonal, gradually rotating XP-Base units in separate columns. Therefore, weak sections could occur on the straight section as XP-Curve exhibits less interlocking on straight sections than XblocPlus. The concepts are illustrated in Figure 3.15.

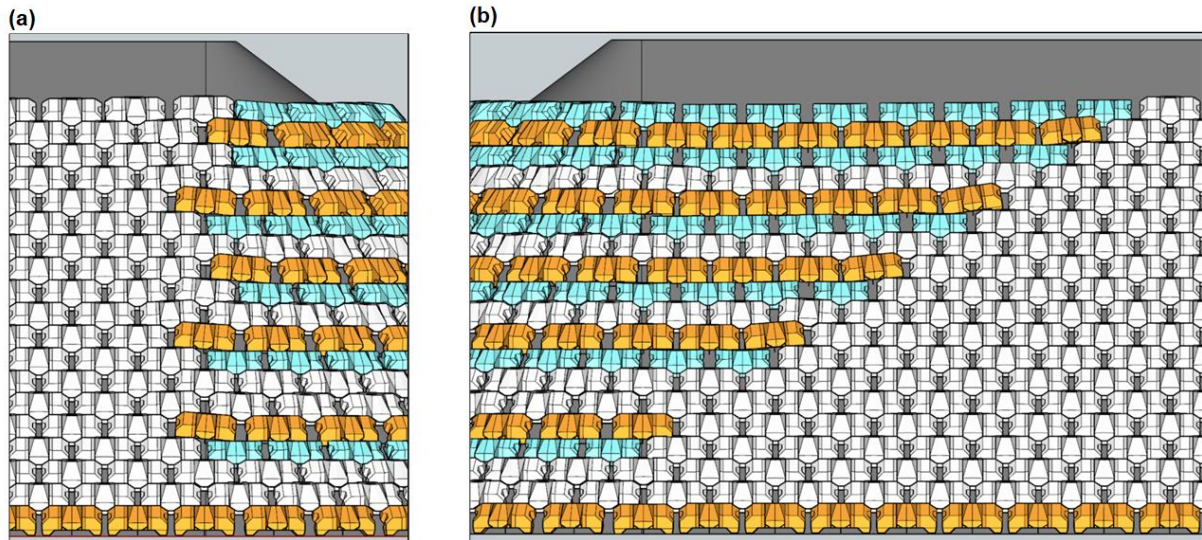


Figure 3.15. Comparison of transition concepts, **(a)** column and **(b)** diagonal.

For the grid configuration consisting of XblocPlus, XP-Base and XP-Curve, placed based on a constant A_s , the column transition is deemed within reasonable limits as the units show relatively low additional rotations. However, the grid of XP-Base and XP-Curve requires almost double corrections to XP-Base rows, complicating the transition in a column. Hence, a transition over a diagonal is proposed for this configuration.

4. Physical model

This chapter provides a description of the physical models applied in the DMC wave flume in Gouda, The Netherlands. Among the topics are the characteristics and dimensions of the flume and roundhead, a description of the constructed models and an explanation of the production process of the scaled units.

4.1. Flume dimensions

The DMC wave flume located in Gouda, The Netherlands, has a length, width and height of 25, 0.6 and 1 meters respectively. The water depth is restricted to a maximum of approximately 0.7 meters, whereas the maximum wave height produced by the wave paddle is 0.3 meters. The length of the flume is subdivided into ten 2.5 meter sections. Due to the dimensions of the flume, the radius of the roundhead model is limited to 0.6 meters.

4.2. Test configuration

The design proposed in Chapter 3 is based on XblocPlus units of 2.5 m^3 volume. The volume is related to the nominal diameter through $D_n = \sqrt[3]{V}$, hence obtaining $D_n = 1.357 \text{ m}$. The scale applied to the physical model is based on the smallest available XblocPlus units at the DMC facility, which weigh 58.5 grams, have a density of 2.36 g/cm^3 and a nominal diameter of 2.91 cm. The corresponding scale is approximately 1:47.

4.2.1. Foreshore

Due to the limited dimensions of the flume, a foreshore is installed to ensure sufficient water depth in the deep water section to prevent depth-limited wave breaking at higher significant wave heights. The foreshore consists of panels, each 2.5 m long, which are placed on a 1:100 slope, consistent with Wiersma (2021) and De Raad (2021). Between the deep water section and the foreshore, a transition slope no steeper than 1:10 should be applied (Wolters et al., 2009). Furthermore, the distance between the wave paddle and the transition slope should be larger than 3 to 5 times the water depth, i.e. usually 3 to 5 meters. Correspondingly, the foreshore is constructed by a 2.5 m panel placed in approximately a 1:10 slope representing the transition slope, followed by four panels placed under a 1:100 slope. The transition slope transfers the height of the foreshore from 0 cm at the deep water section to 26.5 cm. Subsequently, the 1:100 slope adds an additional 10 cm to the bottom height at the roundhead. Additionally, to increase the deep water depth further, the structure is raised 10 cm with core material like proposed in De Raad (2021), see Figure 4.1. The raise is constructed level, with a height of 10 cm at the centre of the segment.

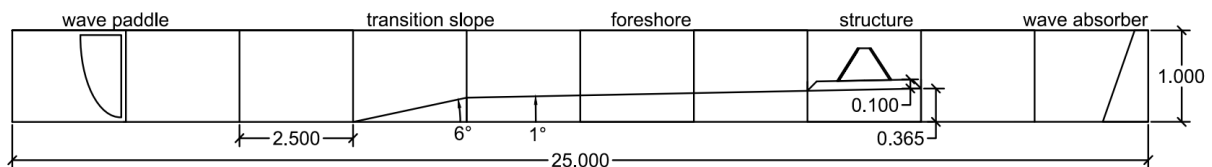


Figure 4.1. Flume cross-section, dimensions in meters and scale $x:y = 1:2$.

4.2.2. Armour layer

As aforementioned, the armour layer of the prototype consists of 2.5 m³ XblocPlus units, corresponding to a scaled nominal diameter of 2.91 cm. The XP-Base and XP-Curve units are geometrically scaled accordingly. The units are placed under a 3:4 slope, standard for XblocPlus (Xbloc, 2023). To achieve similitude, numerous criteria have to be fulfilled. Firstly, the flow hydrodynamics need to conform to the Froude criterion. Secondly, to check for dynamic similarity, Wolters et al. (2009) proposes the following condition:

$$Re_{model} = \frac{\sqrt{gH_s}D_n}{\nu} > 30,000 \quad (4.1)$$

The preceding criterion depends on the wave heights scheduled in the test programme and will be checked accordingly in Chapter 5.

4.2.3. Underlayer

The gradings in the underlayer are prescribed by the XblocPlus Design Guidelines (2023). The M_{50} of the underlayer should be 1/8th to 1/20th of the unit mass. For 2.5 m³ units, the minimum and maximum M_{50} are defined as 0.30 and 0.75 tonnes respectively. Applying the scale and assuming similar density as the units, this corresponds to a grading between 11 and 15 mm. The underlayer gradings available at the DMC facility range from 11 to 16 mm, i.e. $D_{50} \approx 13.5$ mm.

4.2.4. Core

Typically, quarry run is used for the core, which consists of the finer fractions of the quarry yield curve. According to Van den Bos and Verhagen (2017), quarry run has a wide ($1.5 < D_{85}/D_{15} < 2.5$) to very wide grading ($D_{85}/D_{15} > 2.5$). The use of large units in the core is allowed as little to no influence on the stability is found. However, Van den Bos and Verhagen (2017) propose a weight ratio between subsequent layers. The criterion applies to both the transition from the armour layer to the underlayer and from the underlayer to the core. The weight ratio is defined as 1/10th to 1/25th of the previous layer, corresponding to 1/2 to 1/3rd times D_{n50} . Hence, for the prototype underlayer described in Section 4.2.3, core gradings should range between 0.19 and 0.37 meters, i.e. 4 to 8 mm in the model.

Wolters et al. (2014) describes an additional criterion for core scaling, stating that an enlargement factor in relation to Froude scaling should be applied for $2 \text{ mm} < D_{n50,core,Froude} < 9 \text{ mm}$. For $D_{n50,Froude,model} > 4 - 9 \text{ mm}$, the following relationship holds for the enlargement factor:

$$\frac{D_{n50,core,corr}}{D_{n50,core,Froude}} = 1 \quad (4.2)$$

The criterion described by Wolters et al. (2014) relates to the Reynolds number in the filter, and defines that no enlargement of the core diameter is required in case $Re_f > 300$, corresponding to nominal diameters in the core of 7 mm or larger. To ensure this condition is fulfilled, the proposed grading applied in the core is 8 to 11 mm. The forementioned grading is available at the DMC facility in Gouda. The D_{50} of the grading is approximately 9.5 mm. Gradings of 8 to 11 mm were also applied in Wiersma (2021) and De Raad (2021), hence simplifying comparison.

4.2.5. Toe

Guidelines are provided for the design of the toe of XblocPlus breakwaters (Xbloc, 2023). The distinction is made between sandy and rocky seabed. For a sandy seabed, DMC makes the following recommendations: a rock filter layer or a geotextile with a small protective rock layer on top; a foundation layer underneath the first layer of XblocPlus, with typically a W_{50} of the unit divided by 30; a rock toe in front of the units. For a rocky seabed, no filter layers are

required and XblocPlus units are directly placed on the seabed with a rock toe in front. The minimum length of the toe is defined as three times unit D_n , while the height should span at least two times D_n .

When a foreshore representing a sandy seabed is assumed, $1/30^{\text{th}}$ of XblocPlus W_{50} should be applied as a foundation layer. The resulting nominal diameter ranges between gradings of the underlayer and core. However, stability of the toe is not in the scope of this research, so comprehensive design of the toe is neglected and its stability during tests is assured by applying larger than recommended gradings. The gradings are applied as bed protection for the 10 cm raise with an additional layer of D_n thickness and three times D_n length as toe, see Figure 4.2.



Figure 4.2. Toe structure applied in physical model.

4.2.6. Crown

Similar to the toe, the crown is not included in the scope of this research, so its stability during tests should be assured to prevent premature failure of crown units, as well as erosion to the core and underlayer. Hence, additional row(s) of XP-Base and XP-Curve, initially not planned in the design, are placed on top to increase the freeboard and provide more stability to the rows underneath. Additionally, larger gradings, i.e. $D_{n50} > 16 \text{ mm}$, are placed on the exposed underlayer at the crown to prevent wash out.

4.2.7. Roundhead dimensions

Both configurations described in Section 3.2 will be tested in the DMC wave flume. As the width of the flume is 600 mm, the maximum radius will be likewise. The physical models are devised based on the maximum radius and a slope of $H/V = 4/3$, a slope sufficiently steep for Xbloc and XblocPlus breakwaters to ensure effective interlocking of the armour units (Xbloc, 2023). The configurations differ slightly in height. However, as the slope and radii are equal, the same core and underlayer can be used. Hence, reconstruction between test series is limited to the

armour layer. The core consists of half a truncated cone with base width, top width and height of 1019 mm, 40 mm and 367 mm respectively, equating to a volume of 0.208 m³. The underlayer is placed on top of the core and consists of a 11 to 16 mm grading, i.e. $D_{50} = 13.5 \text{ mm}$ with $t = 2 D_{n50}$. The underlayer has a base and top width of 1109 and 59 mm respectively, i.e. 0.0604 m³. The underlayer provides support for the armour layer configurations. Table 4.1 describes the number of units required according to the designs to construct the physical roundhead model, whereas Figure 4.3 depicts the cross-section.

Table 4.1. Number of armour units required for physical roundhead model.

Unit	Design 1	Design 2	Cumulative
XblocPlus	164	0	164
XP-Base	120	208	208
XP-Curve (version 2)	0	201	201
XP-Curve (version 3)	121	0	121

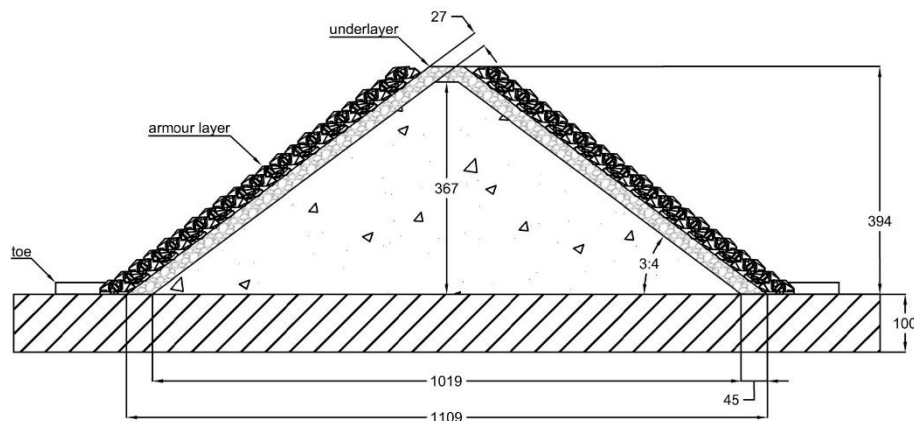


Figure 4.3. Roundhead cross-section, dimensions in millimetres.

4.2.8. Construction

To ensure successful construction of the roundhead model in the flume, a construction plan is defined. Furthermore, if several configurations are tested, a plan minimizes the discrepancies between the construction methods and improves reproducibility. The procedure is defined as follows:

1. The dimensions of the roundhead are drawn on the glass walls of the flume. This includes the section, as well as the elevation.
2. The core, underlayer and crown materials are thoroughly rinsed to prevent substances from significantly clouding the water in the flume.
3. Gradings of 8 to 11 mm are placed and compacted according to the predefined elevation and core dimensions. Subsequently, the underlayer is constructed of 11 to 16 mm grading. For both layers, a smooth and conical shape is achieved by the tool shown in Figure 4.4 and Figure 4.5. The tool consists of two 180° hinges connected to wooden slats sawn in 3:4 angles, enabling the disposal of any residual core and underlayer material.

4. Upon successful construction of the underlayer, the first row of armour units can be installed. The armour units are secured by the aforementioned toe structure.
5. The remaining armour layer is constructed based on the dimensions defined in Section 4.2.7.
6. Following completion of the armour layer, the remaining areas are filled in with underlayer gradings. Furthermore, the armour layer is secured on top using a chain. The chain is applied to secure the armour units at the transition with the glass. Ultimately, the crown is constructed as described in Section 4.2.6.

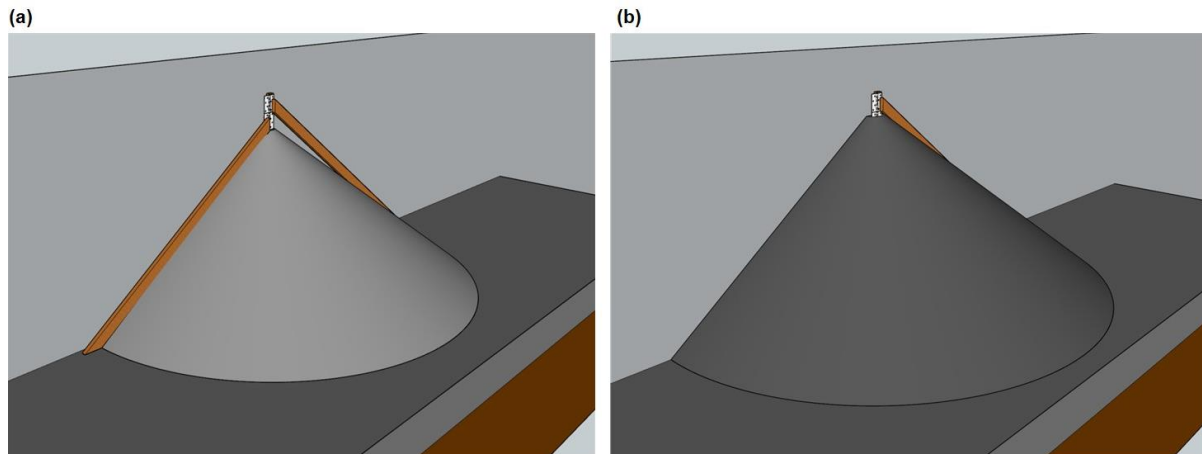


Figure 4.4. Tool to ensure a conical shape of (a) the core and (b) underlayer.



Figure 4.5. Tool to ensure a conical shape of the core applied in practice.

4.3. Models

The previous section described the test configuration, covering the flume setup, the dimensions and composition of the core and underlayer, and the construction method. This section outlines the different models constructed within this test configuration and will be referenced to for a description of the models in the remainder of this thesis.

4.3.1. Model 0

Initially, the armour units of Design 1 were placed following the specifications of the digital model described in Section 3.2. The predefined D_x was approximated by cutting out of wood the scaled radii from the model and marking the planned placement positions along the curve. However, the core and underlayer were built slightly too wide due to margins on the tool described in Section 4.2.8. With the number of units placed corresponding to the digital model, D_x increased (see Figure 4.6a) and hence A_s decreased, as a result reducing interlocking. This erroneous model is henceforth labelled Model 0 and is shown in Figure 4.7.

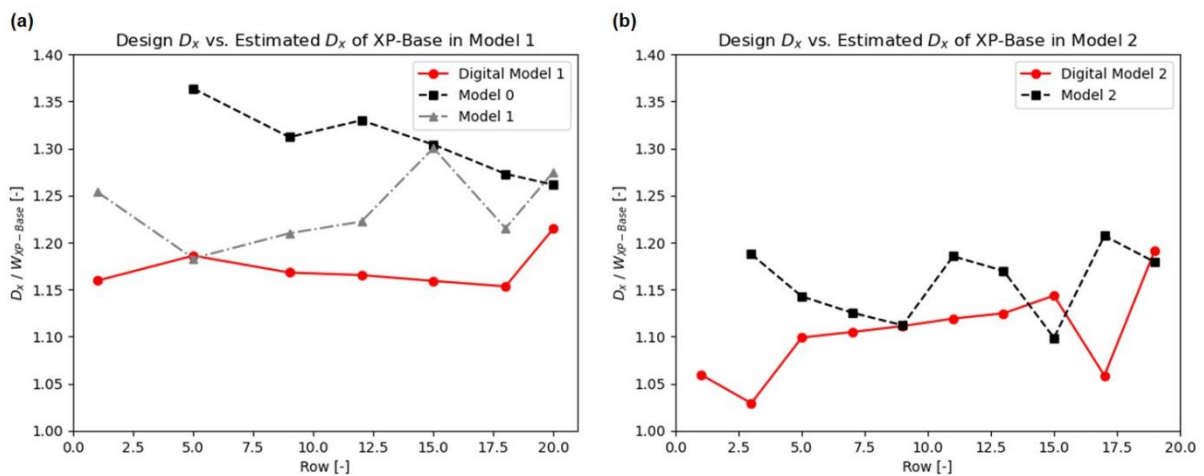


Figure 4.6. Comparison of design D_x and estimated D_x , for (a) Model 0, Model 1 and (b) Model 2.



Figure 4.7. Top view of Model 0.

4.3.2. Model 1

The D_x of all XP-Base rows, depicted in Figure 4.6, was estimated based on photo analysis and compared to the design D_x according to the digital model. Based on these findings, an additional XP-Base unit was included in every applicable row, subsequently adding an XblocPlus and XP-Curve to every row in the grid to better approximate the predefined D_x . An

exception was made in row 15, where an additional XP-Base unit would have obstructed placement of XblocPlus on top. The model better approximated the D_x values devised in the digital model. The packing density was estimated to range between 26.90 and 28.21 1/100 m² translated to 2.5 m³ prototype units, slightly lower than XblocPlus on a straight section. Design 1 was reconstructed accordingly for the remainder of the study, with the model termed Model 1, shown in Figure 4.8.



Figure 4.8. Top view of Model 1.

4.3.3. Model 2

The second design outlined in Section 3.2, termed Design 2, was constructed with the highest packing density achievable with manual placement to approximate the D_x devised in the digital model as closely as possible, see Figure 4.6b. On average, the measured D_x was slightly larger than initially planned in the digital model. Moreover, based on the wider core and underlayer dimensions, the estimated packing density ranged between 27.97 to 29.34 units of 2.5 m³ per 100 m² in the prototype. Model 2 is depicted in Figure 4.9.



Figure 4.9. Top view of Model 2.

4.3.4. Xbloc

Section 1.2 provides a description of the main research question along with the corresponding sub-questions. One of these sub-questions, question 2c, was stated as follows: “What are the limitations of testing in a 2D configuration?” The limitations, based on theoretical considerations, are previously described in Section 2.7. Additionally, to assess these limitations in practice, two methods will be applied, of which one is presented in this section.

In addition to the armour layer configurations outlined in Chapter 3, further reference tests involving Xbloc are scheduled. The tests could enable assessment of the influence of the test configuration, i.e. testing a three-dimensional structure in a 2D configuration, as stability of Xbloc on roundheads has been explored in various research and project contexts. The Xbloc size applied in the scaled physical model is determined by the design wave height (Section 5.1.1), the relative density (Section 4.4.5) and the stability number $N_s = 2.77$ (Xbloc, 2023). The Xbloc Design Guidelines (2023) prescribe several correction factors on the unit weight, depending on local phenomena. Firstly, for strongly curved sections and breakwater heads, Xbloc is designed with a factor of 1.25 compared to the unit size on the trunk. Secondly, for large water depths, a correction factor of 1.5 is applied when $h > 2.5 H_s$, accounting for a higher ratio between the highest wave heights in the spectrum and the significant wave height which can extend up to 1.8 – 2.0. This criterion will be checked in Section 6.4, after which the implications will be discussed in Chapter 7. Applying the aforementioned design parameters and the highest applicable correction factor, a theoretical unit weight is obtained for the physical model. The DMC facility in Gouda provides a range of scaled model units. The 59.3 to 62.4 gram classification approximates the theoretical unit weight best, resulting in an underestimated correction factor of 1.23 and obtaining a stability number of 2.54 for $H_{s,d}$. The model constructed with this classification is depicted in Figure 4.10. The next closest classification has an average unit weight of 74.6 g, corresponding to an overestimated correction factor of 1.65.



Figure 4.10. Top view of Xbloc model.

4.4. Armour units

4.4.1. Production process

The armour layer consists of scaled XblocPlus, XP-Base and XP-Curve units. XblocPlus has been tested multiple times at the DMC facility, so scaled units are readily available. The weight of 1:47 (with respect to 2.5 m³) XblocPlus units are calibrated at 58.5 grams with a density of 2360 kg/m³. XP-Base and XP-Curve are recent concepts which need to be newly produced. A production plan is devised to ensure similar properties for each scaled unit and type:

1. The designed blocks are produced of plastic with a three-dimensional printer.
2. To produce moulds, the blocks are placed upside-down in a wooden formwork and are pinned down using screws to prevent drifting. Subsequently, the remaining volume is filled with casting rubber.
3. The rubber mould hardens in approximately 8 hours, after which the wooden formwork is removed to obtain an empty mould.
4. The model units are produced by filling the moulds with a concrete mixture. The mixture consists of casting mortar and water, with the addition of baryta powder to increase the density. The baryta powder and water are added to 2.4 kg mortar in a ratio of 0.630 kg and 485 millilitres, respectively. After 24 hours, the blocks are demoulded and the surfaces polished. The units are distinguished through a different colour of paint for each type.
5. Ultimately, the dry and wet weight of the blocks is determined to establish the density. The target density is the density of the scaled XblocPlus units, i.e. 2360 kg/m³.

The production of moulds was limited by the amount of 3D printed units available, namely 12 XP-Base, 18 XP-Curve (version 2) and 18 XP-Curve (version 3). Production of units with mortar started as soon as the first moulds were completed. The mix ratio of the mortar was not precisely known beforehand, hence the first batch of units consisted of a density below 2.3 g/cm³, i.e. 2300 kg/m³. Aforementioned units were reserved separately to be applied on non-critical sections of the roundhead, for example XP-Base on the bottom row. Due to continuously altering conditions, for example temperature and humidity, the density can vary while applying the same ratios, similar to what is expected in the prototype. However, to ensure a representative density of the armour units, the density of the remaining armour units is approached statistically as described in the following sections. The density is measured through the difference between dry and submerged mass. The scale used to weigh the units has a resolution of 0.1 grams, limiting the data to three significant numbers. Ideally, the density is recorded for all produced units providing a distribution with maximum accuracy. However, due to time limitations, a sample size of 50 was chosen for each type of unit, distributed over the different production batches. The samples provide an approximated overview of the produced density and the ability of comparison to the target density of 2360 kg/m³.

4.4.2. XP-Base

Due to differing unit and mould shapes, as well as the quality of compacting, the density is variable within each batch of casted mortar. As aforementioned, the mass and density of the units is described statistically by its mean and standard deviation obtained from a sample with $n = 50$. The XP-Base units contain an average mass of 52.2 grams with a density of 2.38 g/cm³, sampled from a total of 218 units.

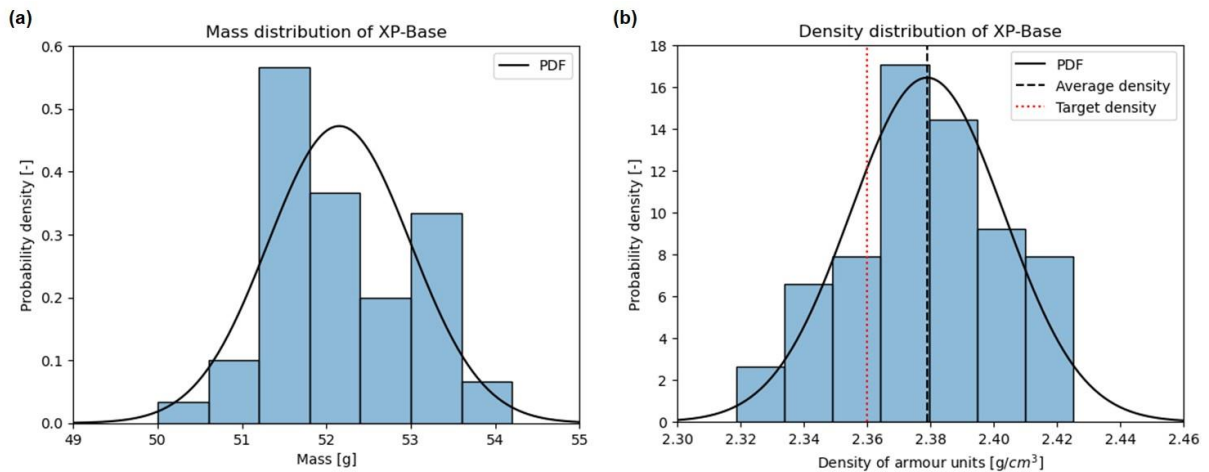


Figure 4.11. Mass (a) and density (b) distributions of XP-Base sample.

4.4.3. XP-Curve (version 2)

The production of XP-Curve (version 2) required a total of 201 units for Model 2, which amounted to 206 due to batch sizes. The sampled units have an average mass of 57.0 grams with a 2.38 g/cm³ density. The distributions are shown in Figure 4.12.

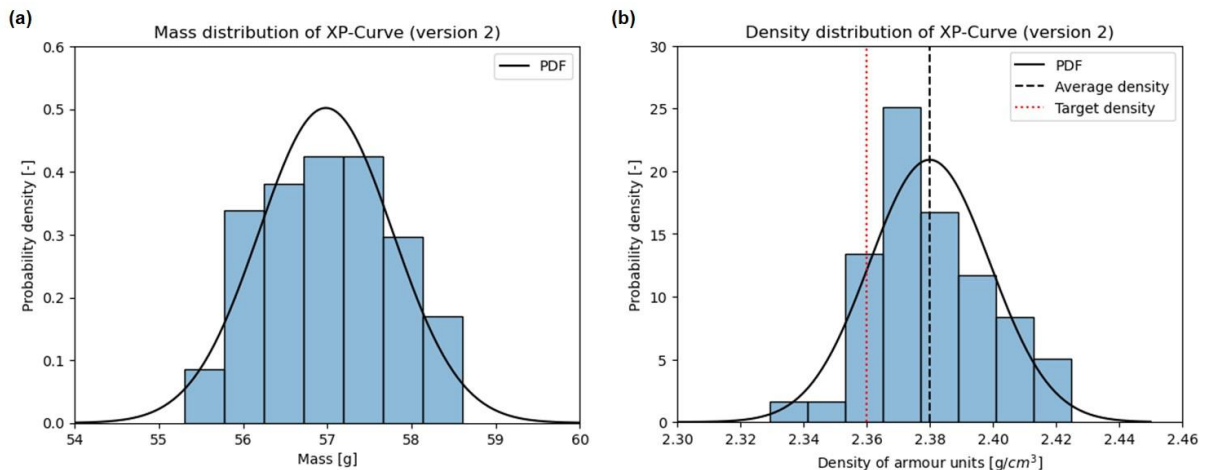


Figure 4.12. Mass (a) and density (b) distributions of XP-Curve (version 2) sample.

4.4.4. XP-Curve (version 3)

The mass and density of the third version XP-Curve is obtained from 50 samples out of 125 units. The average mass amounts to 53.9 grams with a density of 2.37 g/cm³, see Figure 4.13.

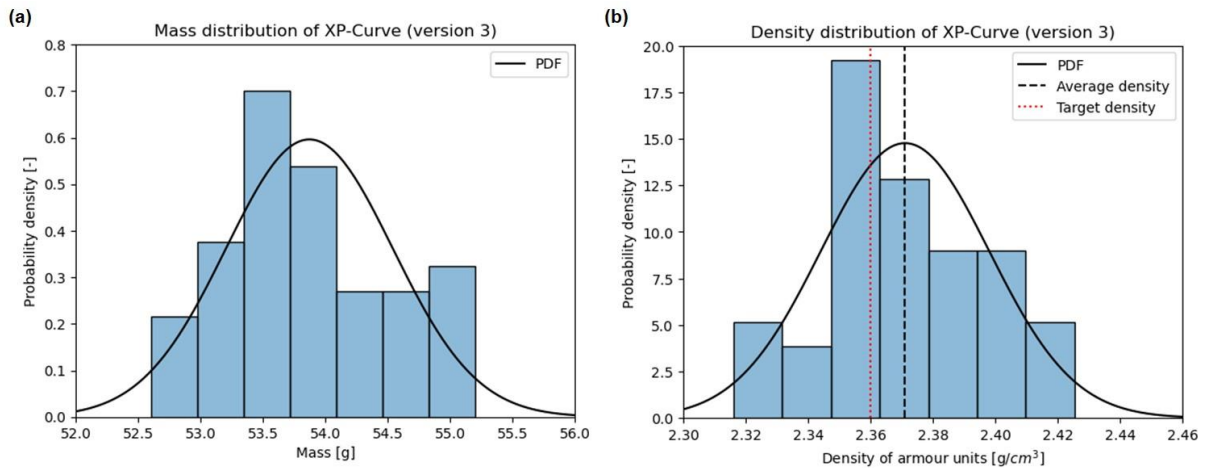


Figure 4.13. Mass (a) and density (b) distributions of XP-Curve (version 3) sample.

For the production of the units, the target density was equal to the density of the calibrated XblocPlus units, i.e. 2360 kg/m^3 . However, due to conditions previously mentioned, there is discrepancy between the target and obtained density, similar to what is expected in the prototype. However, to ensure a representative density, the differences are assessed. The difference in average is limited to 20 kg/m^3 , see Figure 4.14. The discrepancy corresponds to a change in stability number of 0.03, or alternatively 0.14 cm in H_s in the model and 6.53 cm in the prototype. However, the density is an influencing factor on the results and will be considered accordingly in Section 7.2.6.

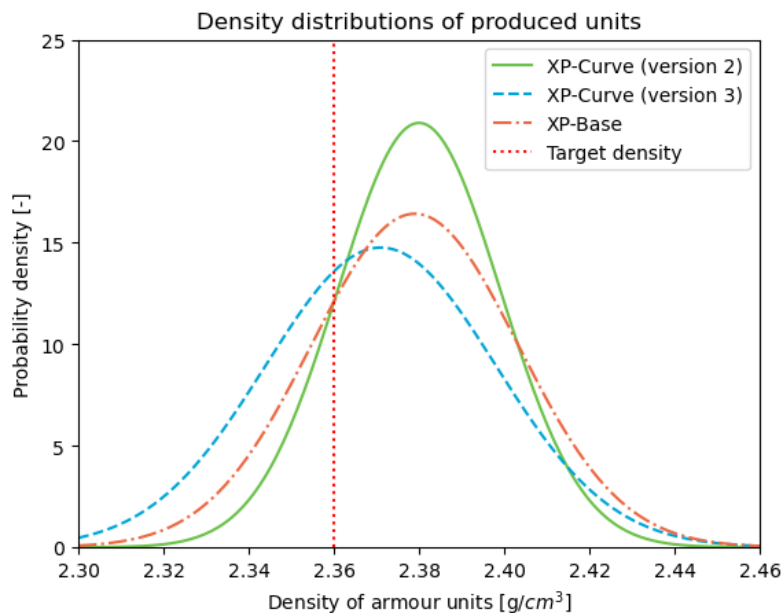


Figure 4.14. Density distributions of produced units, obtained from 50 samples per unit type.

4.4.5. Xbloc

As aforementioned in Section 4.3.4, DMC offers Xbloc model units within a range of unit weights. According to DMC (n.d.), 670 units are available of the 59.3 gram classification with an average density of $2,349 \text{ kg/m}^3$ and a 4.23 cm unit height. Similarly, 350 units are accessible with 62.4 gram unit weight, a $2,301 \text{ kg/m}^3$ average density and a unit height of 4.33 cm. However, the described classifications were mixed in storage at the DMC facility. Therefore, the model is constructed with units sampled from both distributions. Additionally, there is a

spread in weight and density due to repeated use and colouring of the units. Hence, a sample is taken of the units applied in the physical model to estimate the weight and density. Due to time limitations, only a restricted sample of 20 units was taken. The units averaged a weight of 59.28 grams with a density of 2,323 kg/m³. The thickness of the armour layer is calculated as $\sqrt[3]{3V} = 4.25 \text{ cm}$. The nominal diameter is defined as 2.94 cm.

5. Test programme

This chapter describes the test protocol to which the physical models are subjected, including the wave heights and steepness, water levels, measurement equipment and test procedure.

5.1. Waves

5.1.1. Wave height

The waves in the DMC wave flume are generated using the Wave Synthesizer software. This programme is able to produce waves based on a JONSWAP spectrum (see appendix A). The input parameters of the JONSWAP spectrum are the significant wave height and peak period. The height is determined based on the stability number desired for XblocPlus, $N_s = 2.5$. Using the scaled nominal diameter and density, the wave height is obtained as follows:

$$H_s = N_s \Delta D_n = 2.5 * \frac{2360-1000}{1000} * 2.91 = 9.9 \text{ cm} \quad (5.1)$$

The design significant wave height ($H_{s,d}$), which for a JONSWAP spectrum is approximately equal to H_{m0} , is used as a target value for stability. To assess the stability and damage development, the physical models are subjected to tests with ranging percentages of design H_{m0} . For randomly placed armour units, i.e. Xbloc in this study, generally lower percentages (0.6 $H_{s,d}$) are used for the initial wave height to allow for settlements in the layer to occur. However, Bakker et al. (2019) observed no significant settlements in the XblocPlus layer if the rock toe is stable. Nevertheless, to still accommodate possible settlements in the underlayer, 80% of $H_{s,d}$ is proposed in this research as initial wave height for the XblocPlus armour layers. The proposed upper limit is 140% due to limitations regarding the water depth in the wave flume. To ensure an accurate representation of the JONSWAP spectrum and obtain statistically reliable results, test durations should encompass approximately 1,000 waves, corresponding to a prototype storm with durations ranging from 3 to 6 hours, as suggested by Wolters et al. (2009).

The defined wave heights, as mentioned in Section 4.2.2, should oblige by the criterion formulated by Wolters et al. (2009) to achieve turbulent flow conditions throughout the primary armour layer. For a nominal diameter of 2.91 cm and a design wave height of 9.9 cm, the criterion accords to $Re_{model} = 28,677$, which approximates the boundary value. Furthermore, the structure is expected to show deformations and failure at higher percentages of the design wave height, hence turbulent flow conditions are likely to exist throughout the primary armour layer.

5.1.2. Wave steepness

The wave steepness is defined as the ratio between the wave height and length, expressed in fractions or percentages. According to the EurOtop Manual (2007), wave steepness of 1% to 2% indicates a typical swell sea while steepness of 4% to 6% implies a typical wind sea. Following Mutray and Reedijk (2012), Ruwiel (2020) proposes the application of wave steepness $s_{0,p} = 0.02$ as this would cause more intense failure compared to $s_{0,p} = 0.04$. Furthermore, it is associated with wave theory regarding the lift and drag forces. De Raad (2021) executed tests with $s_{0,p} = 0.02$ and $s_{0,p} = 0.04$ and confirmed that a deep water wave steepness of 2% was normative for the stability of XP-Curve. However, differences in wave steepness can trigger different failure mechanisms, depending on the type of armour unit. To ensure establishment of the normative failure criteria for the newly developed XblocPlus

armour layer configurations, tests with 4% deep water wave steepness are also employed in this research. However, due to time limitations in the wave flume availability, the Xbloc model described in Section 4.3.4 is tested solely with $s_{0,p} = 0.02$ as it is expected to be normative based on the results of Muttray and Reedijk (2012). Hence, Table 5.1 and Table 5.2 can be defined, with addition of local wavelength and steepness at the toe derived from the water levels described in Section 5.2. Note, the wave steepness at the toe can be expressed as $s_{toe,p} = H_{m0}/L_{toe,p}$ using the actual wavelength or as $s_{0,p} = H_{m0}/L_{0,p}$, calculated with the deep water wavelength using the wave period at the toe of the structure (Pullen et al., 2007).

Table 5.1. Wave parameters for 2% wave steepness.

Wave parameter	0.8 H_{m0}	1.0 H_{m0}	1.1 H_{m0}	1.2 H_{m0}	1.3 H_{m0}	1.4 H_{m0}	
H_{m0} [cm]	7.92	9.90	10.89	11.88	12.87	13.86	
T_p [s]	1.59	1.78	1.87	1.95	2.03	2.11	
$L_{0,p}$ [m]	3.96	4.95	5.45	5.94	6.44	6.93	
$h_{toe} = 33.5$ cm	$L_{toe,p}$ [m]	2.63	3.00	3.17	3.33	3.48	3.63
	$s_{toe,p}$ [-]	0.030	0.033	0.034	0.036	0.037	0.038
$h_{toe} = 38.5$ cm	$L_{toe,p}$ [m]	2.78	3.18	3.36	3.53	3.70	3.86
	$s_{toe,p}$ [-]	0.028	0.031	0.032	0.034	0.035	0.036

Table 5.2. Wave parameters for 4% wave steepness.

Wave parameter	0.8 H_{m0}	1.0 H_{m0}	1.1 H_{m0}	1.2 H_{m0}	1.3 H_{m0}	1.4 H_{m0}	
H_{m0} [cm]	7.92	9.90	10.89	11.88	12.87	13.86	
T_p [s]	1.13	1.26	1.32	1.38	1.44	1.49	
$L_{0,p}$ [m]	1.98	2.48	2.72	2.97	3.22	3.47	
$h_{toe} = 33.5$ cm	$L_{toe,p}$ [m]	1.68	1.96	2.08	2.20	2.32	2.43
	$s_{toe,p}$ [-]	0.047	0.051	0.052	0.054	0.055	0.057
$h_{toe} = 38.5$ cm	$L_{toe,p}$ [m]	1.75	2.05	2.18	2.32	2.44	2.56
	$s_{toe,p}$ [-]	0.045	0.048	0.050	0.051	0.053	0.054

Table 5.1 and Table 5.2 serve as input for the aforementioned Wave Synthesizer software. The input parameters are the deep water level, H_s and T_p to generate a JONSWAP spectrum and additionally a multiplication factor to compensate for the difference between the perceived wave production of the wave paddle and the measured production. The input parameters are calibrated to approximate the predefined wave conditions at the structure. The software operates with four decimal values, which is unreasonably accurate with respect to the wave paddle production. Therefore, the accuracy of the input is lowered to two decimals.

5.1.3. JONSWAP spectrum

As aforementioned, the wave height and length are related through the wave steepness. Furthermore, the wave length is correlated with the wave period through the dispersion relation, see Appendix A. As the JONSWAP spectrum describes the wave height in deep waters, the period can be assumed independent of the depth. The wave period obtained from the significant wave height is T_s or $T_{1/3}$, which, according to the EurOtop Manual (2007), is approximately identical to the peak period T_p . The significant wave height calculated in Section 5.1 is used in combination with the wave steepness to obtain the JONSWAP spectrum. Figure 5.1 illustrates the JONSWAP spectrum for both $s_{0,p} = 0.02$ and $s_{0,p} = 0.04$.

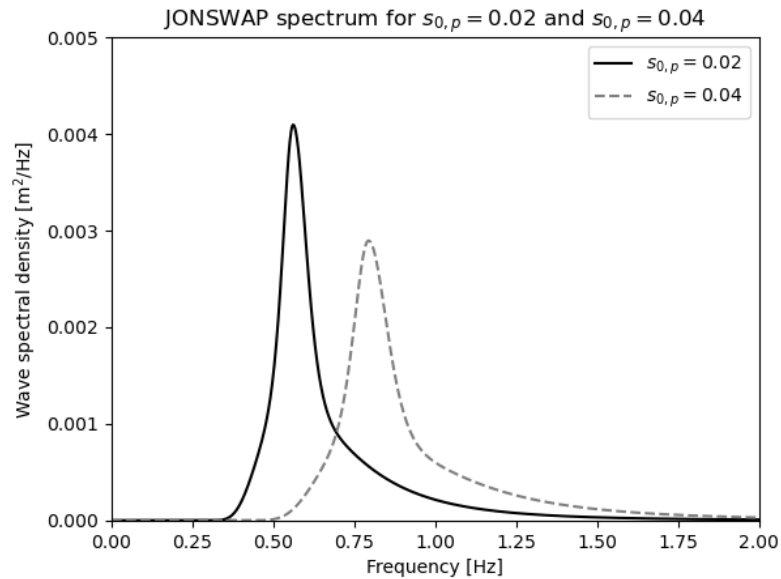


Figure 5.1. JONSWAP spectrum.

5.2. Water depth

Several criteria are posed for the water depth in the wave flume. Firstly, Wolters et al. (2009) prescribes a minimum deep water depth of $h/H_s > 3$. The maximum wave height planned for the tests is 140% of $H_{s,d}$, which corresponds to 13.86 cm. Hence, the deep water depth should exceed 41.58 cm. Secondly, Holthuijsen (2007) poses a minimum water depth at the toe of $H_{s,max}/0.45$, equal to 33.00 cm. Moreover, Janssen (2018) states that top row XblocPlus units show high stability for relative freeboard ($R_c/H_{s,d}$) values above 1.0.

To prevent depth limited wave breaking in the flume, Wiersma (2021) and De Raad (2021) applied a water depth of 67.5 cm in the deep water section. With the foreshore described in Section 4.2.1, this amounts to a water depth of 33.5 cm at the toe of the structure, hence satisfying the aforementioned condition. Furthermore, with the significant wave heights described in Sections 5.1.1 and 5.1.2, the relative freeboard criterion posed by Janssen (2018) is satisfied for all models. Hence, to simplify comparison between previous research, a deep water depth of 67.5 cm is applied in this research, with $h_{toe} = 33.5$ cm. The water depth will be assessed at the toe before every test series. Due to possible inconsistencies in gauging location of the water depth compared to Wiersma (2021) and De Raad (2021), discrepancies may arise in the measured values. An overview of the physical roundhead models of Design 1 and Design 2 with the defined water level is shown in Figure 5.2 and Figure 5.3.

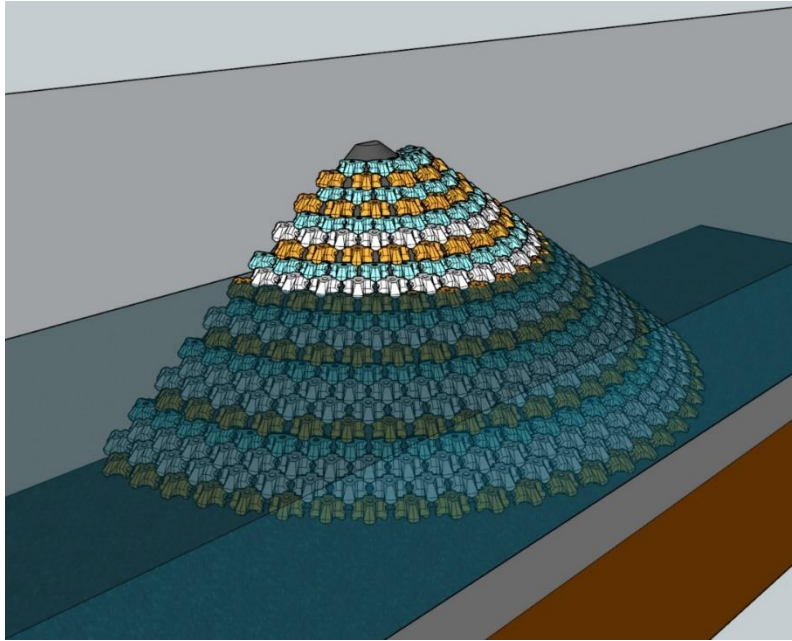


Figure 5.2. Roundhead model of XblocPlus, XP-Base and XP-Curve (version 3) with h_{toe} of 33.5 cm.

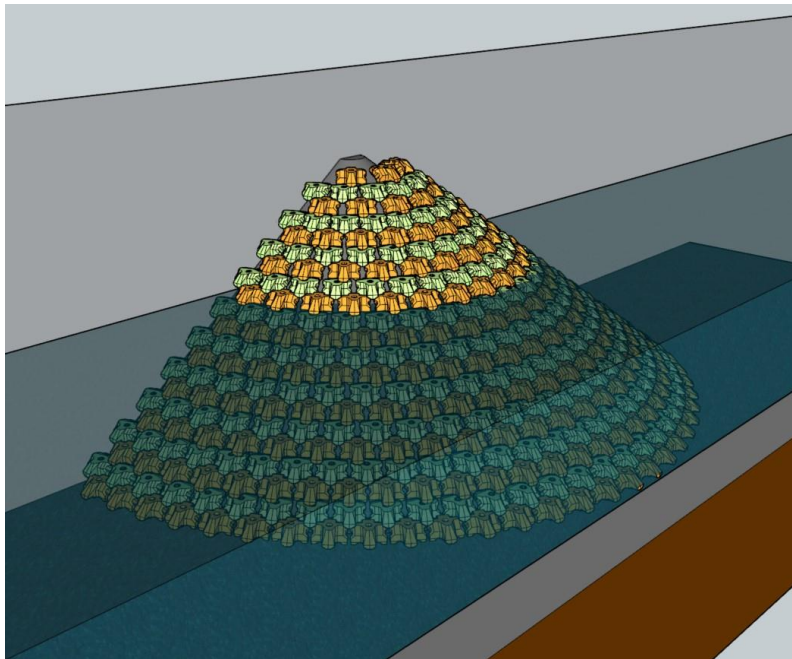


Figure 5.3. Roundhead model of XP-Base and XP-Curve (version 2) with h_{toe} of 33.5 cm.

Because the structure devised according to the design in this thesis allows higher construction height than Wiersma (2021) and De Raad (2021), a higher freeboard is achieved at the aforementioned water depth. Hence, additional test series are planned with 5 cm added water depth. The goal is to examine stability of units on higher rows as stability is expected to be lower due to higher differences in rotations around the z-axis between consecutive units. The relative freeboard with respect to design H_s is decreased to a value of approximately 1.0, at which, according to Janssen (2018), the crest units should still provide sufficient stability. Furthermore, no correction factors on unit weight are required for Xbloc or XblocPlus for relative freeboard values above 1.0 (Xbloc, 2023). Additionally, DMC defines a minimum radius criterion at design water level for a breakwater head section with Xbloc armour, equal to $R > 2.5 H_s$. Alternatively, if larger armour units are applied than based on the correction factor of

1.25, the lower limit of the radius is defined by six times the characteristic height (D) of the Xbloc size. Due to the underestimated correction factor on unit weight (1.23) for the units defined in Section 4.3.4, the criterion amounts to $R > 2.5 * 9.9 = 24.8 \text{ cm}$, which is approximately equal to the radius of the model at $h_{toe} = 38.5 \text{ cm}$. The positioning of the increased water level on the XblocPlus configurations is shown in Figure 5.4 and Figure 5.5.

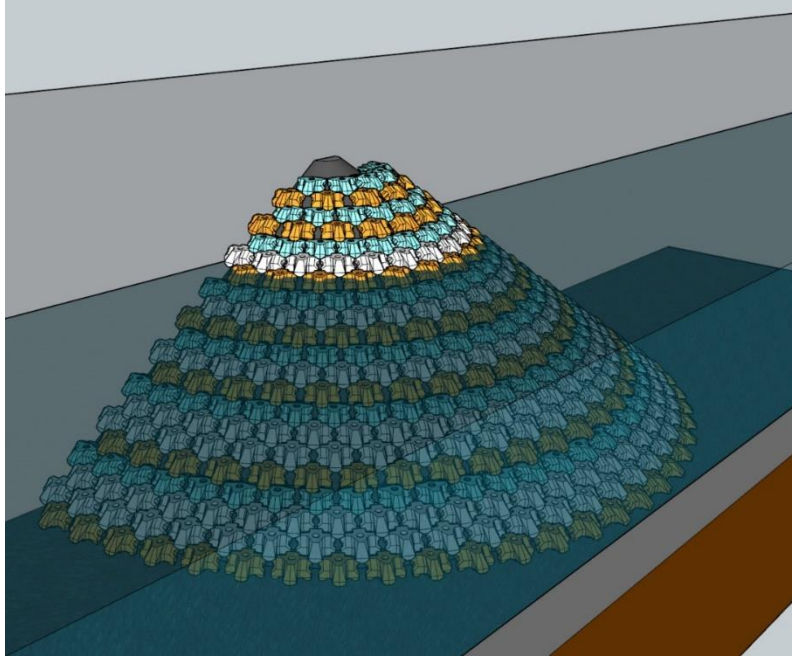


Figure 5.4. Roundhead model of XblocPlus, XP-Base and XP-Curve (version 3) with h_{toe} of 38.5 cm.

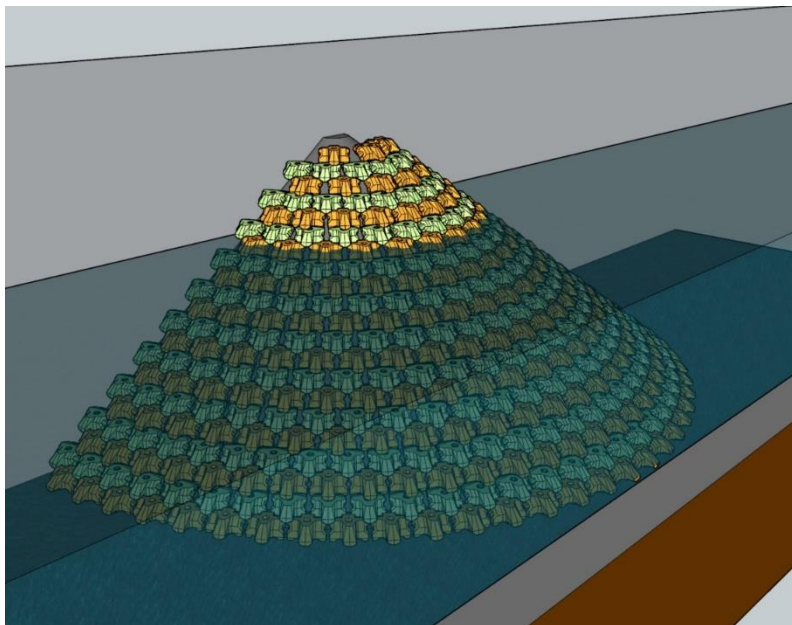


Figure 5.5. Roundhead model of XP-Base and XP-Curve (version 2) with h_{toe} of 38.5 cm.

5.3. Measurement equipment

5.3.1. Wave gauges

During the tests, wave gauges measure the surface elevation in the flume. The DMC facility provides connections for eight gauge rods which measure surface elevation at a frequency of 128 Hz. To measure wave reflection, the three-point method proposed by Mansard and Funke (1980) is applied. The first and second rod are separated by 0.3 meters, while the second and third rod are offset 0.4 meters. The gauges are installed at locations in the flume with different characteristics. Firstly, a single gauge rod is situated at the deep water section of the flume between wave paddle and transition slope, which is defined by 3 to 5 times the water depth (Wolters et al., 2009). For a deep water depth of 67.5 cm, this region is defined by 202.5 to 337.5 cm from the wave paddle. Due to the gauge consisting of only one rod, no reflection can be measured. However, the gauge is able to monitor the water elevation. An additional single gauge rod is positioned between the transition slope and the structure for a similar purpose. Secondly, two sets of three gauge rods are installed in parallel in front of the structure to measure wave reflection on the roundhead. The rods are evenly separated along the width of the flume by 0.2 meters. Regarding the distance to the structure, Wolters et al. (2009) proposes at least 0.4 times the peak wave length L_p , while Goda alternatively suggests 1.5 times the local wave length. The criterion posed by Wolters et al. (2009) results in a distance of approximately 2 meters for $s_{0,p} = 0.02$ and 1 meter for $s_{0,p} = 0.04$, see Figure 5.6 and Figure 5.7.

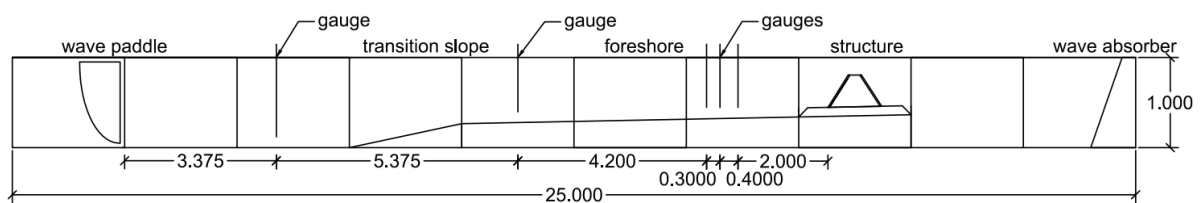


Figure 5.6. Gauge positioning in flume cross-section, dimensions in meters and scale $x:y = 1:2$.

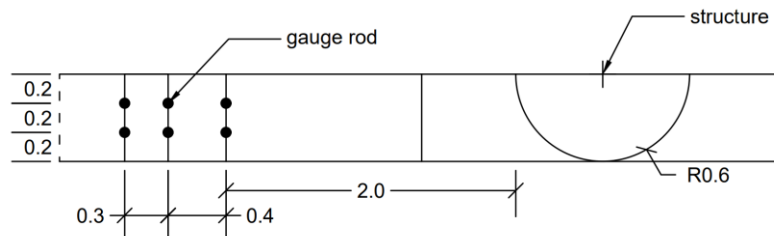


Figure 5.7. Top view of gauge positioning in front of structure, dimensions in meters.

During installation of the test configuration it was noted that one connection of the wave rods was defect, hence only seven remaining intact. The decision was made to remove the planned wave rod between the deep water section and the structure, which was deemed least decisive for this research.

5.3.2. Cameras

Photos are taken before every test run to record the initial state of the structure. Subsequently, photos are taken after the test run to assess the occurred settlements and damage. However, not all unit displacements can be observed in static pictures, so cameras are installed to record the structure during the tests. Furthermore, failure mechanisms can possibly be distinguished from recordings. As described in Section 2.1.3, failure is likely to occur at the leeward side of the breakwater. Hence, a camera is mounted above this section of the structure, providing a top view recording. Additionally, two cameras are positioned to observe the front of the structure and potentially identify currents between the roundhead and the flume wall by peering through the glass. The cameras are placed in opposing angles towards the flume, one above

and one below the waterline to minimize disturbances due to wave impact, see Figure 5.8. All cameras operate at a resolution of 1080p and a rate of 48 frames per second.

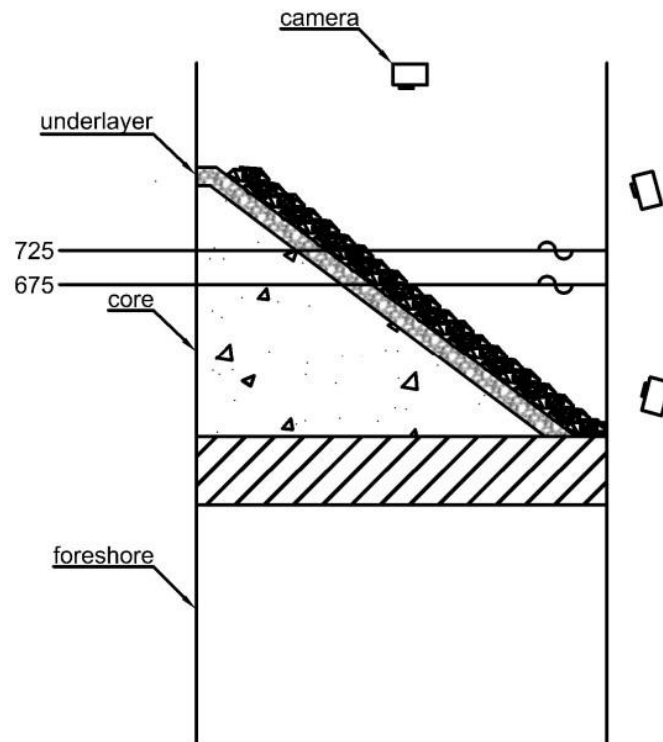


Figure 5.8. Camera positioning in flume cross-section, dimensions in millimetres.

5.4. Damage description

As described in Section 2.6, different qualitative definitions of damage can be used. Gómez-Martin (2015) defines three states of damage, namely 'Initiation of Damage' (IDa), 'Initiation of Destruction' (IDe) and 'Destruction' (De). 'Initiation of Damage' is defined at removal or displacement of some isolated units, whereas 'Initiation of Destruction' expresses the removal of several adjacent units. Similarly, Bakker et al. (2019) distinguishes between 'no damage', 'start of damage', 'damage, no failure' and 'failure'. In this research, definitions similar to the terminology of Gómez-Martin (2015) and Bakker et al. (2019) will be utilized. However, the criteria of the states are amended to the specific designs tested.

The following damage mechanisms are defined by Ten Oever (2017) and Van der Lee (2020) for Xbloc and XblocPlus units on the trunk respectively, with uplift added in this study:

- Rocking, which is characterized by repeated movement of an individual unit and is observed by visual observations. A unit is marked as damaged or failed by rocking if the repeated movement occurs at more than 2% of the waves. For prototype XblocPlus units smaller than 10 m³, rocking is accepted for less than 2% of the total units in design conditions. Furthermore, during overload conditions, defined as 120% of design condition, acceptable rocking is limited to 4%. Below $H_{s,d}$, rocking of less than 1% of the units is deemed acceptable. Failure of a unit due to rocking is termed N_{or} .

- Displacement, defined as dislodgement of a unit from the grid. In this research, due to the unit orientations and rotations around the z-axis on the roundhead, displacement is further subdivided into displacement or rotation and uplift. Damage of the former classification will be quantified by $N_{o,rd}$, i.e. failure due to rotation or displacement.
- Uplift, which, following the results of De Raad (2021), is distinguished in this research as an additional displacement mechanism. Uplift forces on the armour units are caused by the inability of the phreatic surface in the structure to follow the instantaneous water level outside the structure (Vos, 2017). The porosity and permeability of the armour layer are major governing variables for the magnitude of uplift. Damage to the armour layer originating from uplift is termed $N_{o,up}$. The cumulative number of displaced or extracted units is labelled N_{od} , i.e. $N_{od} = N_{o,rd} + N_{o,up}$. Similarly, the cumulative number of moving units is described by $N_{o,mov} = N_{od} + N_{or}$.
- Settlement, a less quantifiable damage mechanism which describes the general compaction of the armour layer, after which a higher packing density is obtained on the slope and a lower packing density towards the crest. The mechanism can be assessed by comparing photos taken from a fixed point before and after the test run.
- Sliding, which describes the downward movement of (part of) the XblocPlus matrix along the slope. However, due to the overdesigned toe structure described in Section 4.2.5, sliding is unlikely.

The aforementioned description of damage mechanisms is utilized to mark the state of individual units as 'failed'. Note, roundhead structures are regularly tested in three-dimensional basins, where rocking is unobservable due to the large viewing distance. Therefore, acceptable rocking criteria are not defined for roundheads. For the result analysis, the assumption is made that the aforementioned conditions also apply to roundheads. Due to the geometry of the roundhead, simultaneous assessment of rocking along the entire structure is impractical. Hence, rocking is solely evaluated in the area of most severe impact depicted in Figure 5.9. The percentage of rocking units will be expressed accordingly.

To assess the state of the armour layer, qualitative descriptions similar to Bakker et al. (2019) are used. Besides stability, resilience and redundancy of the design after damage are evaluated. Hence, criteria are posed to distinguish between the states of damage and assess the remaining strength after failure of a predefined number of units, see Table 5.3. In this study, 'start of damage' is defined as significant loss of one of the contact surfaces depicted in Figure 3.2 due to displacement or rotation of the unit. The state of the armour layer is categorized as 'damage, no failure' if more than one and less than four units have failed. Failure of the armour layer is defined as failure of more than four individual armour units. The descriptions are distinguished by a damage level number to indicate the state of the armour layer in the damage development graphs in Chapter 6.

Table 5.3. Damage descriptions for qualitative analysis of armour layer state.

Damage level	Damage description	Criterion
1	No damage	$N_{o,mov} = 0$
2	Start of damage	$0 < N_{o,mov} \leq 1$
3	Damage, no failure	$1 < N_{o,mov} \leq 4$
4	Failure	$N_{o,mov} > 4$

The damage description method summarized in Table 5.3 qualitatively defines the state of the armour layer while quantifying the absolute number of units failed per failure mechanism.

However, the severity of damage can also be assessed per reference area on the roundhead. Hence, the roundhead is subdivided into two quarter circles, of which the area of most severe impact described in Section 2.1.3 is further divided into four segments. The segments are comprised of 22.5 degrees each and contain approximately an equal number of units, see Figure 5.9. Therefore, damage to the XblocPlus related armour layers can be expressed as failure of individual units divided by the total number of units in the corresponding segment, enabling assessment of the most impacted regions and obtaining $D_{\%}$ as proposed by USACE (1984). Additionally, the segments enable translation of the location of failed units on the roundhead to a two-dimensional visualization. The damage quantification $D_{\%}$ will not be applied to the Xbloc model described in Section 4.3.4 as larger settlements of the armour layer are expected to distort the predefined segments. Additionally, the units are not regularly distinguished through colours so clear distinction between different units is unfeasible.

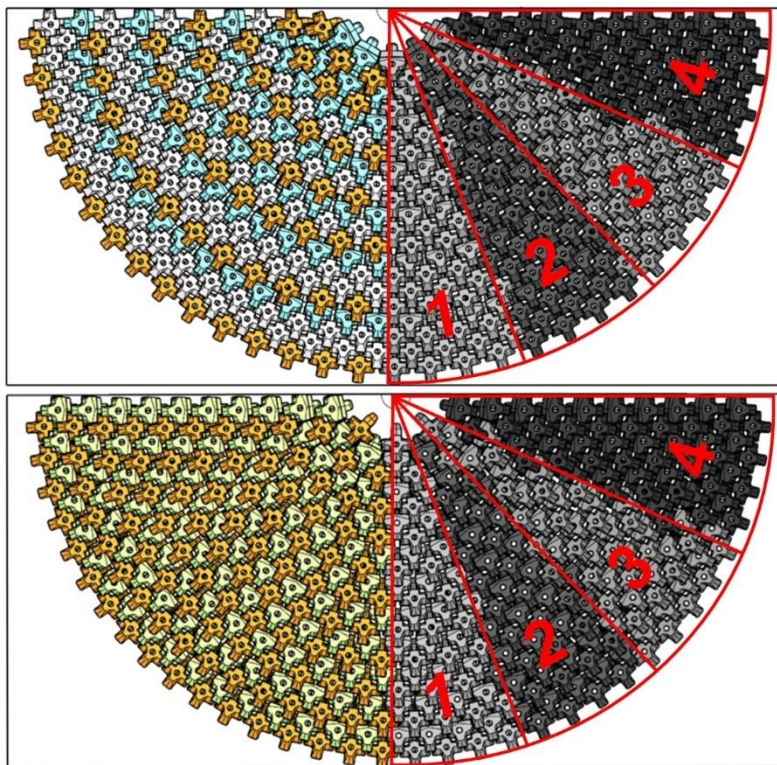


Figure 5.9. Division of roundhead segments for damage assessment of Design 1 (upper) and Design 2 (lower).

5.5. Test procedure

To be able to compare different series of tests, a test procedure is defined, describing the steps followed in each series. The procedure is as follows:

1. The roundhead model is (re)build following the procedure described in Section 4.2.8.
2. The flume is filled with water to the predefined water depth which is gauged at the toe.
3. Photos are made of the roundhead before each test run, specifically of the zone of most severe attack defined in Section 2.1.3.
4. Start of the test run. Recording by cameras is initiated.

5. The test is stopped after at least 1,000 waves are generated, after which photos are made of the result.
6. After test execution, the data of the generated waves is analysed to ensure representative values with respect to the scheduled wave heights.
7. Steps 3 to 6 are repeated throughout the test series until the damage limit is reached or the series is finished.

To prevent unnecessary reconstructions of the armour layer, the test series are scheduled favouring the expected least critical conditions. Additionally, due to production times of the units, Model 0, formerly described in Section 4.3.1, is tested first as less new units are required. The test schedule includes repetition tests of Model 1 (Figure 4.8) for incentives which will be described in Chapter 6. Additionally, repetition tests enable the assessment of reproducibility. The test schedule is summarized in Table 5.4.

Table 5.4. Test schedule.

Series	Model	Armour units	Model description	h_{toe} [cm]	$s_{0,p}$ [-]
0.1	0	XblocPlus XP-Base XP-Curve (version 3)	Section 4.3.1 Figure 4.7	33.5	0.04
1.1				33.5	0.04
1.2.1				33.5	0.02
1.2.2	1	XblocPlus XP-Base	Section 4.3.2 Figure 4.8	33.5	0.02
1.3		XP-Curve (version 3)		38.5	0.04
1.4.1				38.5	0.02
1.4.2				38.5	0.02
2.1				33.5	0.04
2.2	2	XP-Base	Section 4.3.3	33.5	0.02
2.3		XP-Curve (version 2)	Figure 4.9	38.5	0.04
2.4				38.5	0.02
3.1	Xbloc	Xbloc	Section 4.3.4	33.5	0.02
3.2			Figure 4.10	38.5	0.02

6. Results

This chapter presents the findings obtained from the physical model testing conducted to investigate the performance of various configurations of Xbloc and XblocPlus related armour units. A summary of the executed test programme is depicted in Table 5.4 and described in the following section.

Following the test schedule outlined in Table 5.4, Model 0 was tested first due to the lower number of required armour units. As formerly described in Section 4.3.1, the armour units were placed following the specifications of the digital model of Design 1, described in Section 3.2. The predefined D_x was approximated by cutting out of wood the scaled radii from the model and marking the planned placement positions along the curve. However, the core and underlayer were built slightly too wide due to margins on the tool described in Section 4.2.8. With the number of units placed corresponding to the digital model, D_x increased and hence A_s decreased, as a result reducing interlocking. During the first test series, conducted with $h_{toe} = 33.5 \text{ cm}$ and $s_{0,p} = 0.04$, several units failed at $N_s = 2.81$, categorized as 'damage, no failure'. The test continued until $N_s = 3.28$, where failure occurred according to the description defined in Section 5.4. Subsequent measurements revealed that D_x exceeded the design parameters. Therefore, Design 1 was reconstructed. This involved the addition of one XP-Base unit to every applicable row, subsequently adding an XblocPlus and XP-Curve unit to every row in the grid. An exception was made in row 15, where an additional XP-Base unit would have obstructed placement of XblocPlus on top. Design 1 was reconstructed accordingly for the remainder of the test programme, with the renewed model being termed Model 1 (see Figure 4.8). The estimated packing density of the newly built Model 1 ranged between 26.90 and 28.21 1/100 m² translated to the 2.5 m³ prototype units, which is slightly lower than XblocPlus on a straight section. Additionally, the D_x of all XP-Base rows was estimated based on photo analysis and compared to the design D_x according to the digital model, previously illustrated in Figure 4.6a. The D_x in Model 0 was significantly larger than D_x in Model 1. However, the units in the digital model were packed closer together than both models.

Following the reconstruction of Design 1, the test programme was repeated for a configuration of $h_{toe} = 33.5 \text{ cm}$ and $s_{0,p} = 0.04$. No damage was observed in Series 1.1. Subsequent Series 1.2 subjected the structure to longer waves of 2% steepness. However, challenges arose due to an input error in the Wave Synthesizer software. Waves exceeding 130% $H_{s,d}$ were unreasonably large with a measured H_{m0} of 15.97 cm. The structure failed due to large magnitudes of uplift and the test run was deemed erratic. Hence, the armour layer was reconstructed and subsequently Series 1.2 was repeated, with failure occurring at 120% $H_{s,d}$. Similar errors affected Series 1.4. Thereafter, the error was identified and corrected. The remainder of the test programme followed the predefined schedule, with no further repetition tests conducted.

Preliminary results of Series 1 indicated limitations in the interlocking capabilities of XP-Base for relatively large D_x values. Consequently, the decision was made to increase the packing density with respect to the model to the achievable maximum. Based on the wider core and underlayer dimensions, the estimated packing density ranged from 27.97 to 29.34 units of 2.5 m³ per 100 m² in the prototype. Additionally, the estimated D_x is depicted in Figure 4.6b. On average, the measured D_x is slightly larger than initially planned in the digital model.

A third configuration involved testing a roundhead with an Xbloc armour layer, previously described in Section 4.3.4, subjected to longer waves with $s_{0,p} = 0.02$ at both low and high water levels. As Xbloc is regularly placed with a random orientation, the placement of the

armour units, as well as the stability, can vary depending on the model construction. The units described in Section 4.4.5 were positioned in accordance with the placement requirements posed by DMC. The model constructed for Series 3.1 comprised approximately 481 units, resulting in a packing density ranging from 30.24 to 31.72 units of 2.5 m³ per 100 m² in the prototype. Although this met the prescribed packing density for Xbloc on the trunk (31.4 1/100 m²), settlements and displacements indicated areas of relatively low packing density. Consequently, packing density was increased slightly for Series 3.2, resulting in a range of 31.86 to 33.41 units per 100 m². This corresponds to 101 to 106 percent of the prescribed value. For the construction of the prototype, DMC prescribes a packing density between 98 and 105 percent of the design value, whereas the model packing density should be between 98 and 102 percent. The armour layer in Series 3.1 showed no damage up until the 1.0 H_{m0} test run, where multiple units were extracted from the armour layer due to uplift. Subsequently, the armour layer with a higher packing density in Series 3.2 showed no failure in any of the test runs.

The stability numbers of all test runs where no damage occurred are summarized in Figure 6.1, whereas Figure 6.2 depicts the damage development of the armour layers.

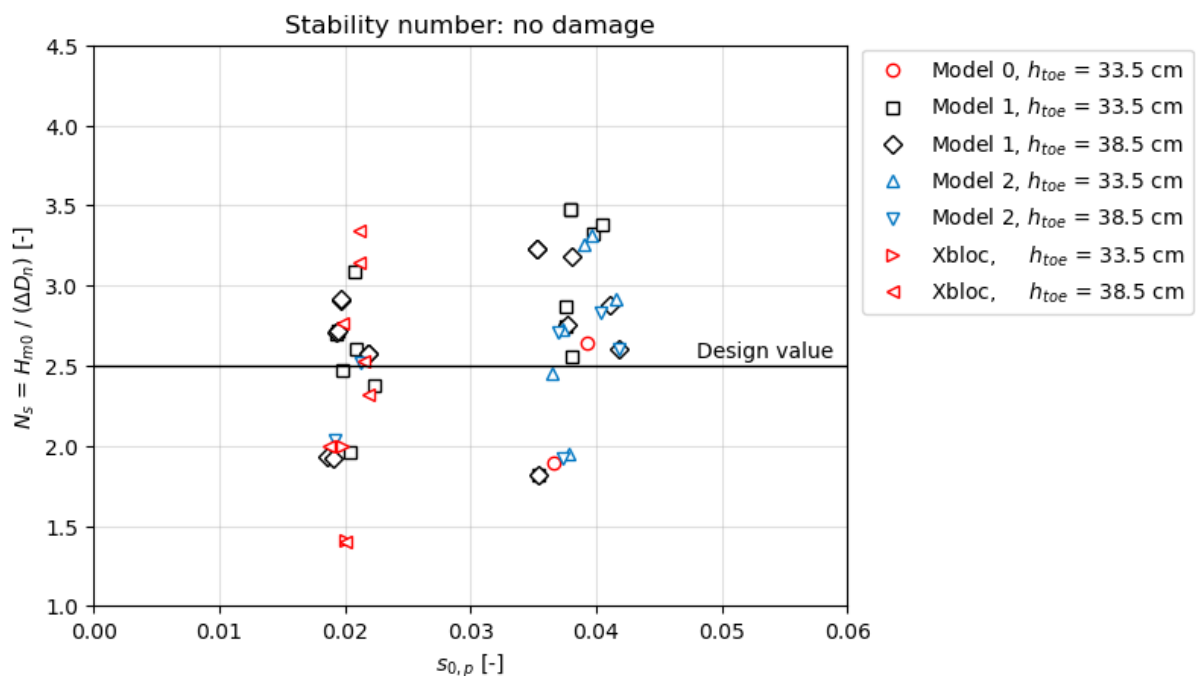


Figure 6.1. Stability number of all test runs with no recorded damage in the armour layers.

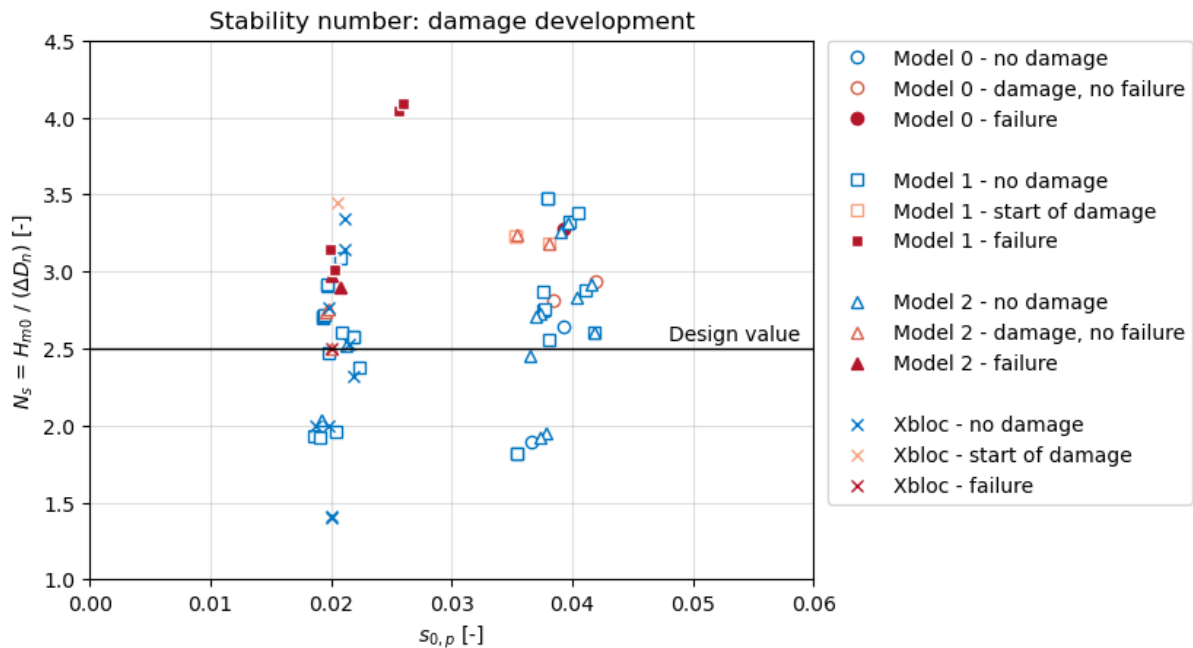


Figure 6.2. Stability number of all test runs until failure, where the condition of the armour layer is described by the formulation defined in Section 5.4.

6.1. Model 0

As previously discussed in Section 4.3.1, the construction of the core and underlayer resulted in slightly wider dimensions than intended, inducing an increase in D_x when maintaining the same number of armour units as the model. Precision in unit placement was required to ensure sufficient support surface, particularly towards the crown where spacings between neighbouring units were relatively large compared to the model.

Model 0 was solely subjected to a test programme (Series 0.1) with $h_{toe} = 33.5 \text{ cm}$ and $s_{0,p} = 0.04$. This series marked the initial submersion of the core and underlayer in water and exposure to wave attack, resulting in settlement of both the structure and the armour layer from the $0.8 H_{m0}$ to $1.0 H_{m0}$ test runs. Settlements led to a slight reduction in interlocking, primarily due to larger spacings between neighbouring XP-Base units. Additionally, XP-Base units positioned in a column with the underlying XP-Curve exhibited relatively more displacement and rotations, obtaining unfavourable positioning as illustrated in Figure 6.3. At $110\% H_{m0}$, failure occurred of initially an XP-Base unit in the 9th row of the grid, four rows beneath the water level. The interlocking of the unit was severely reduced due to a relatively high collapsing wave (see Appendix A), of which the breaking impact zone was positioned in the area of damage. Subsequently, another high collapsing wave extracted the XP-Base unit from the armour layer. Following the failure of the XP-Base unit, the underlying XP-Curve lost the stabilizing force from above and was later removed from its stable position due to the turbulence caused by the wave impact. At $1.2 H_{m0}$, the XP-Curve unit was removed from the armour layer during the impact of a breaking wave. No further damage occurred during this run. However, interlocking of the surrounding units was severely reduced. Continued exposure to wave impacts during the 1.2 and $1.3 H_{m0}$ test runs resulted in gradual lowering of the XblocPlus units above the damaged region, leading to loss of stability and subsequent failure due to breaking wave impacts. The $130\% H_{m0}$ test run was stopped after 847 incident waves, with damage classified as 'damage, no failure' at $N_s = 2.81$ in accordance to the description provided in Section 5.4. Moreover, failure occurred at a stability number of 3.28. The damage

was exclusively located in segment one of the critical roundhead section, around the position of the wave breaking impact zone.



Figure 6.3. Unfavourable positioning of column-positioned XP-Base and XP-Curve due to settlements and a large D_x . The lower marked pair initiated failure.

As described in Section 5.4, damage progression of the armour layers is quantified in terms of the absolute number of displaced units $N_{o,mov}$. However, no rocking of intact units was observed in Series 0, 1 or 2. Therefore, damage to the XblocPlus armour layers is expressed in N_{od} , further subdivided into failure due to rotation or displacement ($N_{o,rd}$) and failure due to uplift ($N_{o,up}$). The damage development is summarized in Figure 6.4, whereas the sectional damage is depicted in Figure 6.5. For sectional damage visualization, each section is divided into columns corresponding to the number of armour units in a specific row, with individual unit failures represented at relative locations within each section. Damage per section is quantified as $D\%$, with $D\%_{total}$ indicating the percentage of failed units relative to the total number on the critical roundhead section. The damage level of the armour layer is indicated by the corresponding number defined in Table 5.3.

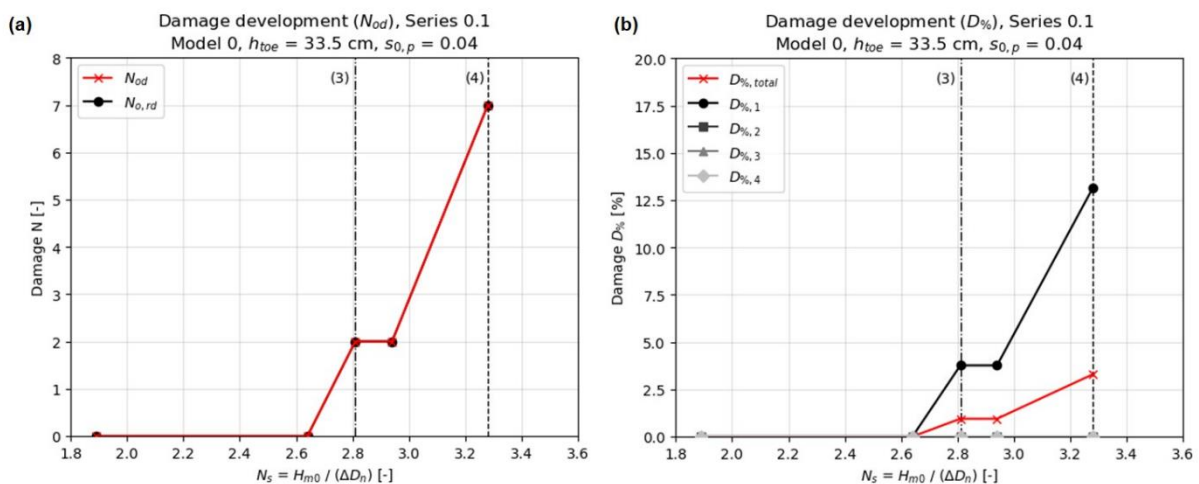


Figure 6.4. Damage development, expressed in (a) N_{od} and (b) $D\%$, of Model 0, with h_{toe} of 33.5 cm and $s_{0,p}$ of 0.04.

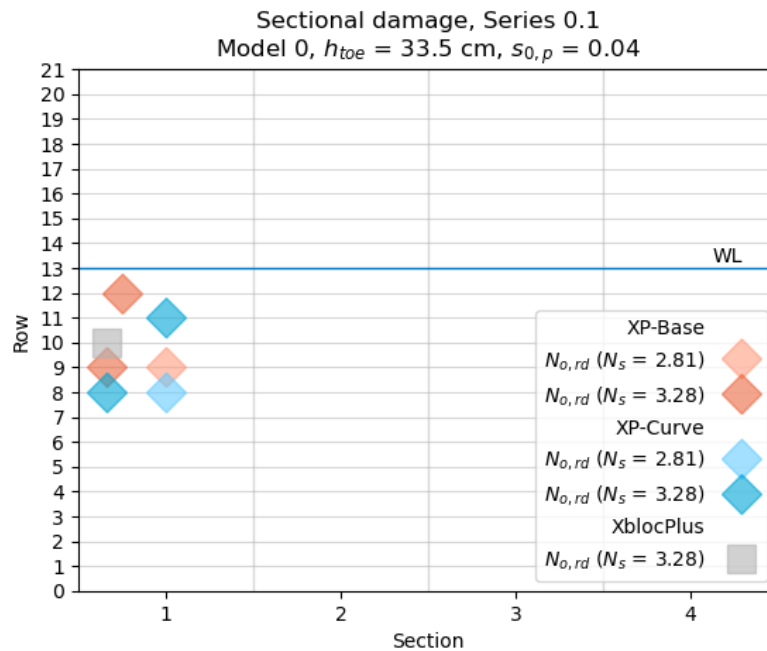


Figure 6.5. Positioning, with respect to the critical section of the roundhead, of the units failed in Series 0.1.

6.2. Model 1

After completing the test series described in Section 6.1, adjustments were made to the packing density of the model. An additional unit was added to each row of XP-Base, XP-Curve and XblocPlus, except for row 15, where adding another XP-Base unit would have obstructed placement of XblocPlus. The reconstructed armour layer consisted of 426 units, resulting in an estimated packing density ranging from 26.90 to 28.21 units of 2.5 m³ per 100 m² in the prototype, with D_x depicted in Figure 4.6a. Consequently, each segment illustrated in Figure 5.9 averaged 53.25 units. Ultimately, six test series were executed with this model, detailed in the following sections.

6.2.1. Series 1.1

This series replicated the test programme of Series 0.1 for the reconstructed armour layer, maintaining parameters of $h_{toe} = 33.5$ cm and $s_{0,p} = 0.04$. Less observable settlements occurred due to compaction of the core and underlayer during the previous series. No individual unit failures occurred in any test run, and no significant displacements or rotations were noted. However, one XP-Curve unit obtained a slightly unfavourable orientation (see Figure 6.6), though this fault was not addressed between test series and the armour layer was not reconstructed for Series 1.2.1.



Figure 6.6. Unfavourable orientation of XP-Curve unit after Series 1.1.

As aforementioned, no units were marked as ‘failed’ in Series 1.1. After the $1.3 H_{m0}$ test run, wave heights at the structure’s toe increased only marginally. Due to the difference in wave height production by the wave paddle and the wave heights observed at the toe, the wave paddle needed to generate significantly higher waves. Due to the steeper character of the waves, the produced wave heights were limited by the available power of the wave paddle. Additionally, the production of larger wave heights led to wave breaking on the transition slope and foreshore. However, wave breaking and the corresponding turbulence due to air entrainment occurred and dissipated before the gauges’ location, so the measured values were deemed reliable. Deep water H_{m0} measurements in the 130% test run averaged 14.84 cm, with 13.14 cm at the toe. In comparison, the deep water gauge measured 15.99 cm on average during the $1.5 H_{m0}$ run with 13.78 measured at the toe, only 93% of the intended wave height. This indicates that the tests with $s_{0,p} = 0.04$ were limited in wave height by the test configuration. Series 1.1 concluded with a stability number exceeding 3.48.

6.2.2. Series 1.2.1

This series featured the lower water level ($h_{toe} = 33.5 \text{ cm}$) with 2% wave steepness. No significant settlements, displacements or rotations occurred in the 0.8 and $1.0 H_{m0}$ test runs. Starting from 110% H_{m0} , the armour layer deformed permanently on multiple occasions due to uplift caused by the highest waves in the spectrum. After passing of a long wave, the phreatic surface in the armour layer cannot follow the instantaneous water level outside the structure, after which large head differences cause uplift pressures. However, no significant damage or unfavourable displacements were caused by uplift of the armour layer during the 1.1 and $1.2 H_{m0}$ runs. Conversely, during the $1.3 H_{m0}$ test run, failure of the XP-Curve unit highlighted in Figure 6.6 occurred as uplift bulged the armour layer. After passing of the wave, the unit was positioned atop of the underlying unit without its wings interlocking (see Figure 6.7a). Additionally, due to the forward displacement of the XP-Curve unit, the supported XP-Base unit rotated forward around its y-axis leading to a loss of interlocking (Figure 6.7b). Due to a lack of residual interlocking, the units were extracted from the armour layer at subsequent waves. Consequently, the surrounding units failed due to a combination of uplift and a lack of interlocking. The damage was predominantly concentrated in segment 3 of the critical section, see Figure 6.10. As aforementioned, there was an error in the input from the Wave Synthesizer software which caused the wave heights to be unreasonably high. Failure of the armour layer

during Series 1.2.1 occurred at a stability number of 4.04, corresponding to 162% H_{m0} with $H_{max} = 19.33 \text{ cm}$. Therefore, the decision was made to rebuild the armour layer and repeat the test programme, termed Series 1.2.2.

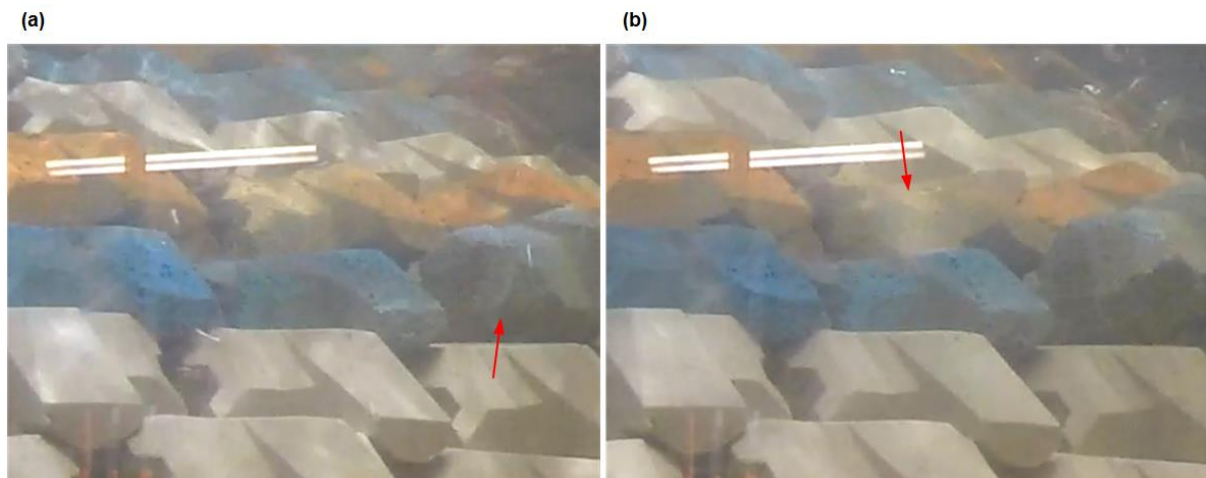


Figure 6.7. 'Damage, no failure' during 1.3 H_{m0} test run of Series 1.2.1.

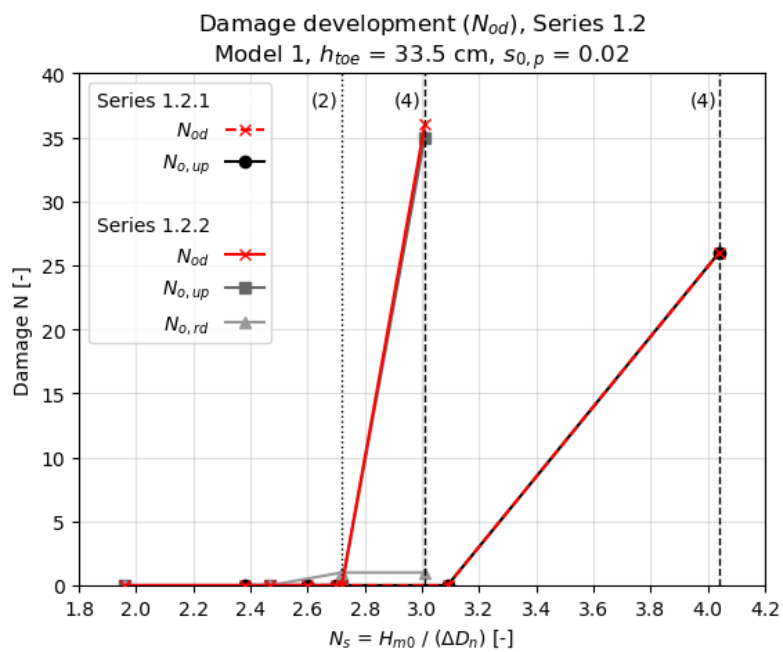


Figure 6.8. Damage development, expressed in N_{od} , of Model 1, with h_{toe} of 33.5 cm and $s_{0,p}$ of 0.02.

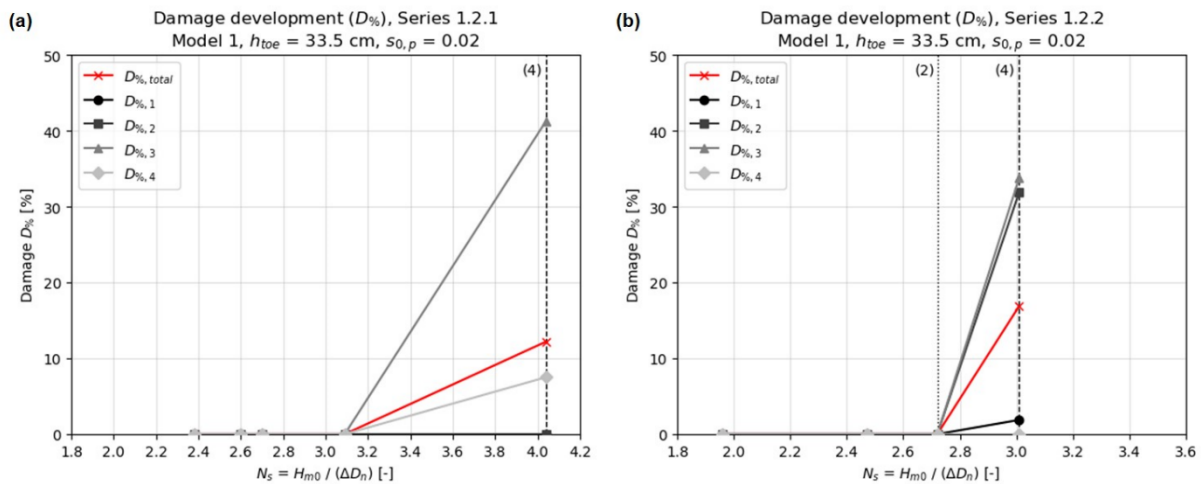


Figure 6.9. Damage development, expressed in $D\%$, of Model 1, with h_{toe} of 33.5 cm and $s_{0,p}$ of 0.02.

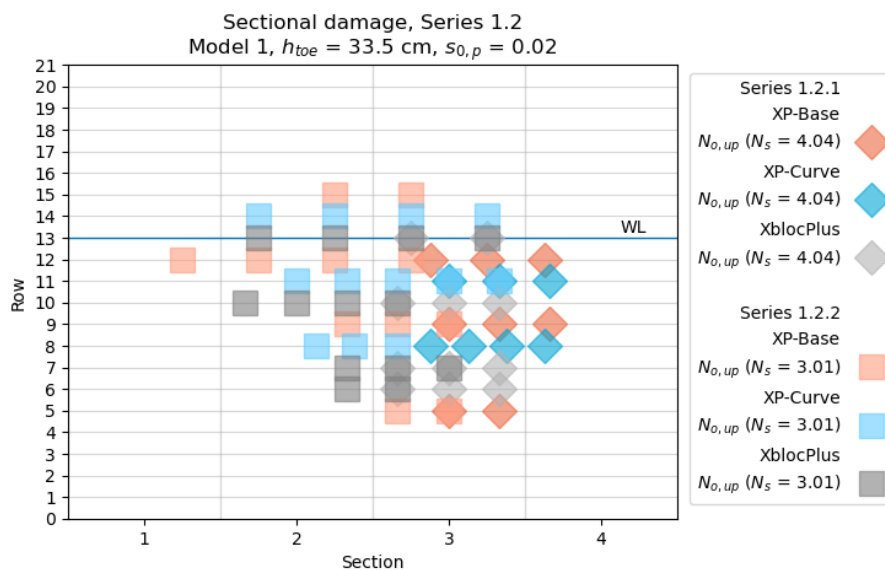


Figure 6.10. Positioning, with respect to the critical section of the roundhead, of the units failed in Series 1.2.1 and Series 1.2.2.

6.2.3. Series 1.2.2

The damage development pattern in Series 1.2.2 resembled Series 1.2.1 closely, with uplift influencing unit orientation and stability from the 1.1 H_{m0} test run onward. Relatively insignificant permanent bulging of the armour layer occurred, with one XP-Base unit experiencing unfavourable rotation, positioning one leg atop of the underlying armour unit. At 120% H_{m0} , increased uplift impact led to the failure of multiple units at two separate locations. Firstly, the aforementioned XP-Base unit with an unfavourable orientation lost interlocking with the surrounding units, after which it was extracted from the armour layer by a subsequent wave. Secondly, two rows below the XP-Base unit, simultaneous failure occurred of one XP-Base and one XP-Curve unit, see Figure 6.11. The failure of the three units reduced interlocking in the surrounding area significantly, gradually leading to failure of 36 units cumulatively. The armour layer showed no significant damage until 110% H_{m0} , where the XP-Base unit rotated significantly. Ultimately, failure occurred at $N_s = 3.01$, see Figure 6.8. Damage to the armour layer was substantially wider spread than in Series 1.2.1. Failure occurred in sections one to three. Sectional damage comparisons are depicted in Figure 6.9 and Figure 6.10.

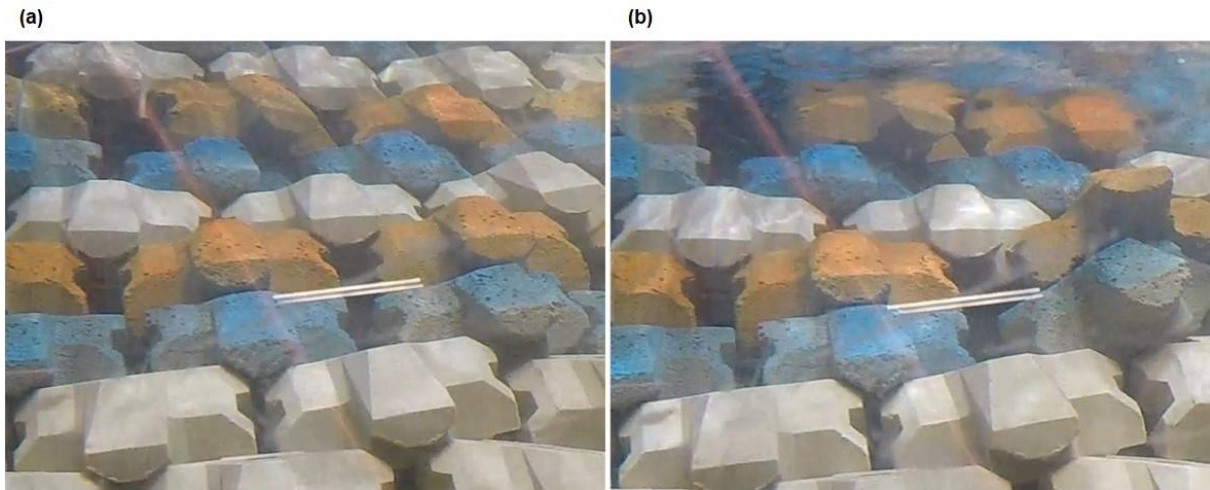


Figure 6.11. ‘Damage, no failure’ during 1.2 H_{m0} test run of Series 1.2.2.

6.2.4. Series 1.3

Series 1.3 involved steeper waves with $s_{0,p} = 0.04$ and a high water level $h_{toe} = 38.5$ cm. The armour layer exhibited minor displacements, rotations or deformations up until 120% of design wave height. At the 1.3 H_{m0} test run, the wing of an XblocPlus unit in the 16th row slipped off the underlying XP-Base. As previously noted in Section 4.3.2, the 15th row was constructed with the originally planned number of XP-Base units. Hence, D_x was larger than initially planned in the virtual model. Consequently, the XblocPlus unit was only marginally supported, leading to loss of one contact surface but remaining stable. During the 1.4 H_{m0} test run, an XP-Base unit located in the 15th row obtained an unfavourable rotation, positioning one leg atop the underlying XP-Curve, thereby reducing interlocking. This rotation occurred gradually as waves curled around the structure towards the leeward side. Similar to Series 1.1, the wave heights generated were limited by the available power of the wave paddle. Due to the higher water level, the wave paddle required increasingly more power. The wave heights at the toe were limited to 12.79 cm, equivalent to 129% of $H_{S,d}$. No damage was observed up to a stability number up to $N_s = 2.88$, as shown in Figure 6.12.

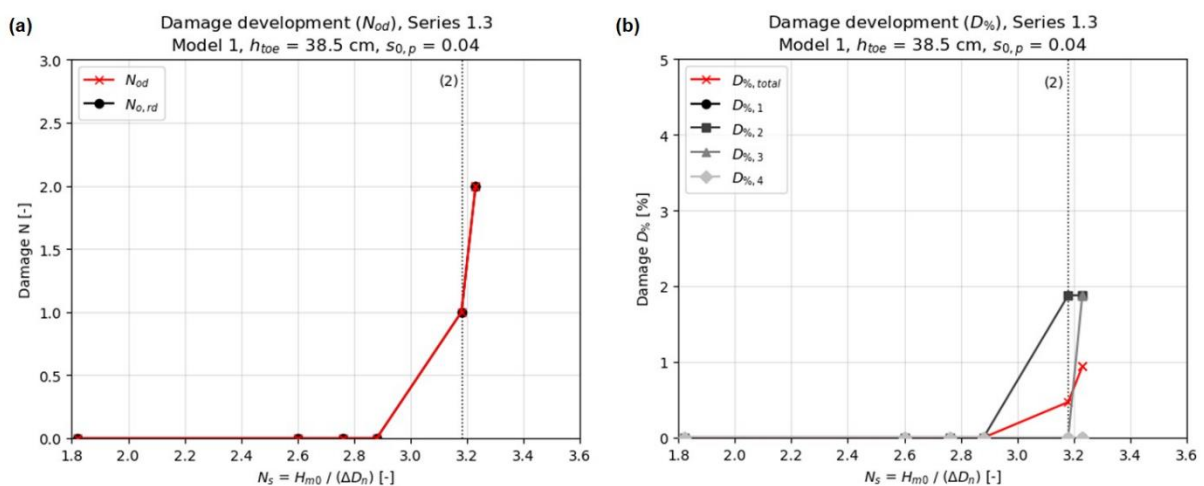


Figure 6.12. Damage development, expressed in (a) N_{od} and (b) $D\%$, of Model 1, with h_{toe} of 38.5 cm and $s_{0,p}$ of 0.04.

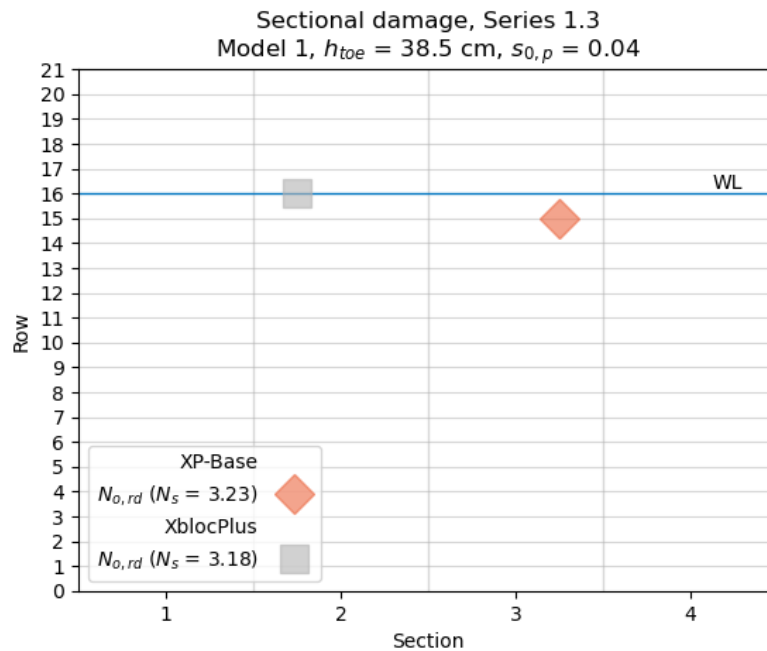


Figure 6.13. Positioning, with respect to the critical section of the roundhead, of the units failed in Series 1.3.

6.2.5. Series 1.4.1

Series 1.4 consisted of a test programme with waves of $s_{0,p} = 0.02$ and a high water level of 38.5 cm at the toe. The armour layer displayed no settlements, displacements or rotations for any of the test runs up to $1.2 H_{m0}$, except for minor influences of uplift at $120\% H_{m0}$. At $1.3 H_{m0}$, the effects of uplift increased significantly, incrementally bulging the armour layer on multiple occasions. This expansion of the armour layer gradually reduced the interlocking of the units, resulting in the extraction of an XP-Base unit (Figure 6.14b). Subsequently, the underlying XP-Curve unit lost stability and was extracted due to the absence of the support on top. Following a damage progression pattern similar to Series 1.2.1 and 1.2.2, the interlocking of surrounding units decreased significantly, resulting in failure of 12 units in total. However, the location of the occurred damage shifted more towards the flume wall, exclusively in section 4 (Figure 6.17). Due to the aforementioned error in the input of the Wave Synthesizer software, the armour layer failed at a stability number of 4.09, i.e. $164\% H_{m0}$. After analysis of the incident wave data, the fault was identified and corrected for Series 1.4.2.

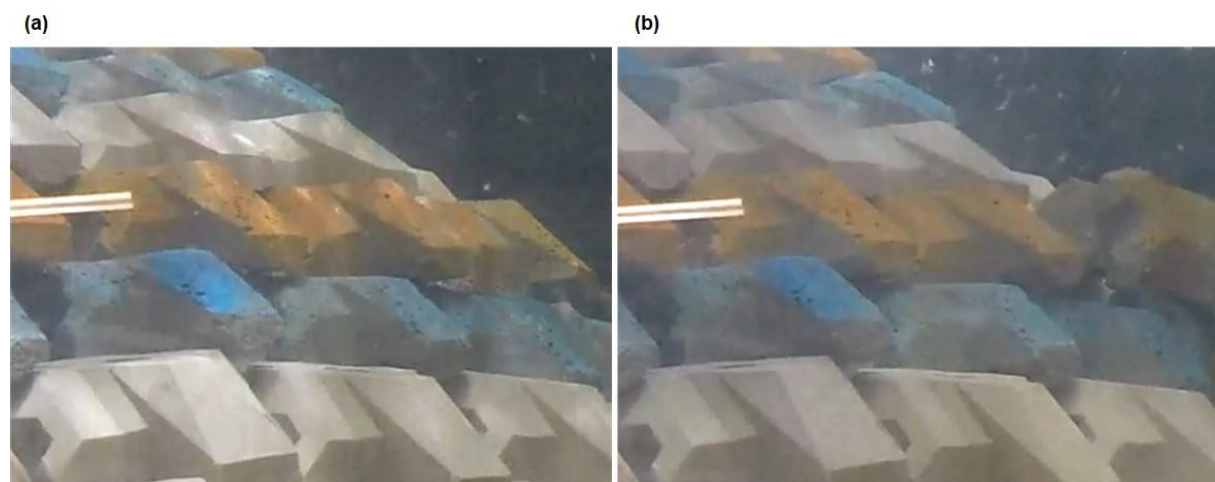


Figure 6.14. 'Damage, no failure' during $1.3 H_{m0}$ test run of Series 1.4.1 due to uplift of an XP-Base unit.

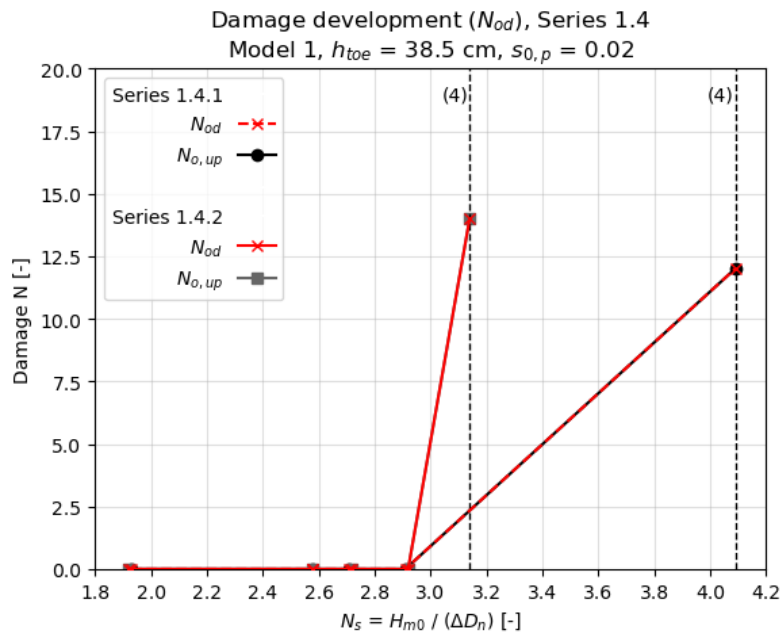


Figure 6.15. Damage development, expressed in N_{od} , of Model 1, with h_{toe} of 38.5 cm and $s_{0,p}$ of 0.02.

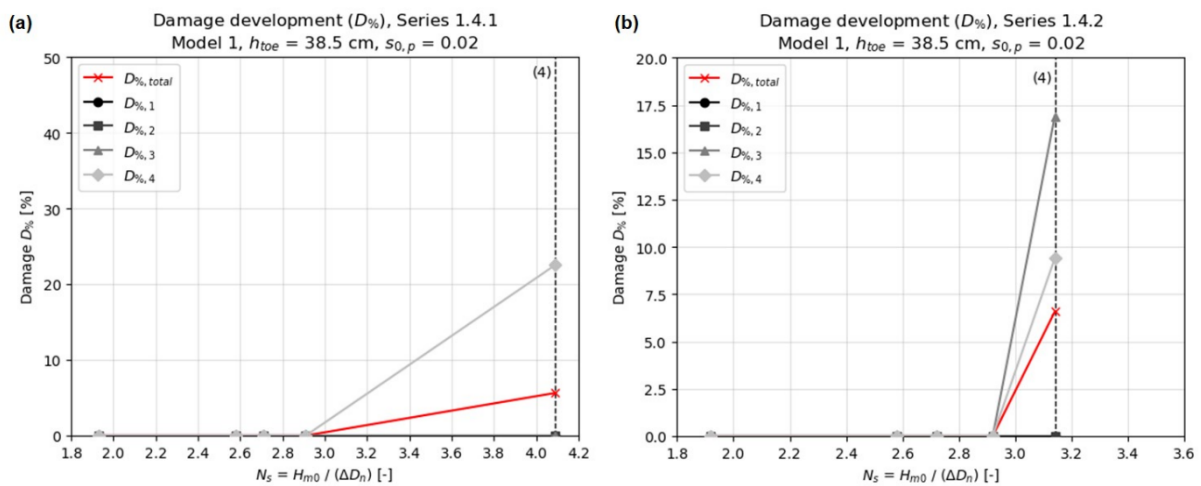


Figure 6.16. Damage development, expressed in $D\%$, of Model 1, with h_{toe} of 33.5 cm and $s_{0,p}$ of 0.02.

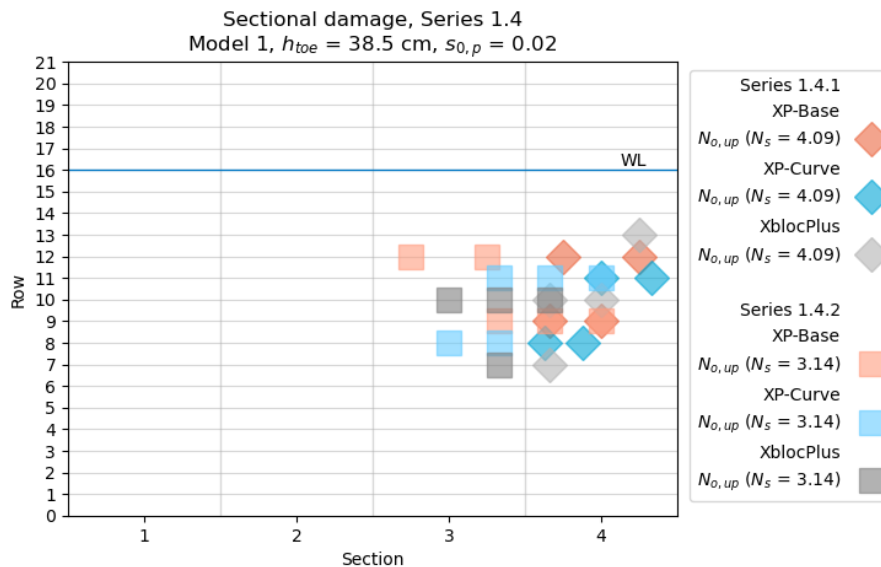


Figure 6.17. Positioning, with respect to the critical section of the roundhead, of the units failed in Series 1.4.1 and Series 1.4.2.

6.2.6. Series 1.4.2

Series 1.4.2 showed similar damage development to Series 1.4.1. However, the effects of uplift were slightly more pronounced in the armour layer during the 1.1 and 1.2 H_{m0} test runs. Consequently, increased deformations were observed. Two relatively large consecutive waves caused uplift during the 130% H_{m0} test run, which reshaped the armour layer to a suboptimal configuration. The weakened area was gradually worsened further by subsequent waves. Ultimately, an XP-Base unit was extracted from the armour layer due to turbulence from a large passing wave. The loosened region was further damaged by the effects of uplift, resulting in failure of 14 units at $N_s = 3.14$ (Figure 6.15). The damage, depicted in Figure 6.17, was located slightly further from the flume wall with respect to Series 1.4.1, while the amount of armour units failed was similar.

6.3. Model 2

Based on the preliminary results of Series 1, Model 2 was constructed with a higher packing density than described in Section 3.2 to possibly improve the interlocking of XP-Base. An increase in packing density and interlocking correlates to a decrease in porosity and permeability. The model consisted of 443 units, corresponding to 55.38 units per section as depicted in Figure 5.9. Since the entire test program was previously conducted in Series 1, the wave heights in Series 2 were effectively calibrated and closely matched the target values.

6.3.1. Series 2.1

In Series 2.1, tests were executed with steeper waves ($s_{0,p} = 0.04$) and a water level of 33.5 cm at the toe. The H_{m0} ranged from 7.71 cm to 13.12 cm, reaching a maximum of 132% $H_{s,d}$. The armour layer remained stable throughout each test run, showing only marginal settlements. Although some XP-Base units positioned directly atop the underlying XP-Curve displayed slight displacements and rotations, none were substantial enough to classify as 'failed'.

6.3.2. Series 2.2

Series 2.2 subjected the model from Series 2.1 to longer waves ($s_{0,p} = 0.02$) at the same water level. Wave data from the 0.8 H_{m0} test run was not recorded due to a temporary error in the

wave paddle's operating system. However, no displacements were recorded during this test run. The first occurrence of damage was observed during the 1.0 H_{m0} test run, where an XP-Base unit rotated significantly due to effects of uplift of a passing wave. One of the legs was lifted atop the underlying XP-Curve, reducing its interlocking (Figure 6.18). The unit was later extracted due to turbulence of two consecutive passing waves. Due to removal of the XP-Base, the underlying XP-Curve lost its interlocking from above and was extracted due to uplift. With the two armour units removed, no damage progression occurred during the 110% H_{m0} run. At $H_{m0} = 11.75$ cm, the surrounding units obtained an unfavourable orientation due to separate instances of uplift and eventually failed due to uplift caused by a large wave. The test concluded with significant damage to the armour layer at a stability number of 2.97. The damage was concentrated around the initially failed units in section 3 (see Figure 6.20).

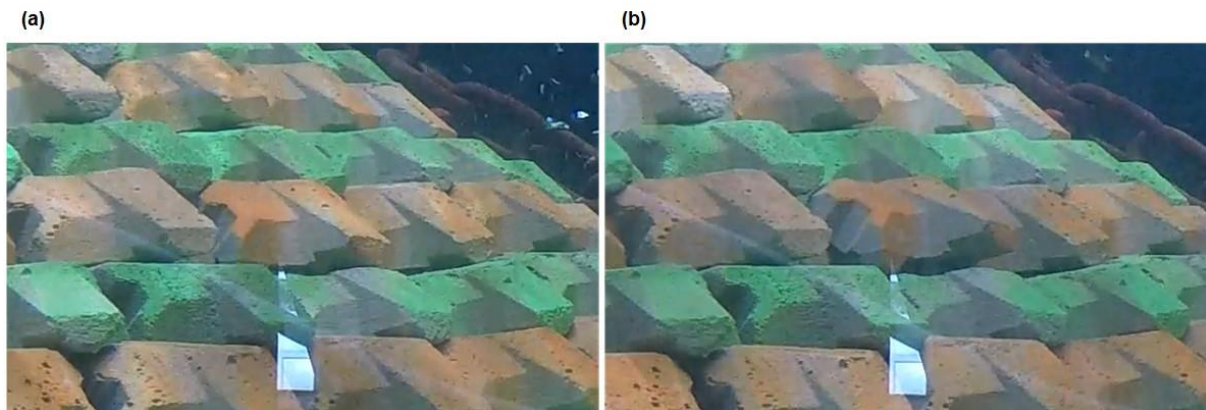


Figure 6.18. 'Start of damage' during 1.0 H_{m0} test run of Series 2.2 due to uplift of an XP-Base unit.

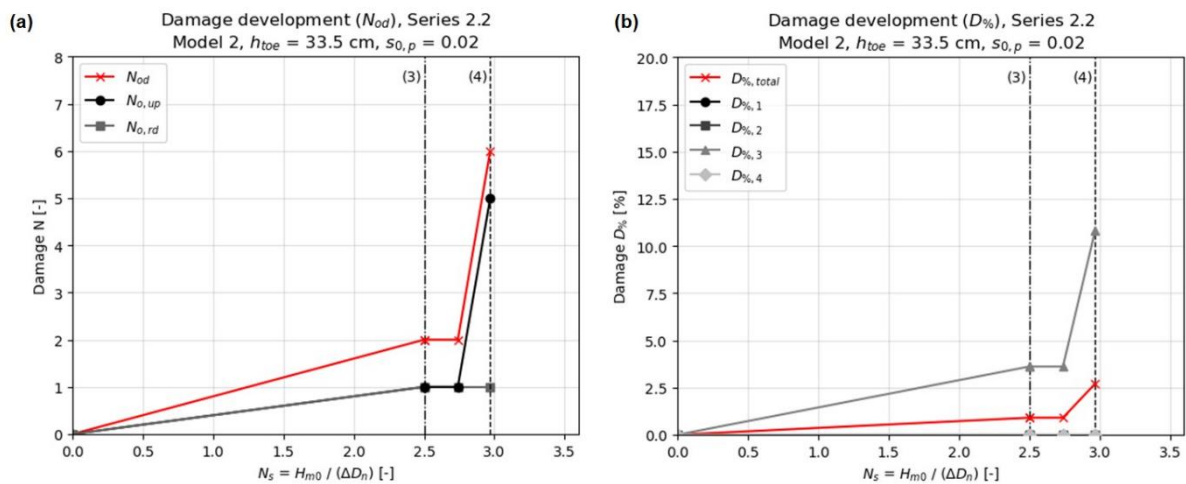


Figure 6.19. Damage development, expressed in (a) N_{od} and (b) $D\%$, of Model 2, with h_{toe} of 33.5 cm and $s_{0,p}$ of 0.02.

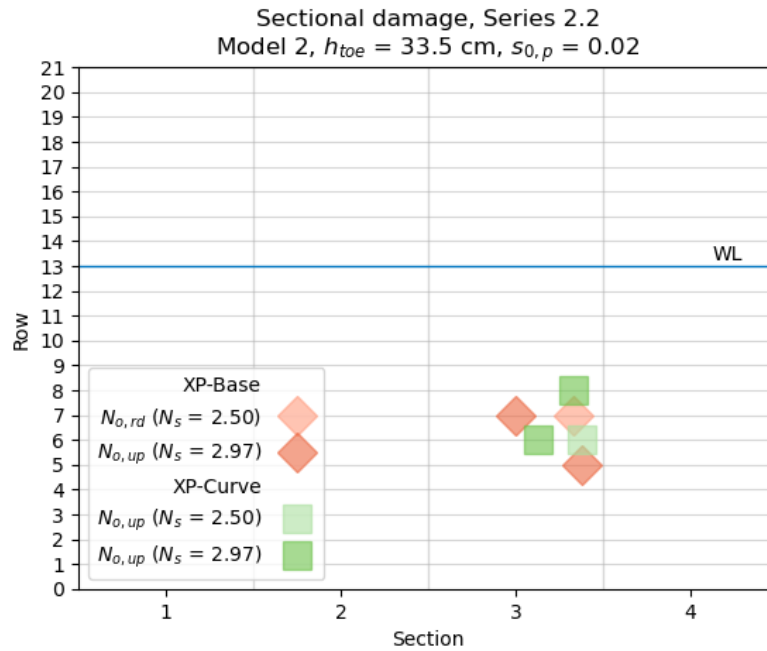


Figure 6.20. Positioning, with respect to the critical section of the roundhead, of the units failed in Series 2.2.

6.3.3. Series 2.3

After Series 2.2, the armour layer was rebuilt in the same configuration. Series 2.3 involved test runs with 4% wave steepness at a water level at the toe of 38.5 cm. Following the 1.0 H_{m0} test run, some deformations were observed in the armour layer. This primarily affected XP-Base units with lower degrees of interlocking due to their positioning relative to surrounding units. At 130% H_{m0} , an XP-Base unit in the 11th row, positioned towards the centre of the structure (see Figure 6.22), rotated out of the armour layer due to turbulence and rotary motion around the roundhead caused by larger waves. In the following test run, at $N_s = 3.24$, another XP-Base unit in the 7th row gradually rotated around its z-axis, losing significant stability.

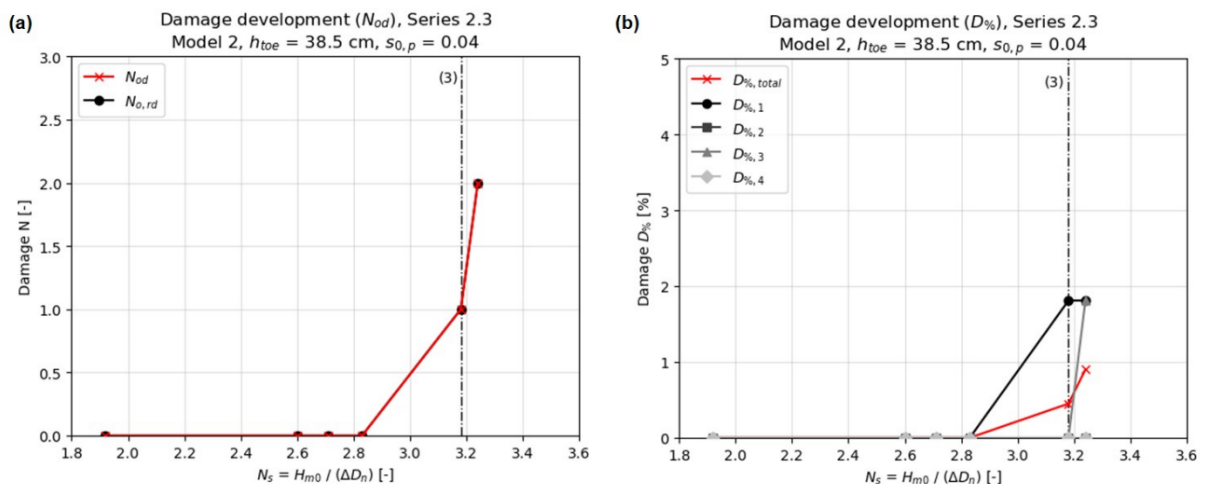


Figure 6.21. Damage development, expressed in (a) N_{od} and (b) $D\%$, of Model 2, with h_{toe} of 38.5 cm and $s_{0,p}$ of 0.04.

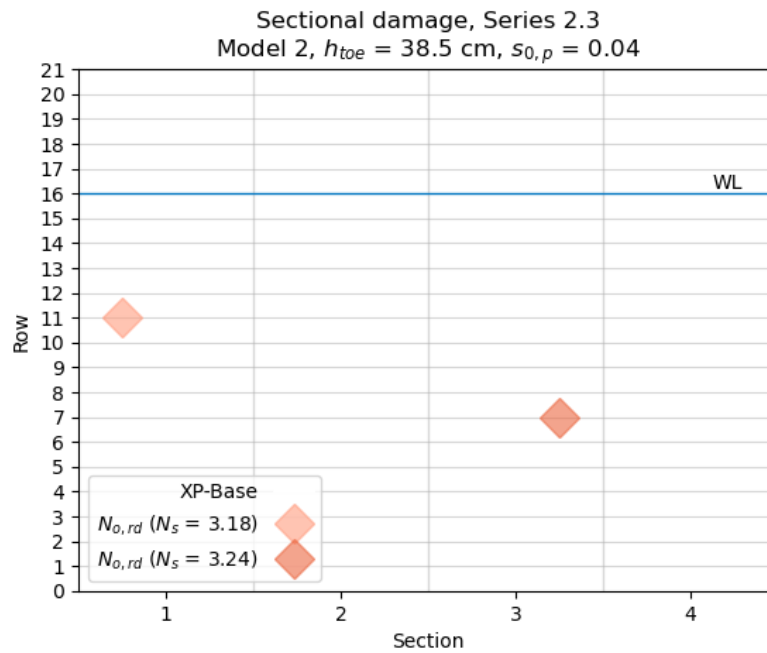


Figure 6.22. Positioning, with respect to the critical section of the roundhead, of the units failed in Series 2.3.

6.3.4. Series 2.4

Series 2.4 consisted of test runs with a steepness of 0.02 and a water level of 38.5 cm at the toe. Minor deformations were observed in the armour layer during the $1.0 H_{m0}$ test run. After increasing the incident wave height to 110% of $H_{s,d}$, units in sections 3 and 4 became unfavourably oriented due to uplift effects. Subsequently, a column of four units lost contact with the underlying units on one side. The column rotated around the x-axis due to uplift ('damage, no failure', see Figure 6.23 and Figure 6.24). Decreased residual interlocking in the area led to a large section of the armour layer failing due to uplift at $N_s = 2.90$. The sectional damage was distributed across sections 2, 3 and 4, as depicted in Figure 6.25.

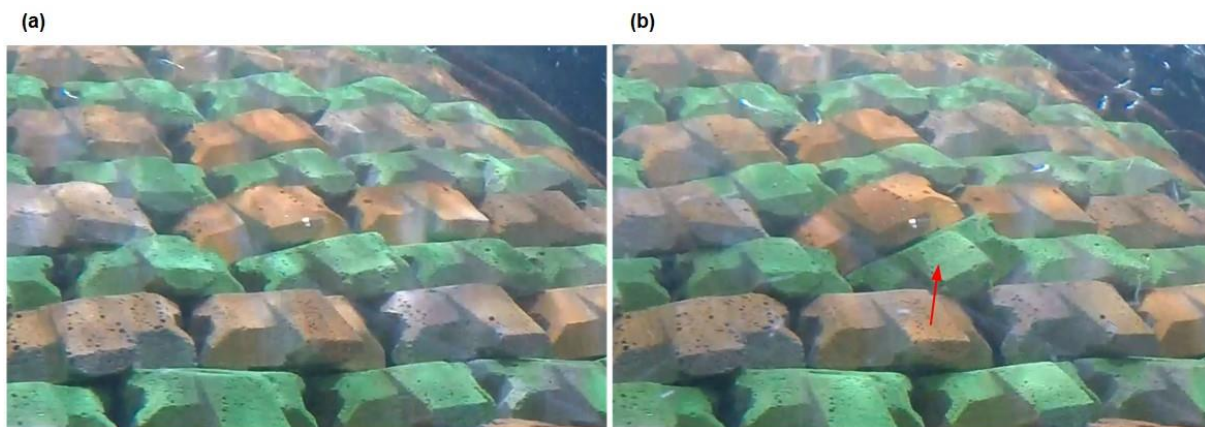


Figure 6.23. 'Damage, no failure' during $1.1 H_{m0}$ test run of Series 2.4, due to simultaneous rotation of a column of four units, where the lowest unit is indicated in (b).

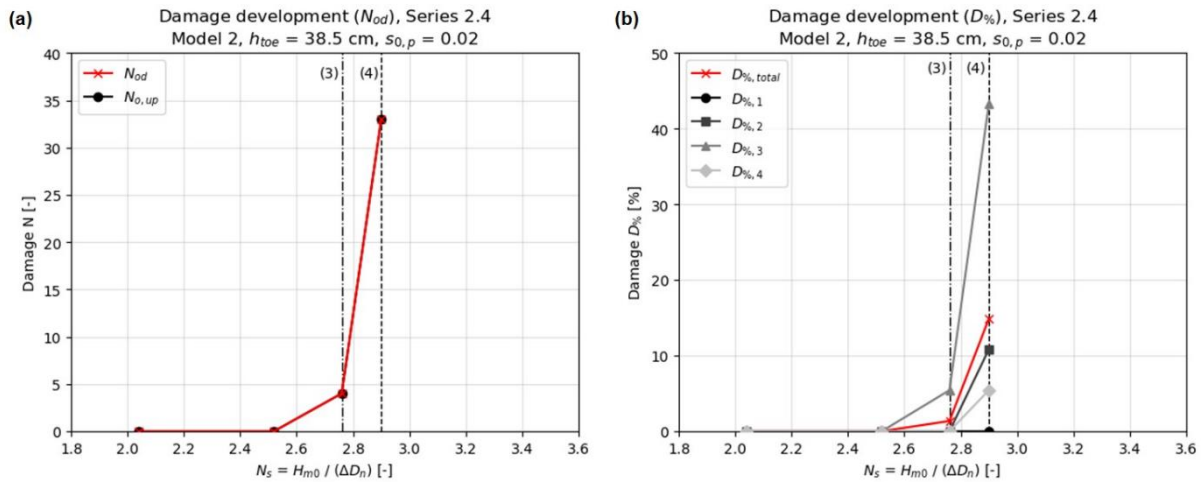


Figure 6.24. Damage development, expressed in (a) N_{od} and (b) $D\%$, of Model 2, with h_{toe} of 38.5 cm and $s_{0,p}$ of 0.02.

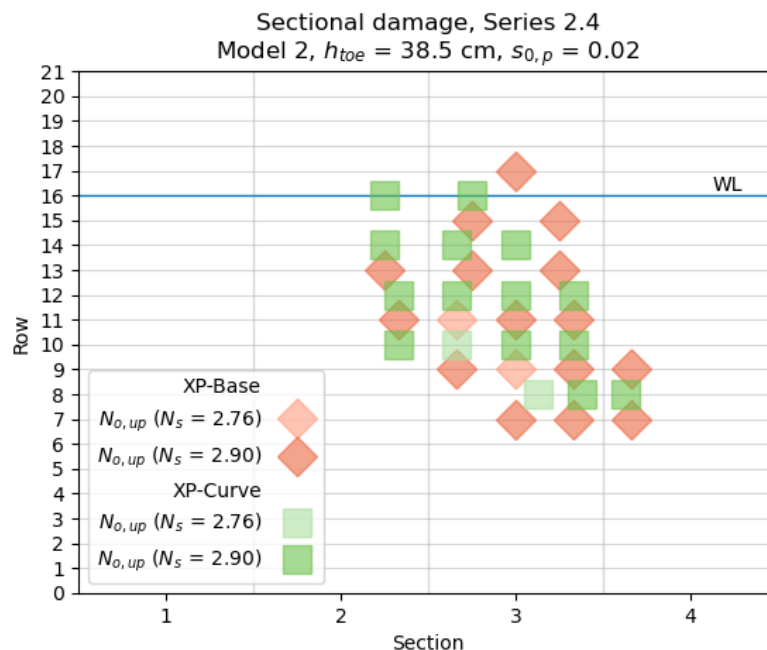


Figure 6.25. Positioning, with respect to the critical section of the roundhead, of the units failed in Series 2.4.

6.4. Xbloc

The fourth model tested featured an Xbloc armour layer, previously described in Section 4.3.4. The layer was constructed for two separate series. Both series were executed with waves of 2% steepness, with different water levels of $h_{toe} = 33.5$ cm and $h_{toe} = 38.5$ cm. The configuration of Series 3.1 was constructed with 481 units, resulting in a packing density of 30.24 to 31.72 units of 2.5 m³ per 100 m². The armour layer constructed for Series 3.2 had an increased packing density between 31.86 and 33.41 1/100 m². The hydraulic stability of the armour layer was assessed by observance of rocking through the glass flume wall. Furthermore, additional analysis was conducted on the recordings.

As previously described in Section 4.3.4, a correction factor was applied to the unit weight of Xbloc to account for the roundhead structure and deep water configuration. For roundheads,

DMC prescribes a 1.25 factor compared to the unit size on the trunk, whereas 1.5 is applied for deep water conditions where $h > 2.5 H_s$. This criterion accounts for a higher ratio between the highest wave heights in the spectrum and the significant wave height. Typically, this ratio falls within the range of 1.2 – 1.4 for nearshore breakwater cross sections, but can extend up to 1.8 – 2.0 for deep waters. As previously mentioned, a correction factor of 1.23 was applied, which corresponded to a design stability number of 2.54. To check the validity of the correction factor, the ratios achieved during the test runs are assessed.

The measured ratio in critical runs initially reached 1.84 during Series 3.1. However, the ratio decreased to 1.65 in the 1.2 H_{m0} run. Higher ratios were observed during Series 3.2 as the water depth was increased. The maximum value of 2.01 was measured during the 1.1 H_{m0} test run, after which it decreased to 1.68 in subsequent runs due to a relatively constant H_{max} . The 0.6 and 0.8 H_{m0} test runs recorded ratios below 1.7 in both series. The ratios calculated for $H_{1\%}$ were approximately equal to 1.5 or less, see Figure 6.26b. The achieved ratios indicate an underestimation of the correction factor for critical test runs with $H_{max}/H_{m0} > 1.8$. The implications of this underestimation will be discussed further in Chapter 7.

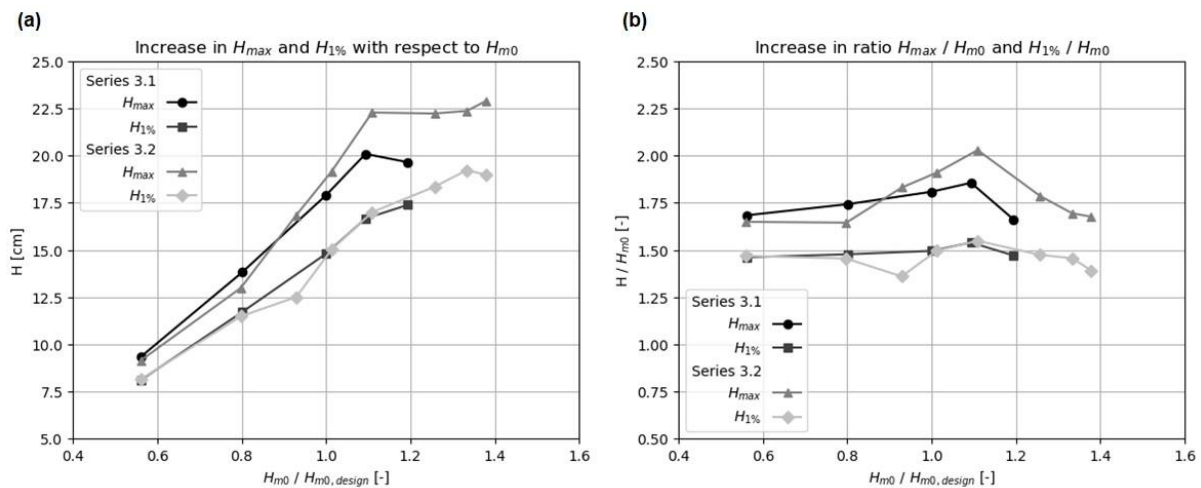


Figure 6.26. Increase in H_{max} and $H_{1\%}$ with respect to H_{m0} for Series 3.1 and Series 3.2.

6.4.1. Series 3.1

Series 3.1 began with a 60% $H_{s,d}$ run (5.94 cm) to accommodate for initial settlements as suggested by DMC. An individual unit showed repeated rotational movement before settlement, but the criterion for rocking as described in Section 5.4 was not met. However, at 80% H_{m0} , a unit in the 5th row of the configuration showed repeated rotational movement for more than 20 waves, thus passing the criterion and failed due to rocking. At 100% H_{m0} , five units were extracted due to uplift effects. Due to the decreased packing density, rocking of at least three units was subsequently observed. Despite redundancy from higher units sliding down, nine additional units were extracted at 1.2 H_{m0} . Additionally, significant settlements were observed, indicated in Figure 6.27b. The initial positions of the extracted units could not be determined as the units are not regularly distinguished through colours like in series 0, 1 and 2. The concluded stability number was $N_s = 2.00$, see Figure 6.28.



Figure 6.27. Xbloc model of Series 3.1 (a) before $0.6 H_{m0}$ test run and (b) after failure at $1.2 H_{m0}$ test run with settlements and extracted units indicated.

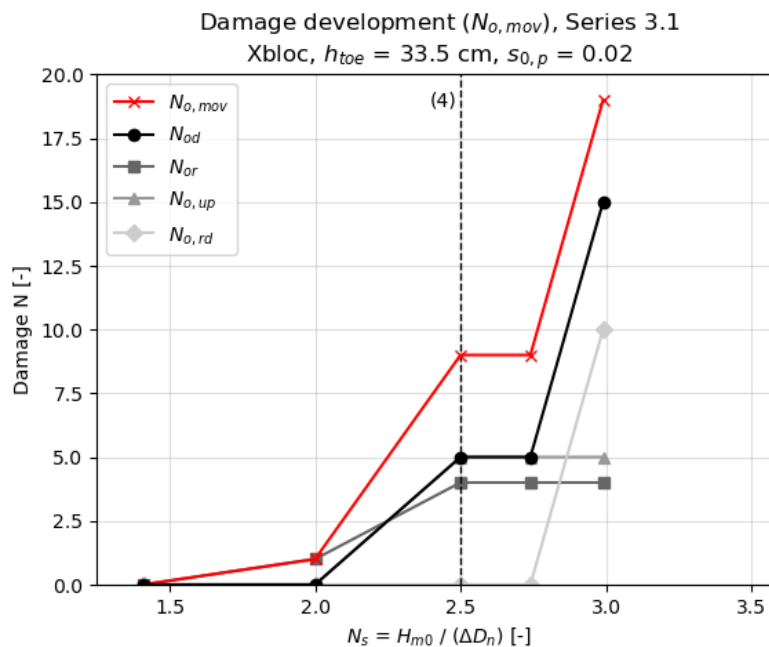


Figure 6.28. Damage development, expressed in N_{od} , of Xbloc configuration, with h_{toe} of 33.5 cm and $s_{0,p}$ of 0.02.

6.4.2. Series 3.2

A $0.9 H_{m0}$ test run was added in Series 3.2 as failure occurred at $100\% H_{m0}$ in Series 3.1. Series 3.2 was conducted with the same steepness as Series 3.1, but a higher water level of $h_{toe} = 38.5$ cm. Due to the increased packing density, settlements of the armour layer were significantly decreased at $0.6 H_{m0}$ with respect to Series 3.1. At $80\% H_{m0}$, two rocking units were observed, corresponding to 0.79 percent of the critical roundhead section. An additional unit started rocking during the $0.9 H_{m0}$ test run. Effects of uplift were observed at $100\% H_{m0}$. However, no unit failures occurred. The number of rocking units increased by one during both the 110 and 120 percent test runs. Additionally, the influences of uplift increased significantly for the highest waves. At $1.4 H_{m0}$, an Xbloc unit was displaced significantly out of the armour layer, see Figure 6.29b. However, following the description in Section 5.4, no failure occurred at the maximum achievable incident wave height of 13.65 cm, see Figure 6.30.



Figure 6.29. Xbloc model of Series 3.2 (a) before $0.6 H_{m0}$ test run and (b) after failure at $1.2 H_{m0}$ test run with extracted unit indicated.

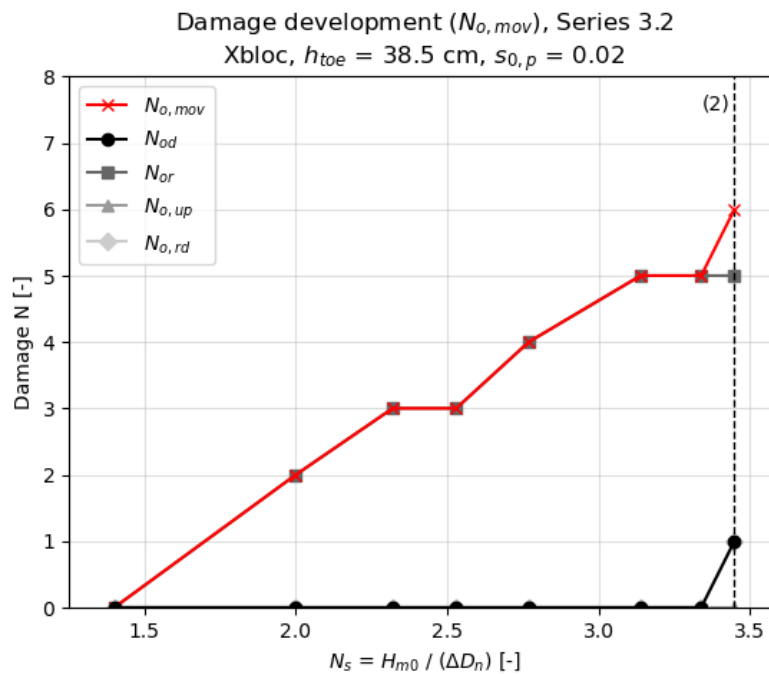


Figure 6.30. Damage development, expressed in N_{od} , of Xbloc configuration, with h_{toe} of 38.5 cm and $s_{0,p}$ of 0.02.

6.5. Reflection analysis

To evaluate the influence of the structure's orientation in the wave flume on wave reflection, parallel measurement gauges were situated in front of the structure (see Figure 5.6). This allowed the comparison of water elevation time series for the assessment of waves perpendicular to the incident wave direction. The average reflection coefficient, determined separately by gauges 2, 3 and 4 as well as gauges 5, 6 and 7 (Figure 6.31), provided insight into reflection variations caused by the structure.

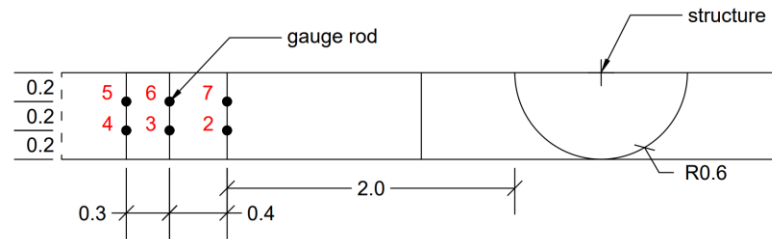


Figure 6.31. Wave gauge labels used for reflection analysis.

The average reflection coefficient recorded by gauges 2, 3, and 4 across all test runs was 27.20 percent, while gauges 5, 6 and 7 measured an average of 27.17 percent. The largest gauged difference between the sets was 0.4 percent, both negative and positive. However, minor differences in reflection coefficient do not exclude the possibility of waves perpendicular to the wave attack. Therefore, elevation time series from each test configuration – comprising all combinations of wave steepness and water level – were compared across both gauge sets, depicted in Figure 6.32. Additionally, Table 6.1 describes the bounding range and absolute average of the difference.

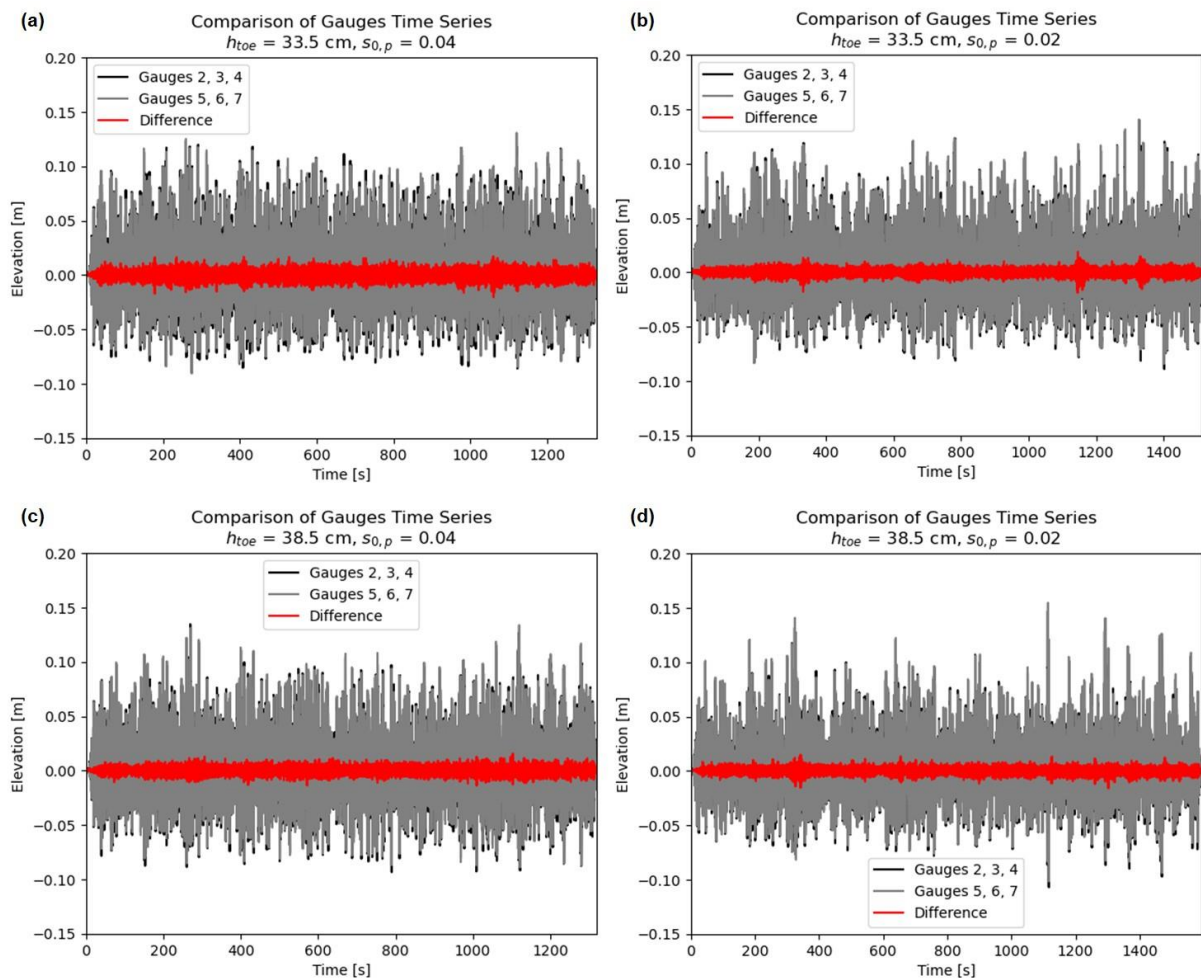


Figure 6.32. Gauges time series comparison of each test configuration.

Table 6.1. Description of the minimum, maximum and absolute average differences between two gauged time series.

h_{toe} [cm]	$s_{0,p}$ [-]	Max. negative difference [cm]	Max. positive difference [cm]	Avg. of absolute difference [cm]
33.5	0.04	2.05	1.71	0.297
33.5	0.02	1.89	1.88	0.206
38.5	0.04	1.39	1.57	0.245
38.5	0.02	1.61	1.49	0.208

According to Table 6.1, the most significant difference in surface elevation perpendicular to wave attack occurs at $h_{toe} = 33.5$ cm and $s_{0,p} = 0.04$. Here, the maximum negative difference – the difference in surface elevation when the measurements by gauges 5, 6 and 7 exceeded the values of the second gauge set – is equal to 2.05 centimetres. This extreme value occurs closely after the peak of a wave at $t = 1060.1$ s in the time series. The wave had a total height of 13.59 cm as measured by gauges 2, 3 and 4, whereas gauges 5, 6 and 7 measured $H = 14.15$ cm. The wave period was approximately equal. Both waves were included in the percentile of the significant wave height of their respective gauge sets. The difference in total wave height between the gauge sets, along with the incident and reflected waves, is depicted in Figure 6.33. Additionally, the difference in gauged H_{max} ($t = 259.7$ s) is 0.118 centimetres at the structure's side of the flume, see Figure 6.34.

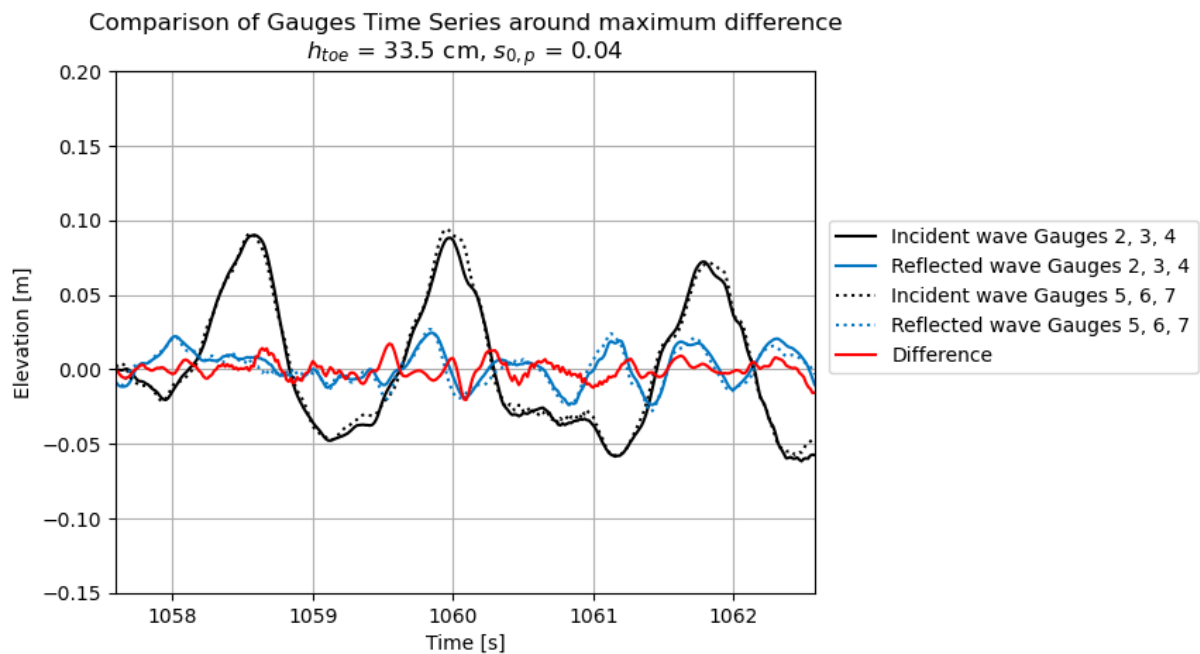


Figure 6.33. Gauges' incident and reflected wave time series comparison around the epoch of the maximum difference.

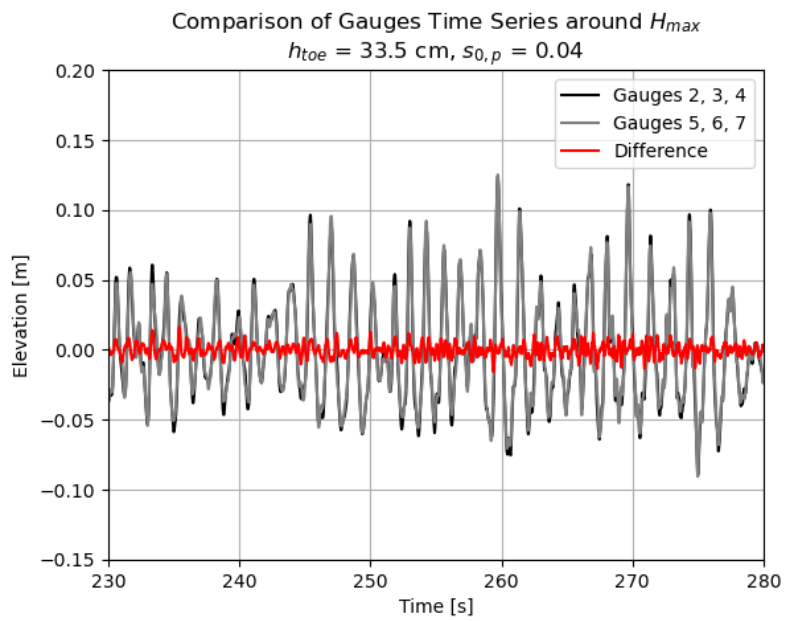


Figure 6.34. Gauges' total wave time series comparison around the epoch of H_{max} .

7. Discussion

This chapter provides a comparative analysis between the two designs devised in Section 3.2, focusing on their stability, constructability and production speed. Additionally, a comparison is drawn to previous research to contextualize the findings. Moreover, the impacts of the flume, wave steepness and wave programme variations are explored. This discussion provides an interpretation of the results objectively described in Chapter 6.

7.1. Design comparison and analysis

Firstly, the designs are compared based on their stability and constructability. Additionally, the performance is evaluated with respect to Xbloc.

7.1.1. Xbloc

Section 6.4 outlines the Xbloc roundhead test series. The first series consisted of a configuration with 0.02 wave steepness and a low water level. However, the packing density of the model was estimated to be relatively low compared to recommendations by DMC. The concluded stability number was 2.00. Failure occurred due to rocking and uplift-induced extraction of armour units. The packing density was increased for the second configuration, executed with a water level of $h_{toe} = 38.5 \text{ cm}$. However, the damage observed during Series 3.2 was not significant enough to satisfy the failure conditions described in Table 5.3. Therefore, a stability number exceeding 3.45 was obtained.

The two test series conducted with an Xbloc armour layer showed relatively ambiguous results for different water levels. Before interpreting these results in the following sections, the factors influencing the validity of the test series are discussed. Firstly, as previously mentioned in Section 6.4, the correction factor on unit weight to account for deep water conditions was underestimated for several critical test runs in the wave programme. However, with a design stability number of 2.54, hydraulic stability similar to the XblocPlus armour layers was to be expected.

Secondly, DMC imposes limitations on the maximum number of rows on the slope to limit possible settlements, set at 20 rows of Xbloc. When this criterion is exceeded, DMC recommends to increase the unit size or alternatively raise the toe level using a rock berm. However, approximately 22 rows of Xbloc armour units were required for the test configuration applied in this study. Consequently, settlements beyond the critical threshold may have occurred. Moreover, a minimum radius for the breakwater head section at the design water level is specified by DMC. This requirement is only roughly met by the roundhead model.

Thirdly, the validity of the Xbloc test results could have been influenced by the placement, which is based on a regular, diamond-shaped pattern with random unit orientations. Due to the staggered pattern, the packing density of Xbloc on the trunk of the structure can be assessed and compared to the design value defined by DMC. However, when units are placed on a roundhead or bend, D_x will decrease progressively when going up the slope and units should be left out occasionally (Ten Oever, 2017). Therefore, in combination with the more complex geometry of a roundhead, assessment of the packing density and comparison to the design value becomes more difficult. Although DMC proposes a range for the packing density, properties such as packing density, permeability and interlocking may vary within that range for each roundhead model iteration. According to Pardo et al. (2012), armour porosity and placement patterns affect the hydraulic stability, as well as wave reflection, run-up and

overtopping. Additionally, the units need to be placed sufficiently random to ensure interlocking, which is not always achievable as illustrated in Figure 7.1. Due to large settlements observed in Series 3.1, the packing density was increased for Series 3.2. However, Series 3.2 introduced a variation in test configuration by raising the water level at the toe, complicating stability comparison between the two series. Series 3.1 resulted in a stability number of 2.00, whereas Series 3.2 exceeded 3.45.



Figure 7.1. Unfavourable orientation of two Xbloc units due to a lack of randomness in placement in Series 3.1.

Two possible interpretations of these results are provided here. Firstly, the difference in stability numbers may originate from the varying degrees of interlocking caused by the discrepancy in packing density. The armour layer of Series 3.1 was constructed with a packing density ranging from 96 to 101 percent of the DMC recommendation. The packing density in Series 3.2 ranged from 101 to 106 percent. According to the placement requirements of DMC, the model should be constructed with a packing density between 98 and 102 percent of the design value. Compliance or exceedance of this criterion is possible for both series. However, the actual packing density is hard to determine. Therefore, the model should be tested further to provide a definitive assessment of the stability. Secondly, the discrepancy in stability could be attributed to the difference in water level. Higher water levels may mitigate negative influences of the narrow flume by providing a larger flow opening between the structure and flume wall, a point to be elaborated in Section 7.2.3.

7.1.2. Stability

In Section 4.3.1, Model 0 was described as a variant of Design 1 with a too large D_x compared to the digital model. Therefore, the model is not discussed further here.



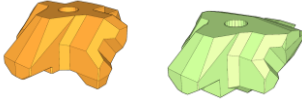
Model 1, previously described in Section 4.3.2, underwent six test series, including two configurations with waves of 4% steepness at varying water levels. In Series 1.1, no damage was recorded across all test runs, resulting in a stability number exceeding 3.48. In Series 1.3, damage was observed to two individual armour units after the 1.3 and 1.4 H_{m0} test runs. Both units were positioned around the 15th row of the grid, which was constructed with a larger D_x than the digital model, see Figure 4.6. Model 1 was designed with the placement grid based on support area as described in Section 3.1.5. As Figure 3.8 shows, D_x in XP-Base rows of this grid design is relatively large. An increase in D_x most likely led to a significant reduction of interlocking capabilities of the XP-Base armour units in the 15th row, as well as the XblocPlus atop. A stability number of 2.88 was concluded, but the armour layer remained stable for wave heights up to $H_{m0} = 12.79 \text{ cm}$ and $H_{max} = 20.83 \text{ cm}$.

A total of four test series were conducted with $s_{0,p} = 0.02$. Series 1.2.1 recorded a stability number of $N_s = 3.09$, after which failure occurred rather abruptly due to large magnitudes of

uplift. Damage originated from the unit depicted in Figure 6.6, but large influences of uplift were recorded beforehand. Series 1.2.2 showed comparable damage progression but failed prematurely at $N_s = 3.01$. Series 1.4.1 and 1.4.2 concluded stability numbers of 2.91 and 2.92 respectively, with occurrence of failure due to uplift. For both series, damage was initiated by displacement or extraction of XP-Base units and was located close to the flume wall.

Model 2 (see Section 4.3.3) underwent four test series. No damage was observed in Series 2.1, concluding $N_s > 3.31$. In Series 2.2, damage occurred at $H_{m0} = 9.88 \text{ cm}$. The damage originated from the rotation and subsequent extraction of an XP-Base unit and progressed due to uplift. Due to missing data of the $0.8 H_{m0}$ test run, no factual stability number can be concluded. However, an approximation can be provided based on the significant wave height gauged in Series 1.2, resulting in $N_s = 1.96$. In Series 2.3, at $s_{0,p} = 0.04$ and $h_{toe} = 38.5 \text{ cm}$, damage to two individual XP-Base units was observed due to a lack of interlocking. The armour layer remained stable for wave heights up to 12.83 centimetres. However, significant 'damage, no failure' occurred in an earlier stage, resulting in a stability number of 2.83. No damage was observed in Series 2.4 up to a stability number of 2.52, after which failure occurred due to uplift. See Table 7.1 for a summary of the concluded stability numbers for all armour layer configurations.

Table 7.1. Concluded stability numbers of Xbloc, Model 1 and Model 2.

Model	Configuration	$s_{0,p}$ [-]	$\frac{h_{toe}}{H_{s,d}}$ [-]	N_s [-]
Xbloc		0.02	3.38	2.00
		0.02	3.89	≥ 3.45
1		0.04	3.38	≥ 3.48
		0.02	3.38	$2.72 \leq N_s \leq 3.09$
		0.04	3.89	2.88
		0.02	3.89	2.91
2		0.04	3.38	≥ 3.31
		0.02	3.38	1.96
		0.04	3.89	2.83
		0.02	3.89	2.52

Note. The water depth at the toe is expressed as a ratio to the design significant wave height to enhance reproducibility in different test configurations.

Both armour unit configurations show similar stability for waves with 4% steepness. No damage was observed at a toe water level of $3.38 H_{s,d}$ and only minor displacements or rotations without failure for $h_{toe} = 3.89 H_{s,d}$. Notably, damage in both cases was either caused by or associated with XP-Base units. However, differences between the models are observed based on the test series with $s_{0,p} = 0.02$. Model 1 showed superior stability compared to Model 2 for a toe water level of $3.38 H_{s,d}$. Failure occurred in both armour layers due to uplift, but Model 1 outperformed Model 2 by approximately 20 percent of $H_{s,d}$. For example, failure occurred in the $1.0 H_{m0}$ test run of Series 2.2 due to the extraction of two column-positioned armour units. Similarly, failure occurred in Series 2.4 with four units. In contrast, Series 1.4.1 and 1.4.2 experienced failure due to uplift at the $1.3 H_{m0}$ test run. The difference in stability at $s_{0,p} = 0.02$ could be attributed to the increased packing density of Model 2 and the corresponding reduction in permeability, making the structure more viable to effects of uplift.

Overall, Model 1 demonstrated greater stability compared to Model 2. Besides increased permeability, this difference could be attributed to the higher interlocking capabilities facilitated by the inclusion of XblocPlus units in Model 1. The absence of lateral support at the bottom of XP-Base introduced the unit as a potential weakness in the grid, with six out of eight failed configurations credited or related to XP-Base. The increased number of XP-Base rows in the sequence of Model 2 introduced more weak areas on the roundhead, especially where the units are positioned in a column. For example, failure of two individual column-positioned units occurred during Series 2.3, as depicted in Figure 7.2. Model 2 contained 35 pairs of column-positioned XP-Base and XP-Curve, whereas this phenomenon occurred only 13 times in Model 1. Moreover, Model 2 had forward unit rotations closer to the ideal value for 3:4 slopes, see Figure 3.14. Therefore, the interlocking capabilities of Model 1 should be significantly larger to compensate this disadvantage and still exhibit higher levels of stability.



Figure 7.2. Rotation out of the armour layer of two individual column-positioned XP-Base units during Series 2.3.

7.1.3. Constructability

Section 3.2 outlined the construction advantages and disadvantages of both designs. Production of Design 1, comprising three unique types of armour units, is more challenging compared to Design 2. Additionally, unit placement is simplified for the latter due to a reduced number of distinct types. However, due to the larger forward rotations of this model, the placement of the armour units was deemed more challenging compared to Model 1. Furthermore, the increased number of rows without pattern placement in Model 2 complicated unit placement and resulted in reduced construction speed. Moreover, the packing density of Model 2 was increased to enhance interlocking between XP-Base units as discussed in Section 6.3, resulting in higher concrete consumption.

As Figure 4.6 shows, all constructed models display larger separations (D_x) than initially planned in the design, according to the measurements based on photo analysis. Therefore, if these values are deemed reasonably accurate, the constructability of the designs in the prototype would be questionable, as additional difficulties are introduced due to wind and wave climates, underwater visibility and the equipment available (Pardo et al., 2012). However, D_x and its assessment method should be investigated further to ensure accuracy as the method applied in this study was deemed a rough estimation.

7.2. Analysis of test influences

The following section provides an analysis and subsequent interpretation of the test influences which were assessed using different methods. The discussed factors include, amongst others, wave steepness, water level and the wave flume.

7.2.1. Wave steepness

The test programme for both models included two distinct values of wave steepness, $s_{0,p} = 0.02$ and $s_{0,p} = 0.04$. According to the EurOtop Manual (2007), these values correspond to swell and wind sea states, respectively. The measured wave steepness closely matched the theoretical wave steepness as shown in Figure 7.3a. However, outliers were observed for $s_{0,p} = 0.02$ in the erroneous test runs of Series 1.2.1 and 1.4.1. Moreover, differences in wave breaking were observed between wave steepness values of 0.02 and 0.04, as illustrated in Figure 7.3b. This figure displays the correlation between deep water wave steepness and the corresponding wave steepness observed in front of the structure. Notably, a higher incidence of wave breaking was observed on the transition slope and foreshore for wave steepness of 0.04. Moreover, a significant reduction in the maximum wave height (H_{max}) was observed for wave steepness of 0.04 in comparison to 0.02, see Figure 7.4.

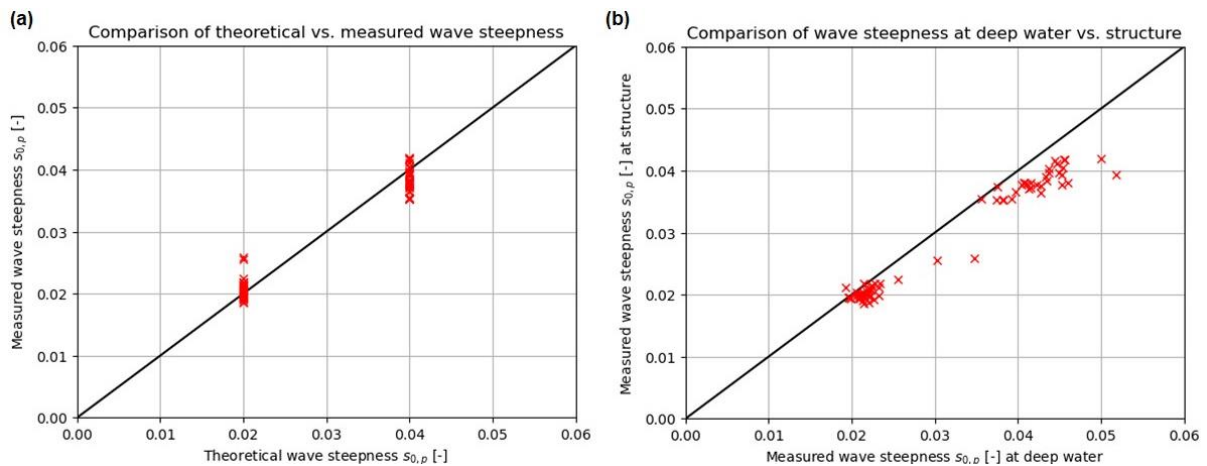


Figure 7.3. (a) Comparison of theoretical vs. measured wave steepness and (b) correlation between local steepness and deep water steepness based on peak period.

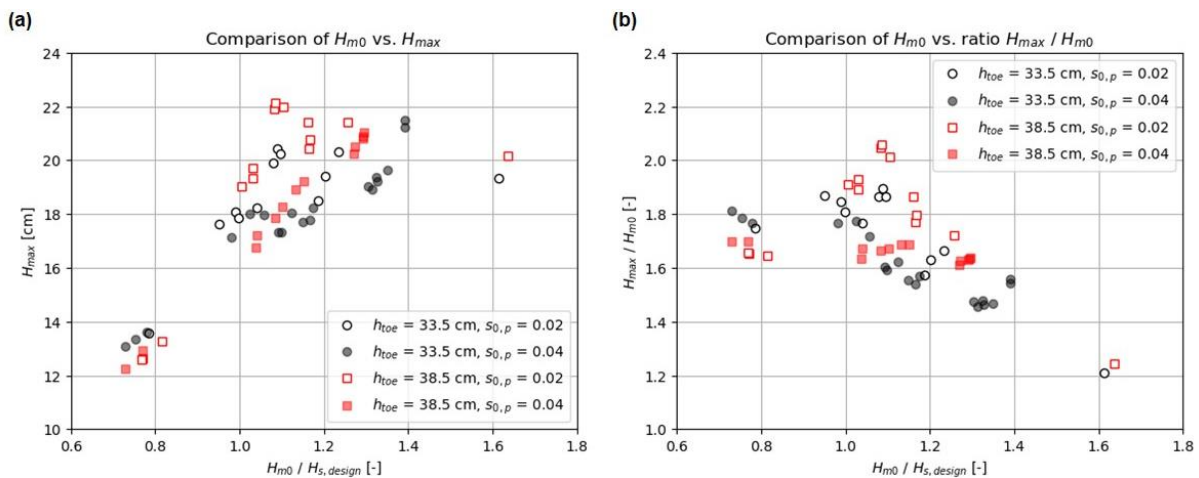


Figure 7.4. Comparison of (a) H_{m0} vs. H_{max} and (b) H_{m0} vs. ratio H_{max} / H_{m0} .

The findings from Muttray and Reedijk (2012) suggest a normative wave steepness of 0.02 for single-layer armour as opposed to 0.04. They observed a 20 percent reduction in armour layer stability when the wave steepness decreased from 0.04 to 0.02. Similarly, Model 1 experienced a stability reduction ranging from 11 to 22 percent at $h_{toe} = 3.38 H_{s,d}$. Stability remained relatively consistent at the higher water level for Model 1, likely due to premature failure in the 15th row which was constructed with too large D_x . Conversely, a reduction of 41 percent in stability was noted for the lower water level when wave steepness decreased from 0.04 to 0.02 for Model 2. At $h_{toe} = 3.89 H_{s,d}$, a decrease of 11 percent in stability was observed. These results suggest confirmation of the normativity of 0.02 steepness as found by Muttray and Reedijk (2012), as well as De Raad (2021). However, note should be taken to the maximum wave heights achieved from the spectra, depicted in Figure 7.4. Due to the test configuration, i.e. the transition slope and foreshore, more wave breaking was observed for 0.04 wave steepness compared to $s_{0,p} = 0.02$. This becomes particularly evident when applying least squares regression, a method fitting a line that minimizes the sum of the squared vertical distances between the line and the points, to the data of Figure 7.4, see Figure 7.5. For $h_{toe} = 3.38$, similar H_{max} is achieved during 0.04 wave steepness test runs at roughly 20 percent higher H_{m0} compared to $s_{0,p} = 0.02$. This effect is reduced for a water level increase, see Figure 7.5b.

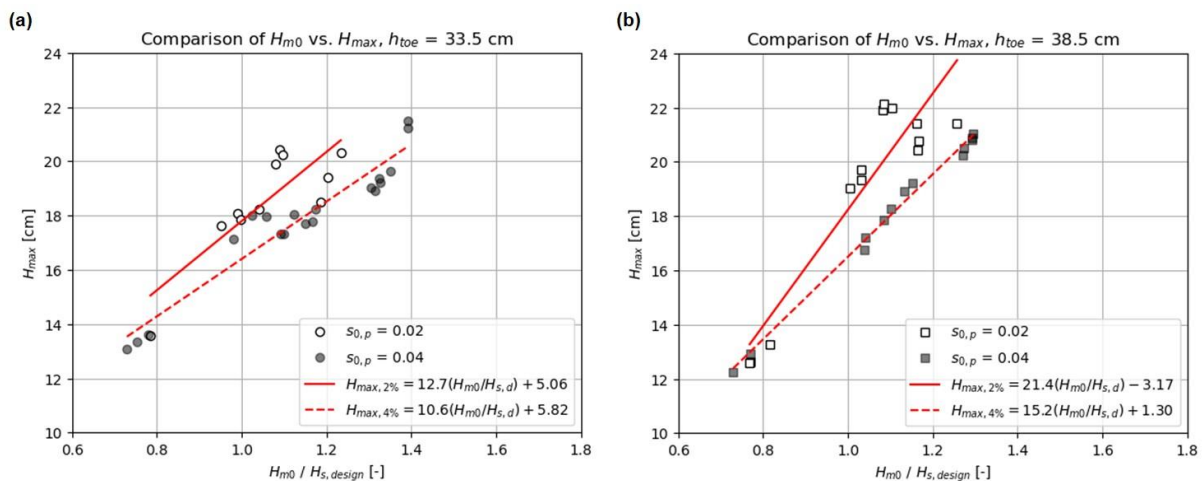


Figure 7.5. Comparison of H_{m0} vs. H_{max} for (a) h_{toe} of 33.5 cm and (b) h_{toe} of 38.5 cm with fitted least squares regression line.

Besides differences in stability, wave steepness also influenced the failure mechanisms observed in the armour layer. Waves with a steepness of 0.02 primarily led to failure induced by uplift, resulting from the difference in water levels inside and outside the structure. This phenomenon causes outward-directed forces which bulge the armour layer. Failure occurred when the outward forces surpassed the stabilizing forces of interlocking. This failure mechanism typically occurred abruptly. Conversely, failure at 0.04 wave steepness was predominantly attributed to wave impact – a brief yet intense inward-directed pressure exerted by waves upon plunging onto the slope. This mechanism often led to gradual failure characterized by the rotation or displacement of individual armour units. Damage resulting from this mechanism is typically less concentrated compared to failure at 0.02 steepness and tends to occur predominantly at weak areas of the section. Conversely, failure at 0.02 steepness primarily manifests at section 3, with progression towards sections 2 or 4.

7.2.2. Water level

The wave programme described in Chapter 5 included two distinct water levels to evaluate the roundhead's stability at different waterline radii. Particularly, this test configuration was applied to assess its resistance to instability towards the crown where less interlocking is expected due to increased variability in unit rotation around the vertical axis. This expectation proved largely

accurate for 0.04 wave steepness, as units with greater differences in vertical axis rotation were more prone to rotations and displacement following brief and intense impacts. For $s_{0,p} = 0.04$, the stability decreased for both models when the water level increased. In contrast, the stability remained largely unaffected by water level increases for 0.02 steepness, and in the case of Model 2 even showed signs of improvement. Hald (1998) observed a reduction in peak force with decreasing water depth, attributing this phenomenon to the diminishing impact of the flow reversal when downrush encounters the subsequent wave. This reduction in force is primarily due to the decelerating effect caused by the limited water depth. Therefore, it would have been expected that observed stability was lower for increasing water level. According to the findings of Hald (1998), this holds particularly true for waves with 0.02 steepness. Additionally, higher water levels correspond to smaller waterline radii, which, according to the hypothesis described in Section 5.2, are expected to display lower stability due to higher differences in rotation around the z-axis. However, as aforementioned, the stability of the armour layer at 2 percent steepness did not exhibit strong dependence on the water level. This could possibly be attributed to the influences of the wave flume, as the flow area between the structure and flume wall is significantly smaller for low water levels. Hence, the forces are increased due to higher flow velocities and the push-up of the waterline against the flume wall. This theory will be elaborated further in the following section.

7.2.3. Wave flume

Wolters et al. (2009) advocates for the utilization of 3D physical model tests for evaluating three-dimensional structures like roundheads. However, given the availability of a 2D wave flume, this thesis primarily conducts principle tests within this constraint. To assess the impact of the wave flume on the test outcomes quantitatively, comprehensive testing in a basin would be necessary. Nonetheless, it is feasible to qualitatively describe this influence based on observations during the tests and theoretical considerations.

As previously discussed, the expectation based on theory suggests that stability tends to increase as water levels decrease. However, findings from Xbloc Series 3.2, previously described in Section 6.4.2, and the high water level series of the XblocPlus configurations contradict this expectation, as stability either remained constant or even increased with rising water level at 0.02 wave steepness. One possible interpretation of this phenomenon can be explained as follows. A comparison of test runs conducted with $s_{0,p} = 0.02$ and low water levels for Xbloc, Model 1 and Model 2 reveals that Model 1 demonstrates superior stability. Both Xbloc and Model 2 experienced failure at $1.0 H_{m0}$, corresponding to significant wave heights of 9.84 and 9.83 cm, respectively. However, Model 1 remained stable until 11.91 cm, representing a 20 percent difference of the design wave height. This would suggest that Model 1 offers greater stability on a roundhead compared to Xbloc designed according to the guidelines. However, as discussed in Section 7.1.1, Xbloc's unit weight was designed with an underestimated correction factor. Nonetheless, the design stability number of the Xbloc armour layer was equal to 2.54, a value comparable to the XblocPlus armour layers.

As the water level increased, the observed stability of the XblocPlus armour layers either remained unchanged or improved, which is contrary to the expectations described by Hald (1998). This phenomenon could be attributed to the influences of the flume. For higher water levels, the flow opening between the flume wall and the structure significantly increases in area by up to 50 percent. Consequently, the disadvantageous effects of the wave flume on the stability of the structure decrease, leading to increased stability. This would explain the results of the Xbloc series when the assumption is made that both Xbloc models maintained a packing density within the range prescribed by DMC. However, this effect is not observed in the XblocPlus armour layers. Based on this interpretation, the conclusion can be drawn that the configuration of Model 1 demonstrates significantly greater stability on a roundhead compared to Xbloc, and that higher water levels, or alternatively smaller waterline radii, have a negative impact on its stability.

7.2.4. Wave programme

The structure was constructed in the wave flume on top of a foreshore with transition slope, see Figure 4.1. The foreshore was installed to raise the structure to obtain deep water conditions at the toe. However, the influence of the foreshore on the wave climate was not known beforehand. As described in Section 5.1.2, a multiplication factor was applied to the input of the wave paddle to compensate for the difference in intended and measured wave production. Typically, calibration tests are conducted for this purpose. However, no calibration tests were executed due to time limitations. The multiplication factors were determined during the model test series, which led to differences between the intended and actual wave heights (Appendix C), see Figure 7.6.

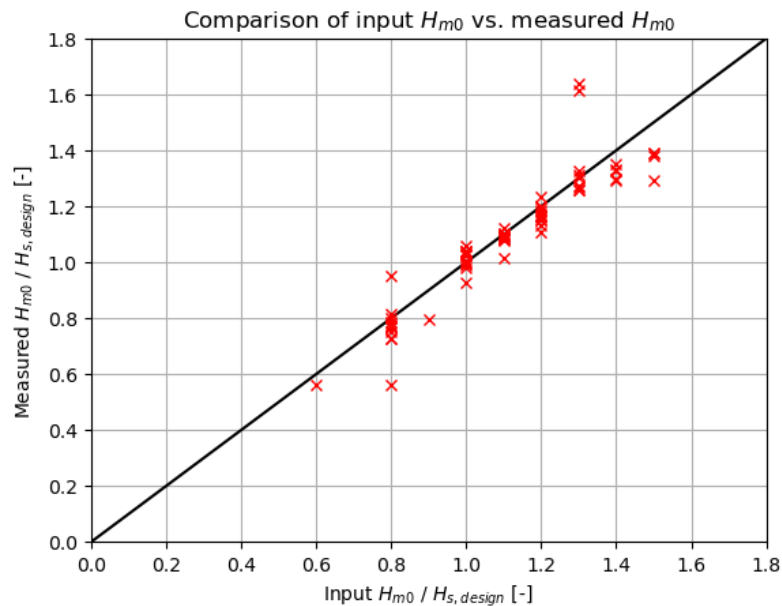


Figure 7.6. Comparison between the intended and measured wave heights.

7.2.5. Wave direction

Due to the orientation of the roundhead in the wave flume, the waves approached the structure at a 90-degree angle. As previously described in Chapter 2, the section with heaviest impact is typically situated on the leeward side of the structure (Van den Bos & Verhagen, 2017). Due to the angle of incidence, the waves refract towards the leeward side, potentially leading to an increase of wave loads due to rotary motion. Furthermore, the structure experienced overtopping when the highest waves in the spectrum exceeded the freeboard, further increasing the loads on the leeward side.

7.2.6. Armour units

As described in Section 4.4, the armour units used in this study were specifically produced for the research conducted in this thesis. Moulds were created from casting rubber and the units were constructed by filling these moulds with mortar. Initially, a mortar recipe with a density closely matching that of the XblocPlus units (2360 kg/m^3) was not available. Consequently, the units exhibit a density distribution as illustrated in Figure 4.14. However, stability numbers were determined based on the density and nominal diameter of the XblocPlus units. As a result, the stability numbers of the produced units vary slightly. Nonetheless, the variability was marginal, leading to relatively narrow confidence intervals as described in Table 7.2.

Table 7.2. Confidence intervals of sampled variables and the corresponding stability numbers.

Armour unit	\bar{m} [g], $CI_{95\%}$	\bar{V} [cm ³], $CI_{95\%}$	$\bar{\rho}$ [g/cm ³], $CI_{95\%}$	$\bar{N}_{s,d}$ [-], $CI_{95\%}$
XP-Base	52.2 (51.9, 52.4)	21.9 (21.8, 22.0)	2.38 (2.37, 2.39)	2.57 (2.55, 2.58)
XP-Curve (version 2)	57.0 (56.8, 57.2)	23.9 (23.8, 24.0)	2.38 (2.37, 2.39)	2.49 (2.48, 2.50)
XP-Curve (version 3)	53.9 (53.7, 54.1)	22.7 (22.6, 22.8)	2.37 (2.36, 2.38)	2.55 (2.53, 2.57)

7.3. Performance in context of previous research

The stability of XP-Curve has been assessed on two different occasions. Firstly, Wiersma (2021) tested configurations with XP-Curve as a transitional element between two consecutive rows of XblocPlus. Secondly, De Raad (2021) validated the findings of Wiersma (2021), and tested an additional configuration consisting solely of XP-Curve. Due to the similar test configuration, the results obtained in this thesis are compared to those of Wiersma (2021) and De Raad (2021).

7.3.1. Stability

The findings of Wiersma (2021) were previously described in Section 2.4.1. Wiersma (2021) observed failure in two subsequent tests, both with $s_{0,p} = 0.02$. Additionally, two different water levels were applied. The first test, executed with a water depth of $h_{toe} = 2.62 H_{s,d}$, was stopped after failure of one XP-Curve unit during the $1.5 H_{m0}$ test run. The second test run ($h_{toe} = 2.87 H_{s,d}$) concluded with failure of three units at $N_s = 3.25$. However, wave climate data of the normative test run is missing in the report of Wiersma (2021). Therefore, this value cannot be compared and the newly devised configurations are solely compared to the results of De Raad (2021).

De Raad (2021) performed tests with the same armour layer configuration as Wiersma but with an increased water level of $h_{toe} = 3.03 H_{s,d}$. The water level was raised to reduce depth-limited wave breaking. The waterline was located at approximately the same level with respect to the roundhead due to the application of a raise using core material, similar to the method applied in this thesis. De Raad (2021) concluded a stability number of $N_s = 2.91$ after failure occurred due to rotation and uplift. Additionally, De Raad (2021) concluded a normative wave steepness of $s_{0,p} = 0.02$, as $s_{0,p} = 0.04$ resulted in a stability number of $N_s \geq 3.50$.

The results of De Raad (2021) are compared to the two models evaluated in this thesis. The normative test run of De Raad (2021) consisted of a configuration with 0.02 wave steepness, $h_{toe} = 3.03 H_{s,d}$ and failure occurring at $H_{m0} = 11.46$ cm at the toe. Damage was observed due to a combination of uplift and rotation of the units. Moreover, the damage was concentrated in an area corresponding to section 2 as illustrated in Figure 5.9. In a comparable test configuration, Model 1 exhibited a stability number ranging between 2.72 and 3.09. Failure occurred at $1.3 H_{m0}$, also due to influences of uplift. The sectional damage was distributed further towards the flume wall, predominantly in section 3. Model 2 proved less stable, with an estimated stability number of 1.96. The test configuration of De Raad (2021) consisted solely of a water depth of $h_{toe} = 3.03 H_{s,d}$, so direct comparison to the high water levels evaluated in this thesis is impeded. Thus, similar values of stability number were found in the normative series of De Raad (2021) and Model 1 of this thesis. However, the introduction of XP-Base in the configuration led to a notable reduction in failure occurring due to rotation of the armour

units. This phenomenon can be attributed to the additional interlocking provided by the legs. Nonetheless, weaknesses persist regarding XP-Base due to the lack of pattern-placement and frequent unfavourable positioning relative to the underlying units which is emphasized in Model 2.

7.3.2. Constructability

The configuration tested by De Raad (2021) was based on the same design as applied by Wiersma (2021). Neither of the reports investigated the transition of the roundhead to the trunk. However, this feature is incorporated in this study for both models, thereby enhancing constructability. Furthermore, constraints were encountered by Wiersma and De Raad regarding the maximum construction height. The previous design disallowed placement higher up the roundhead due to the narrowing radius. Therefore, the XP-Curve designs in this thesis proposed a reduction in width by 10 percent, allowing placement higher up the grid. The construction height is limited by the grid if the radius becomes too narrow for the placement of XP-Curve. Alternatively, XP-Base may need to be positioned with a D_x value so large that XP-Curve loses significant contact area. However, this scenario occurs higher up the grid compared to previous research due to XP-Curve's reduced width.

8. Conclusions and recommendations

In this final chapter, conclusions and recommendations are drawn from the result analysis and discussion of the previous chapters. The findings offer insights into the stability and applicability of XblocPlus or related armour units on roundhead configurations. Additionally, conclusions are drawn regarding the validity of the test configuration.

8.1. Conclusions

The main research question was defined as follows:

How could XblocPlus be redesigned to provide sufficient applicability and stability on breakwater roundheads?

The aim of this study was to explore ways to enhance the applicability and stability of XblocPlus and related concrete armour units on breakwater roundheads. The design built upon findings of previous research. Possible modifications to the unit shape and placement configuration were considered. The altered designs were subjected to physical model testing in a wave flume to evaluate the hydraulic stability, quantified by the stability number (N_s). However, roundheads are three-dimensional structures and testing them in a narrow 2D wave flume is not standard practice. The tests conducted in this thesis were considered as 'principle tests', aimed at obtaining an indication of the hydraulic stability and failure mechanisms of the devised armour unit designs. Furthermore, the limitations of the test configuration were assessed by positioning parallel gauge sets in front of the structure. This set-up allowed the observation of waves perpendicular to the wave attack originating from the reflection on the structure. Additionally, tests with Xbloc armour units were performed. The design of the Xbloc-armoured roundhead adhered to the design guidelines formulated by DMC. This test configuration served as a possible benchmark when tested in the same configuration.

8.1.1. Applicability

The preliminary design consisted of three potential armour units. Firstly, the conventional XblocPlus. Secondly, XP-Base, which is a concept under development by BAM Infraconsult specifically for application on the bottom row of XblocPlus armour layers. This unit features legs designed to enhance underlayer tolerances, see Figure 3.3. Thirdly, the XP-Curve, a variant of XblocPlus with modifications to the backside compared to the standard XblocPlus. This unit, depicted in Figure 3.4, originates from an earlier version previously examined by Wiersma (2021) and De Raad (2021).

The initial sequence outlined in the preliminary design encountered challenges when transitioning to a straight section. Consequently, two distinct modifications to the design were proposed. Firstly, a design retaining the same sequence but featuring an altered shape of the XP-Curve unit, termed Model 1 (see Figure 8.1a). In this adaptation, the tail length of XP-Curve was reduced by 3.5 percent, accompanied by an increase in the length of the top support surface. Placement distances for this model were determined based on the support area (Figure 3.7b) provided by the underlying units, aiming to match that of XblocPlus on a straight section with a separation of $D_x = 1.15 L_2$. Secondly, modifications were proposed to the sequence, utilizing only XP-Base and XP-Curve units in an alternating pattern as illustrated in

Figure 8.1b, labelled Model 2. The dimensions of the units remained unchanged. Placement involved positioning the units as closely together as possible to optimize the interlocking capabilities of XP-Base. The design introduced in this thesis offers several notable improvements regarding applicability:

- The reduction of XP-Curve's width by 10 percent allows for the placement of armour units on smaller radii, facilitating their positioning higher up the roundhead compared to previous design iterations.
- The alterations to the tail length and top support surface of XP-Curve in Model 1, as well as the sequence modification of Model 2, enable connection of 3:4 and 2:3 roundheads to the trunk, a feature that was not feasible with the previous design.

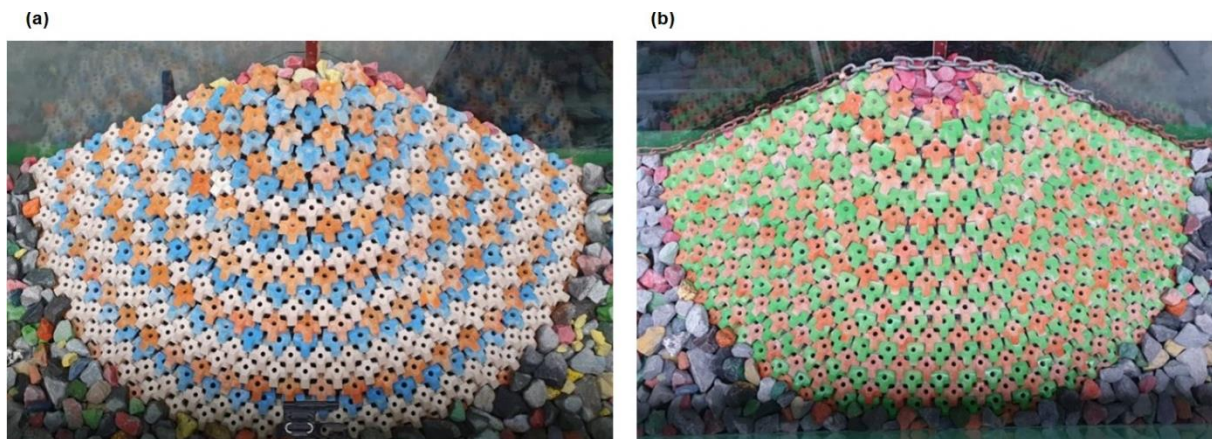


Figure 8.1. (a) Model 1 and (b) Model 2.

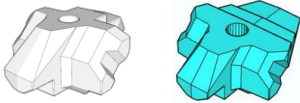

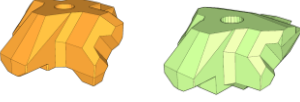
8.1.2. Stability

Both configurations underwent hydraulic testing with $s_{0,p} = 0.02$ and $s_{0,p} = 0.04$ waves, along with two water level variations. The normative steepness was $s_{0,p} = 0.02$, where failure was primarily attributed to uplift of the armour layer. Under these conditions, Model 1 demonstrated significantly greater stability compared to Model 2; Model 2 sustained no damage up to $N_s = 1.96$, whereas Model 1 exhibited stability ranging from 2.72 to 3.09 (see Table 8.1). Compared to the standard test series by De Raad (2021), which used a model of XblocPlus and XP-Curve at $s_{0,p} = 0.02$ with a stability number of 2.82, the newly devised configuration did not show improved stability of the armour layer. However, the following stability-related features can be concluded:

- The inclusion of the XP-Base unit in the configurations introduced in this thesis aimed to enhance interlocking compared to XblocPlus, particularly in rows without pattern placement. This addition resulted in a notable decrease in units failing due to rotation.
- The stability of XP-Base is normative for the hydraulic stability of both armour layer designs, with damage initiated by failure of XP-Base units in six out of eight test series where failure occurred.
- The interlocking of XP-Base is weakest when the unit is column-positioned (see Figure 7.2) with the underlying unit, one of the legs is not situated behind the supporting edge of XP-Curve or the unit's rotation around the y-axis is suboptimal with respect to the prescribed value.

- Model 1, featuring XblocPlus, exhibits superior interlocking capabilities compared to Model 2. Consequently, units can be spaced further apart, enhancing permeability and improving stability against uplift failure in Model 1 relative to Model 2.

Table 8.1. Concluded stability numbers of Model 1 and Model 2 in comparison to the reference test of De Raad (2021).

Model	Configuration	$s_{0,p}$ [-]	$\frac{h_{toe}}{H_{s,d}}$ [-]	N_s [-]
De Raad (2021)		0.02	3.03	2.82
1		0.04	3.38	≥ 3.48
		0.02	3.38	$2.72 \leq N_s \leq 3.09$
		0.04	3.89	2.88
		0.02	3.89	2.91
2		0.04	3.38	≥ 3.31
		0.02	3.38	1.96
		0.04	3.89	2.83
		0.02	3.89	2.52

Note. The armour units in the configurations from left to right. The reference test of De Raad (2021): XblocPlus, XP-Curve (version 1). Model 1: XP-Base, XblocPlus, XP-Curve (version 3). Model 2: XP-Base, XP-Curve (version 2).

8.1.3. Limitations

As previously discussed, conducting tests on a three-dimensional structure in a narrow wave flume deviates from common practice. Therefore, this thesis aimed to provide a qualitative description of the influences of the test configuration, as a quantitative assessment would necessitate testing in a basin for comparison.

To measure the presence of waves perpendicular to the incident wave attack, parallel gauges were positioned in front of the structure. Analysis of the distinct time series allowed for the assessment of observed differences. The average disparity between the gauged wave heights amounted to approximately 3 millimetres, while the maximum difference reached 2.05 centimetres. Although the maximum difference is notable, it falls within the margins of a principle test configuration as applied in this thesis. Moreover, the instances of maximum disparity did not coincide with the epoch of H_{max} , indicating that it is unlikely that these discrepancies occurred during a normative wave event. However, perpendicular waves caused by uneven reflection exerted an influence on the significant wave height. Therefore, the results should be interpreted within the specific test configuration.

Additionally, reference tests were conducted using Xbloc. The design of the Xbloc-armoured roundhead adhered to design guidelines defined by DMC. The units in these tests had a design stability number of 2.54, similar to the XblocPlus armour layers. At a water level of $h_{toe} = 3.38 H_{s,d}$, this configuration experienced premature failure at $H_{m0} = 9.90$ cm, concluding a stability number of $N_s = 2.00$. However, for the second test series the water level was increased to $3.89 H_{s,d}$. The stability number with this configuration exceeded 3.45. Therefore, definitive conclusions cannot be drawn from these test series.

8.2. Recommendations

The following section describes the recommendations formulated based on the previously stated conclusions. Implementation of the suggestions could potentially enhance the applicability and stability of XblocPlus or related concrete armour units on breakwater roundheads.

8.2.1. XP-Curve modifications

As described in Section 7.1.2, XP-Base emerged as a weakness in both configurations, with damage originating from failure of XP-Base units in six out of eight test series where failure occurred. This deficiency in stability is partially attributable to the decreased interlocking capabilities of XP-Base due to a lack of pattern-placement. This phenomenon was specifically notable where XP-Base and XP-Curve were column-positioned. To increase the interlocking of XP-Base within the grid, several modifications are proposed.

The current sequence entails positioning an XP-Base unit atop each row of XP-Curve. Consequently, alterations to XP-Curve will inherently influence the placement and stability of XP-Base. Hence, several modifications are suggested to XP-Curve. Firstly, modifications are suggested to the top support surface of XP-Curve. As aforementioned, XP-Curve was reduced in width by 10 percent to improve applicability and permeability. Additionally, an inclination was introduced to the top surface to enhance water dissipation. The latter was predominantly part of a design optimization. However, the effect was deemed marginal compared to the decrease in width. Nonetheless, the addition of the inclination significantly reduced the height of the edge supporting XP-Base atop. The decreased height of the support edge potentially contributed to the weaker degrees of interlocking observed for XP-Base. Therefore, the proposition is made to reconsider this modification by raising the edge to an optimized height and inclination angle, see Figure 8.2.

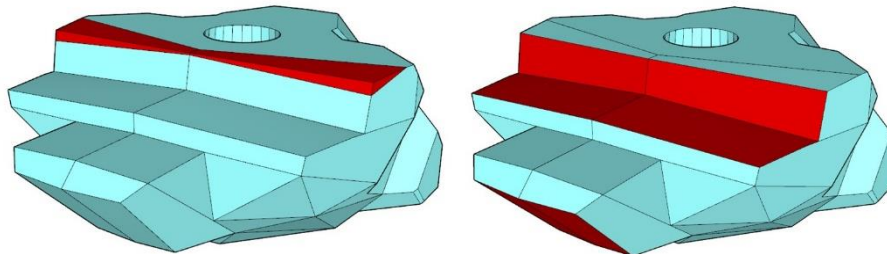


Figure 8.2. Proposed modifications to the edge supporting XP-Base atop, the top support surface and the length of XP-Curve.

The second design modification proposed for XP-Curve comprises the rotation around the y-axis. As aforementioned, Model 2 had forward rotations of the armour units relatively close to the prescribed value for XblocPlus on the trunk (2.75 degrees), as depicted in Figure 3.14. However, Model 1 showed notable differences. XblocPlus generally rotated further forwards due to dimensions unsuited for roundhead applications. Conversely, XP-Base and XP-Curve rotated slightly further backwards. As previously stated in the conclusions, the rotation around the y-axis of XP-Base is expected to influence the interlocking of the unit. Therefore, the proposition is made to optimize the aforementioned design variables of XP-Curve to better approximate the ideal unit rotation. This alteration could possibly increase the friction and interlocking between the units, which would improve hydraulic stability. Additionally, these parameters should be investigated further to enable generalized application on different breakwater slopes and configurations.

8.2.2. XP-Base modifications

The column-positioning of XP-Base and XP-Curve was identified as a potential weakness in the armour layer due to decreased interlocking. Therefore, modifications to XP-Base are

proposed. The suggested alteration involves widening XP-Base to ensure interlocking of both legs behind two individual XP-Curve units below. This modification should reduce the amount of XP-Base units failed due to rotation of one or both legs as observed multiple times in both models during the test series. Additionally, the modification reduces the amount of column-positioned units in the grid. The new XP-Base unit should be investigated regarding applicability. Furthermore, the transition to the trunk should be reconsidered.

8.2.3. Placement grid modifications

The design of Model 1 was based on a placement philosophy which aimed to approximate the support area of XblocPlus on the trunk placed with $D_x = 1.15 L_2$. This criterion allowed the placement of XblocPlus for a larger number of rows and smaller radii with respect to other configurations. However, the design was continued on rows where XblocPlus lost applicability and the pattern was reduced to alternating XP-Base and XP-Curve. Applying the same philosophy to this alternating pattern will inherently decrease the support area of XP-Curve on the underlying XP-Base due to the reduced width of XP-Curve. Based on the same observation, the packing density of Model 2 was increased after Series 1. Therefore, the proposition is made to adjust the placement distances between units after the last possible row of XblocPlus. Closer packing should increase the interlocking of the units. Using Model 1 as a reference, it is noted that the high water level was situated at the last row of XblocPlus. Consequently, the rows of units above experience progressively less uplift, suggesting that increasing the packing density and subsequently reducing permeability should not present significant challenges. However, the prototype constructability of a grid with increased packing density should be investigated further in future research, as D_x exceeded the design values in the constructed models (see Figure 4.6). Additionally, the placement criterion applied to D_x should be optimized to enhance interlocking and possibly decrease column-positioning of units.

8.2.4. Flume influence

A method applied to assess the influence of the wave flume was testing an Xbloc-armoured roundhead in the same test configuration. However, the results yielded ambiguity as significant variations were observed in the stability numbers. Therefore, the proposition is made to conduct additional tests with this configuration prior to conducting basin tests. A higher number of repetition tests could help mitigate the impact of the random unit orientations previously described. Furthermore, the packing density of the units on the roundhead should be investigated closer to adhere to the guidelines posed by DMC. When repetition tests are executed with this configuration, it is advised to repeat the normative test series of Model 1 to ensure consistency.

8.2.5. Basin tests

If the aforementioned assessment method suggests that testing in a narrow wave flume is conservative, the recommendation would be to proceed with basin testing for Model 1, where flume effects are minimized. If not, the advise would be to further optimize the configuration to increase stability. Two alternatives are discussed in the following sections.

8.2.6. Transition

The designs in this thesis are devised to be applied using units of the same size as those on the trunk. An alternative approach to implementing the design proposed in this thesis on a breakwater roundhead involves transitioning the armour size before reaching the roundhead. This would result in the roundhead units being over-dimensioned compared to those on the trunk. Therefore, the stability would be enhanced, allowing the application of the design while ensuring adequate safety margins. Similar transitions in the armour layer are already employed by DMC between various types of armour units, including rock armour, Xbloc and XblocPlus, as well as between units of different sizes.

8.2.7. Density

Alternatively, the density of the concrete armour units could be increased. The denser units would be applied following the design philosophy of Model 1, with the higher density increasing hydraulic stability. It is recommended to evaluate this alternative by an economical optimization, considering production costs and concrete consumption.

8.2.8. Breakwater slope

The design proposed in this thesis was developed to accommodate both 3:4 and 2:3 roundhead slopes, while enabling a transition to the trunk. However, hydraulic tests were conducted exclusively on a 3:4 breakwater slope. Therefore, it is advisable to validate the stability of the design on a 2:3 slope, and potentially on additional slopes as well, to ensure its applicability across various slope configurations.

References

- Bakker, P., Jacobs, R., Van De Koppel, M., Reedijk, B., & Muttray, M. (2019). Hydraulic stability and practical application of XBlocPlus breakwater armouring. *Coastal Structures*, 98–109. https://doi.org/10.18451/978-3-939230-64-9_011
- Burcharth, H. (1992). *Reliability evaluation of a structure at sea*. TU Delft Repositories. <http://resolver.tudelft.nl/uuid:22243a72-a728-4649-97c1-bd1013d7f876>
- Burcharth, H. F., & Andersen, T. L. (2009). Scale Effects Related to Small Scale Physical Modelling of Overtopping of Rubble Mound Breakwaters. *Coastal Structures*. https://doi.org/10.1142/9789814282024_0135
- CIRIA, CUR, & CETMEF. (2012). *The Rock Manual. The use of rock in hydraulic engineering* (2nd ed.). C683, CIRIA. (Original work published 2007)
- De Raad, O. (2021). *Onderzoek naar de toepassing van de XblocPlus op een golfbrekerkop* [Bachelor Thesis]. De Haagse Hogeschool.
- DMC. (2018, July 3). *XblocPlus at the ICCE*. Delta Marine Consultants. <https://www.dmc.nl/news/2018/7/xblocplus-icce>
- Donnelly, J. P., Bakker, P., Reedijk, B., & Qian, Y. Z. (2020). XBLOC-PLUS: THE INTERLOCKING, PATTERN PLACED AND EFFICIENT ARMOUR UNIT. *Proceedings of . . . Conference on Coastal Engineering*, 36v, 18. <https://doi.org/10.9753/icce.v36v.structures.18>
- Hald, T. (1998). *Wave Induced Loading and Stability of Rubble Mound Breakwaters*. Hydraulics & Coastal Engineering Laboratory, Department of Civil Engineering, Aalborg University.
- Holthuijsen, L. H. (2007). *Waves in Oceanic and Coastal Waters*. Cambridge University Press.
- Introduction of the new XblocPlus*. (2018, June 4). Delta Marine Consultants. Retrieved November 17, 2023, from <https://www.dmc.nl/news/2018/6/introduction-new-xblocplus>

- Janssen, D., Aarninkhof, S. G. J., Hofland, B., Van Den Bos, J. P., & Reedijk, B. (2018). *Stability analysis of XblocPlus crest element* [Master Thesis]. Delft University of Technology.
- Jensen, O. J. (1984). *A Monograph on Rubble Mound Breakwaters*. Danish Hydraulic Institute.
- Kaneko, S., Nakamura, T., Inada, F., Kato, M., Ishihara, K., Nishihara, T., & Langthjem, M. A. (2014). Flow-Induced Vibrations: Classifications and Lessons from Practical Experiences. In *Elsevier eBooks* (2nd ed., pp. 359–401). Elsevier Ltd.
<https://doi.org/10.1016/C2011-0-07518-X>
- Latham, J., Xiang, J., Anastasaki, E., Guo, L., Karantzoulis, N., Viré, A., & Pain, C. C. (2014). NUMERICAL MODELLING OF FORCES, STRESSES AND BREAKAGES OF CONCRETE ARMOUR UNITS. *Proceedings of . . . Conference on Coastal Engineering*, 1(34), 78. <https://doi.org/10.9753/icce.v34.structures.78>
- Mansard, E., & Funke, E. (1980). *The Measurement of Incident and Reflected Spectra Using a Least squares Method*. TU Delft Repositories. <http://resolver.tudelft.nl/uuid:840a64af-b113-4372-8f91-47b4d7a3cc78>
- Mares-Nasarre, P., Argente, G., Gómez-Martín, M. E., & Medina, J. R. (2021). Armor damage of overtopped mound breakwaters in Depth-Limited Breaking wave conditions. *Journal of Marine Science and Engineering*, 9(9), 952.
<https://doi.org/10.3390/jmse9090952>
- Muttray, M., & Reedijk, B. (2012). Stability of Low Crested and Submerged Breakwaters with Single Layer Armouring. *Journal of Shipping and Ocean Engineering*, 2.
- Muttray, M., Reedijk, B., & Klabbers, M. (2003). *Development of an Innovative Breakwater Armour Unit*.
- Pardo, V., Herrera, M. P., Molines, J., & Medina, J. R. (2012). Placement grids, porosity and randomness of armor layers. *Coastal Engineering Proceedings*, 1(33).
<https://doi.org/10.9753/icce.v33.structures.37>

- Pullen, T., Allsop, N. W. H., Bruce, T., Kortenhaus, A., Schüttrumpf, H., & Van Der Meer, J. W. (2007). *EurOtop wave overtopping of sea defences and related structures: assessment manual*.
- Rapp, B. E. (2017). *Microfluidics: Modeling, Mechanics and Mathematics*. Elsevier Ltd.
- Reedijk, B., Eggeling, T., Bakker, P., Jacobs, R. M., & Muttray, M. (2018). HYDRAULIC STABILITY AND OVERTOPPING PERFORMANCE OF A NEW TYPE OF REGULAR PLACED ARMOR UNIT. *Proceedings of . . . Conference on Coastal Engineering*, 1(36), 54. <https://doi.org/10.9753/icce.v36.structures.54>
- Reedijk, B., & Muttray, M. (2008). *Design of Concrete Armour Layers*. Delta Marine Consultants.
- Reedijk, B., & Muttray, M. (2023, May 10). *Concrete Breakwater Armour Units . . . and Xbloc / XblocPlus* [Slide show].
- Ruwiel, T., Antonini, A., Janssen, D., Uijtewaal, W., Reedijk, B., & Van De Koppel, M. (2020). *Crest stability of XblocPlus armoured low crested breakwaters* [Master Thesis]. Delft University of Technology.
- Smith, P. (2016). Design and specification of marine concrete structures. In *Elsevier eBooks* (pp. 65–114). <https://doi.org/10.1016/b978-0-08-100081-6.00003-9>
- Ten Oever, E. (2017). *Instruction Xbloc Model Testing*. Delta Marine Consultants.
- USACE. (1984). *Shore Protection Manual* (Vols. 1–2). Dept. of the Army, Waterways Experiment Station, Corps of Engineers, Coastal Engineering Research Center.
- Van De Koppel, M., Qian, Y. Z., Bakker, P., Bruins, R., & Swewczak, T. (2023). FIRST APPLICATIONS OF XBLOCPLUS: EXPERIENCES FROM AFSLUITDIJK AND VISTULA SPLT PROJECTS. *Proceedings of . . . Conference on Coastal Engineering*, 37, 79. <https://doi.org/10.9753/icce.v37.structures.79>
- Van Den Bos, J. P., & Verhagen, H. J. (2017). *Breakwater design: Lecture notes CIE5308* (2017th ed.).
- Van Der Lee, A. (2020). *Instruction XblocPlus 2D-Model Testing*. Delta Marine Consultants.

- Van Der Meer, J. W. (1998). Application and stability criteria for rock and artificial units. In *Van Der Meer Consulting B.V.* Retrieved December 14, 2023, from http://www.vandermeerconsulting.nl/downloads/stability_b/1998_vandermeer_ch11.pdf
- Van Gent, M. R. A. (1995). Porous Flow through Rubble-Mound Material. *Journal of Waterway, Port, Coastal, and Ocean Engineering*, 121(3), 176–181.
- Vos, A. B. (2017). *Exploration into the mechanisms that govern the stability of an XblocPlus armour unit* [Master Thesis]. Delft University of Technology.
- Wiersma, T. (2021). *Toepassing XblocPlus op een golfbrekerkop* [Bachelor Thesis]. Amsterdam University of Applied Sciences.
- Wolters, G., Van Gent, M., Allsop, W., Hamm, L., & Muhlestein, D. (2009). *HYDRALAB III: Guidelines for physical model testing of rubble mound breakwaters* (pp. 559–670).
- Wolters, G., Van Gent, M. R., Hofland, B., & Wellens, P. (2014). Wave damping and permeability scaling in rubble mound breakwaters. *Coastlab 2014*.
- Woodward-Clyde Consultants. (1980). *Assessment of the Morison Equation*. Civil Engineering Laboratory, Naval Construction Battalion Center.
- Xbloc. (n.d.). Xbloc. <https://www.xbloc.com/our-blocks/xbloc>
- Xbloc. (2023). *Xbloc & XblocPlus Design Guidelines 2023*.

A. Theoretical Background

This appendix provides additional explanations to the terms, variables and theories mentioned and referenced throughout this report.

A.1. Wave Theory

Coastal structures are subject to random ocean waves, which can be described based on the notion of summing a large number of independent harmonic waves. Linear theory for surface gravity waves describes in detail such harmonic waves. Linear wave theory is based on two fundamental equations describing certain kinematic and dynamic aspects of waves which are linearised. The theory, also known as Airy wave theory (Airy, 1845), holds when amplitudes of the waves are small compared to the wave length and water depth (Holthuijsen, 2007). The distinction can be made between oceanic- and coastal waters, depending on the water depth, wave length or wave number. The criterion is formulated as follows:

- Deep waters:

$$\frac{d}{L} > 0.5 \quad (\text{A.1})$$

- Intermediate waters:

$$0.05 < \frac{d}{L} < 0.5 \quad (\text{A.2})$$

- Shallow waters:

$$\frac{d}{L} < 0.05 \quad (\text{A.3})$$

A.1.1. Oceanic waters

Linear wave theory is developed assuming an ideal fluid with only Earth's gravitation inducing forces (Holthuijsen, 2007). Except for extreme situations, e.g. when waves are steep, this assumption holds. The mass- and momentum balance equation are the basis for the theory, which, when linearised and specific boundary conditions are applied, result in the Laplace equation:

$$\frac{\partial^2 \Phi}{\partial x^2} + \frac{\partial^2 \Phi}{\partial y^2} + \frac{\partial^2 \Phi}{\partial z^2} = 0 \quad (\text{A.4})$$

The Laplace equation can be solved analytically with particular kinematic boundary conditions, resulting in a long-crested harmonic wave propagating in the positive x-direction with corresponding phase speed c :

$$\eta(x, t) = a \sin(\omega t - kx) \quad (\text{A.5})$$

$$c = \frac{\omega}{k} = \frac{L}{T} \quad (\text{A.6})$$

The formula is expressed in terms of the amplitude $a = \frac{H}{2}$, the radian frequency $\omega = \frac{2\pi}{T}$ and the wave number $k = \frac{2\pi}{L}$, with T the wave period and L the wave length. For deep waters, i.e. when $kd \rightarrow \infty$, the particle velocity components are described as:

$$\hat{u}_x = \hat{u}_z = \omega a e^{kz} \quad (\text{A.7})$$

The expression shows that wave-induced velocities decrease exponentially with the distance to the surface and the particles move in circles. When the free-wave condition is invoked for the above results for the kinematic aspects, the dispersion relationship is obtained:

$$\omega^2 = gk \tanh(kd) \quad \text{or} \quad L = \frac{gT^2}{2\pi} \tanh\left(\frac{2\pi d}{L}\right) \quad (\text{A.8})$$

For deep water conditions, the dispersion relation approaches:

$$\omega = \sqrt{gk_0} \quad \text{or} \quad L_0 = \frac{gT^2}{2\pi} \quad (\text{A.9})$$

From the dispersion relation, the propagation speed of the surface wave profile, i.e. phase speed, is obtained. The resulting conclusion shows that, in general, long waves travel faster than short waves as the phase speed depends on wave number and therefore frequency. For oceanic, deep water waves, the phase speed depends on wave length or frequency and is expressed as:

$$c_0 = \sqrt{g/k_0} \quad \text{or} \quad c_0 = \frac{g}{2\pi} T \quad (\text{A.10})$$

The waves formulated by this expression are termed dispersive waves. When two harmonic waves travelling in the same direction with slightly different frequencies are added, the waves will reinforce each other in phase but cancel each other out of phase, creating a series of wave groups. If the difference between the frequencies is infinitesimal, the group velocity is:

$$c_g = \frac{\partial \omega}{\partial k} = nc, \quad \text{where} \quad n = \frac{1}{2} \left(1 + \frac{2kd}{\sinh(2kd)} \right) \quad (\text{A.11})$$

$$n = \frac{1}{2}, \quad \text{for deep waters}$$

The forementioned expression of water particle velocities imply accelerations caused by forces acting on these particles, provided by wave-induced pressure in the water. Substitution of the velocity potential into the Bernoulli equations results in a formulation of the total pressure, which, for deep waters, is defined as:

$$\hat{p}_{wave} = \rho g a e^{kz} \quad (\text{A.12})$$

A.1.2. Coastal waters

Due to the limited water depth, amplitude and direction of waves entering coastal waters are affected. When propagating over a fixed seabed topography with gentle slopes and no currents, the frequency is retained. The dispersion relationship implies that the wave length will decrease if the depth decreases, and correspondingly the phase speed will decrease. Through conservation of energy, the affected amplitude can be calculated by the process termed shoaling:

$$a = \sqrt{\frac{c_{g,\infty}}{c_g}} a_\infty = K_{sh} a_\infty \quad (\text{A.13})$$

When harmonic waves approach a straight coast under oblique incidence, the direction will change slowly as it approaches the coast, called refraction. Refraction is caused by the depth variation along the wave crest with a corresponding variation in phase speed along that crest. According to the formulation of refraction, theoretically all ocean waves reach the shore at a right angle. The influence of refraction on the amplitude, combined with the influence of shoaling, is expressed as:

$$a = K_{sh} K_{ref} a_\infty \quad (\text{A.14})$$

A third phenomenon occurring in coastal waters is diffraction, which describes the change of direction and amplitude around a headland or breakwater. Diffraction describes the propagation of waves travelling in water of constant depth curving into a shadow area behind the headland, see Figure A.1.

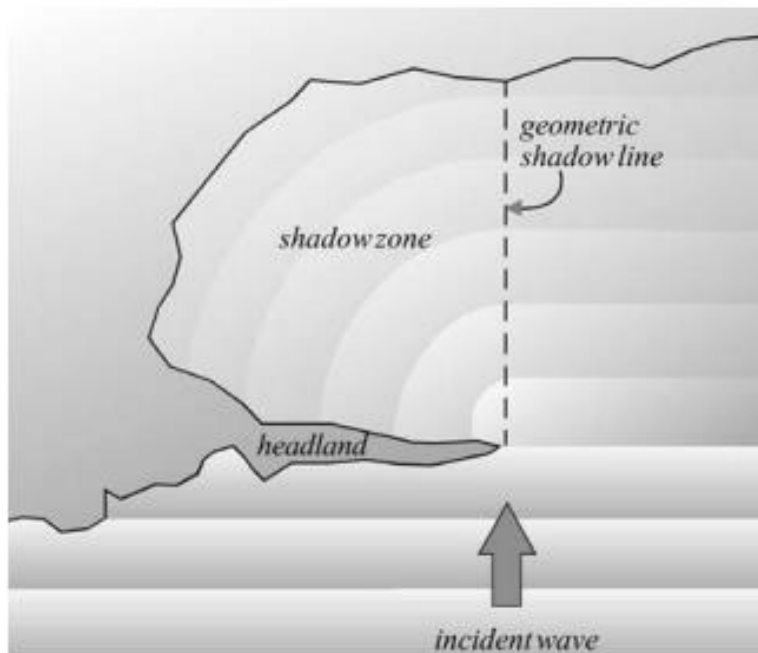


Figure A.1. Diffraction around a headland with a circular wave pattern in the shadow zone (constant depth and no reflections) (Holthuijsen, 2007).

A.1.3. Wave height

The instantaneous elevation of the sea surface relative to some reference level, here between the minimum and maximum points of the oscillation, is the surface elevation. In this context, a wave is defined as the profile of the surface elevation between two successive downward zero-crossings of the elevation (Holthuijsen, 2007). According to this formulation, different interpretations of wave heights exist.

The mean wave height \bar{H} , in a wave record with N waves and i the sequence number of the wave in the record, is defined as:

$$\bar{H} = \frac{1}{N} \sum_{i=1}^N H_i \quad (\text{A.15})$$

Similarly, relevant for energy-related projects, the quadratically weighted average value is used, defining the root-mean-square wave height H_{rms} :

$$H_{rms} = \left(\frac{1}{N} \sum_{i=1}^N H_i^2 \right)^{\frac{1}{2}} \quad (\text{A.16})$$

However, the aforementioned definitions bear little resemblance to the visually estimated wave height. As an alternative, the significant wave height H_s is used, defining the mean of the highest one-third of waves in the waves record:

$$H_s = H_{1/3} = \frac{1}{N/3} \sum_{j=1}^{N/3} H_j \quad (\text{A.17})$$

In this formulation, index j is used as the rank number of the wave based on wave height. In addition to the highest one-third of waves, occasionally the highest one-tenth of waves is used to define $H_{1/10}$.

A.1.4. Wave period

The wave period T is defined as the time interval between the start and end of the wave, alternatively known as the zero-crossing period. The mean \bar{T}_0 , in analogy with the mean wave height, is defined as:

$$\bar{T}_0 = \frac{1}{N} \sum_{i=1}^N T_{0,i} \quad (\text{A.18})$$

Similarly, the significant wave period T_s is specified as the mean period of the highest one-third of waves, i.e.:

$$T_{1/3} = \frac{1}{N/3} \sum_{j=1}^{N/3} T_{0,j} \quad (\text{A.19})$$

A.1.5. Wave spectra

A wave spectrum describes the sea surface as a stochastic process, with an observation formally treated as one realisation of this process. The spectrum originates from a summation of all harmonic wave components through a Fourier series. Repetition of this experiment results in the average amplitude spectrum, of which the variance spectrum can be deduced. The variance is proportional to the energy of the waves and the sum of the variances is equal to the variance of the sum, i.e. the random surface elevation (Holthuijsen, 2007). The variance density spectrum is defined as:

$$E(f) = \lim_{\Delta f \rightarrow 0} \frac{1}{\Delta f} E\left\{\frac{1}{2} \underline{a}^2\right\} \quad (\text{A.20})$$

The statistical characteristics of the variance density spectrum are expressed in terms of the moments, which are defined as:

$$m_n = \int_0^{\infty} f^n E(f) df \quad (\text{A.21})$$

From this expression, several statistical characteristics of the wave height can be obtained theoretically, namely:

- The mean zero-crossing period \bar{T}_0 :

$$\bar{T}_0 = \sqrt{\frac{m_0}{m_2}} \quad (\text{A.22})$$

- The inverse of the mean frequency, which is less dependent on high-frequency noise:

$$T_{m01} = f_{mean}^{-1} = \left(\frac{m_1}{m_0}\right)^{-1} \quad (\text{A.23})$$

- The mean wave height:

$$\bar{H} = E\{H\} = \sqrt{2\pi m_0} \quad (\text{A.24})$$

- The root-mean-square wave height:

$$H_{rms} = E\{H^2\}^{\frac{1}{2}} = \sqrt{8m_0} \quad (\text{A.25})$$

- For deep water, an estimation of the significant wave height:

$$H_{m_0} \approx 4\sqrt{m_0} \quad (\text{A.26})$$

Holthuijsen (2007) distinguishes two common types of wave spectra, namely Pierson-Moskowitz and JONSWAP. The Pierson-Moskowitz spectrum describes a fully developed sea state obtained after longer time periods of steady wind, resulting in an equilibrium between the wind and waves. However, Hasselmann et al. (1973) found that the wave spectrum was never fully developed during the Joint North Sea Wave Observation Project (JONSWAP). In order to improve the fit to their measurements, the Pierson-Moskowitz spectrum was multiplied by an extra peak enhancement factor γ^r , resulting in the following formulation:

$$E_{JONSWAP}(f) = \alpha g^2 (2\pi)^{-4} f^{-5} \exp\left(-\frac{5}{4}\left(\frac{f}{f_{peak}}\right)^{-4}\right) \gamma^r \quad (\text{A.27})$$

$$r = \exp\left(-\frac{1}{2}\left(\frac{\frac{f}{f_{peak}}}{\sigma}\right)^2\right)$$

The JONSWAP study was repeated at different times and locations, obtaining similar averages for the parameters of the spectrum, namely $\gamma = 3.3$, $\sigma_a = 0.07$ (if $f < f_{peak}$) and $\sigma_b = 0.09$ (if $f > f_{peak}$).

A.2. Breakwater design

In this section, a description is provided of the main dimensions and components of a breakwater.

Rubble mound breakwaters typically consist of a core of quarry run or secondary materials with the seaward- and (part of) lee-side slope protected by armour. The core and armour layer are generally separated by a filter- or underlayer. To support the armour layer, a toe is often built. For a schematic overview of a rubble mound breakwater, see Figure A.2.

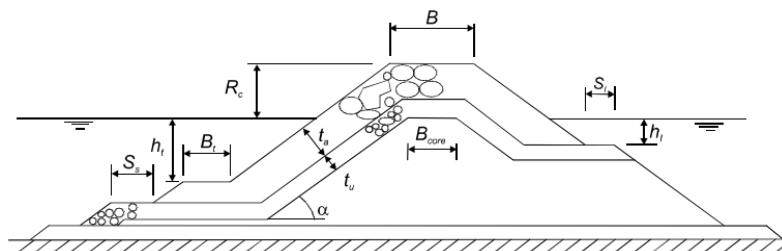


Figure A.2. Definition sketch for a rubble mound breakwater (CIRIA et al., 2007/2012).

The parameters denoted in Figure A.2 are defined as:

- Crest freeboard, R_c (m)
- Crest width, B (m)
- Slope angle, α (deg)
- Armour layer thickness, t_a (m)

- Underlayer thickness, t_u (m)
- Seaward toe level, h_t (m)
- Shoulder level, h_l (m)
- Toe width, B_t (m)
- Shoulder width, S_l (m)

The acceptable overtopping discharge or wave transmission usually dictates the required elevation of the crest, while visual appearance may also contribute. The minimum crest freeboard R_c depends on the overtopping requirements. The crest should be sufficiently wide to enable at least three armour units to be placed to ensure safe placement and interlocking. Faces of a breakwater are constructed under a slope angle α , with the front face ideally as steep as possible (CIRIA et al., 2007/2012). However, due to hydraulic and geotechnical stability considerations, the slope is generally not steeper than 1:1.5, with the exception of armour layers consisting of concrete armour units, where the slope can be as steep as 1:1.33.

Generally, no significant differences exist between the toe details of concrete armour units with respect to natural armour stone. However, for highly interlocking single-layer armour units, stability at the centre of the armour layer is higher than at the edges. To protect the edges in shallow water conditions, the Rock Manual (2007/2012) proposes excavation of the first layer in the sea bed, shown in Figure A.3.

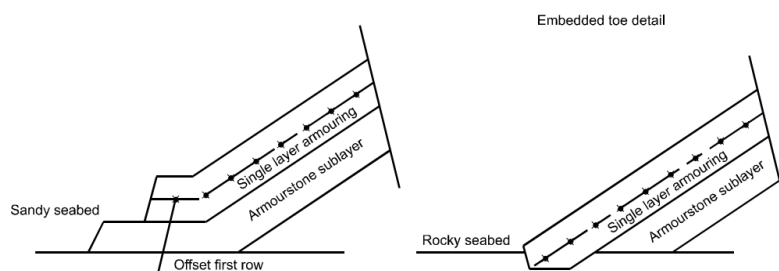


Figure A.3. Toe details for single-layer concrete armour units (CIRIA et al., 2007/2012).

A.3. Dimensionless numbers in fluid mechanics

This section provides an overview of dimensionless numbers used in fluid mechanics most relevant to this thesis, as described by Rapp (2017).

A.3.1. Froude

The Froude number defines the relation between inertia and gravity forces in a system and is defined as:

$$Fr = \frac{\text{inertia forces}}{\text{gravity forces}} = \frac{U^2}{gL} \quad (\text{A.28})$$

Where U is the flow velocity and L the characteristic length. The Froude number denotes the relation between the flow- and wave velocity, with subcritical flow for $Fr < 1$, supercritical flow for $Fr > 1$ and critical flow for $Fr \approx 1$.

A.3.2. Reynolds

The Reynolds number correlates the inertia forces to the viscous forces (through the kinematic viscosity ν), describing the transport properties of a fluid or particle moving in fluid. The quantity distinguishes flow regimes between laminar- or turbulent flow, and is defined as:

$$Re = \frac{\text{inertia forces}}{\text{viscous forces}} = \frac{UL}{\nu} \quad (\text{A.29})$$

A.3.3. Cauchy

The Cauchy number is defined as the ratio between inertia and compressibility forces in a flow and is expressed in terms of the flow velocity, density and elasticity of the fluid as:

$$Ca = \frac{\text{inertia forces}}{\text{elastic forces}} = \frac{\rho U^2}{E} \quad (\text{A.30})$$

A.3.4. Weber

The Weber number relates the inertia forces to the forces resulting from surface tension (σ) and is defined as:

$$We = \frac{\text{inertia forces}}{\text{surface tension}} = \frac{\rho U^2 L}{\sigma} \quad (\text{A.31})$$

A.4. Fluid-structure interaction

A.4.1. Wave reflection

Waves propagating around or against a coast or structure will to some extent reflect. The wave motion at each point of the reflecting structure is described by the sum of the incoming wave and one or more reflected waves. In case of 100% reflection, a standing wave is formed. However, according to Holthuijsen (2007), very often the reflection is less and the resulting wave is a partially standing wave, which can be described as:

$$\eta(x, t) = (a_i - a_r) \sin(\omega t - kx) + 2a_r \cos(kx) \sin(\omega t) \quad (\text{A.32})$$

Hence, for a partially standing wave, the maximum and minimum amplitudes are defined as $a_{max} = a_i + a_r$ and $a_{min} = a_i - a_r$ respectively. And thus, the reflection coefficient, which can readily be measured in a laboratory, $K_{refl} = a_r/a_i$.

A.4.2. Wave breaking

According to Holthuijsen (2007), depth-induced breaking is the most nonlinear process affecting waves in coastal water. Alternatively known as surf-breaking, this phenomenon is described by the Iribarren number, formulated as:

$$\xi = \tan \alpha / \sqrt{H/L_\infty} \quad (\text{A.33})$$

In which $L_\infty = gT^2/2\pi$ is the deep water wave length, H is the wave height at the assessed location and α is the slope of the structure. Different types of wave breaking, visualized in Figure A.4, can be distinguished depending on the Iribarren number:

- Spilling:

$$\xi_\infty < 0.5 \text{ or } \xi_{br} < 0.4$$

- Plunging:

$$0.5 < \xi_\infty < 3.3 \text{ or } 0.4 < \xi_{br} < 2.0$$

- Collapsing or surging:

$$\xi_\infty > 3.3 \text{ or } \xi_{br} > 2.0$$

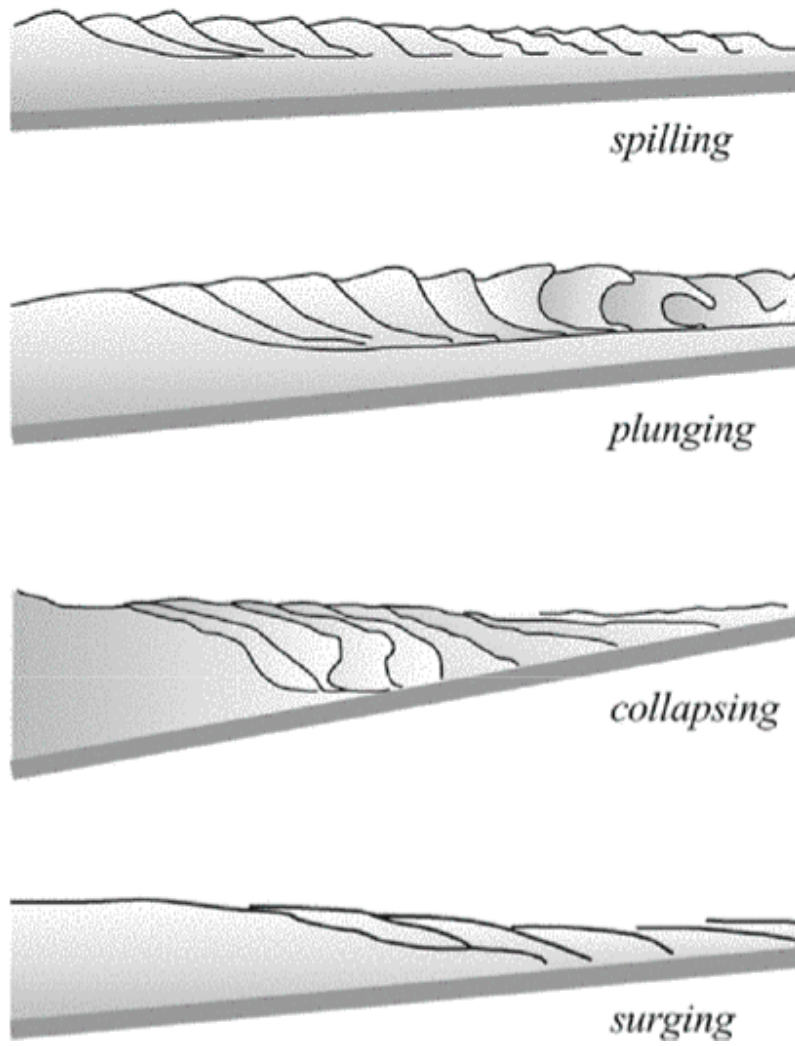


Figure A.4. The four main types of breaking waves (Holthuijsen, 2007).

B. Armour units

This appendix provides a description of the production process of the armour units, paired with an overview of the sampled unit densities on which the distributions in Section 4.4 are fitted.

B.1. Production

The armour units specified in the design are manufactured using a three-dimensional printer, as depicted in Figure B.1. These model units serve as templates within a wooden framework to create moulds from casting rubber, as shown in Figure B.2. The moulds are then filled multiple times with a mixture comprising of 2.4 kg of mortar, 0.630 kg baryta powder and 485 millilitres of water, illustrated in Figure B.3. Following demoulding and subsequent surface polishing of the armour units, the resulting model units are displayed in Figure B.4. Subsequently, densities are sampled by measuring both the dry and submerged masses of the units, which are outlined in Table B.1, Table B.2 and Table B.3. Thereafter, the units are spray painted in the colour corresponding to the digital model, as depicted in Figure B.5.



Figure B.1. Three-dimensional prints of the armour unit concepts.



Figure B.2. Casting rubber moulds for the production of concrete armour units.



Figure B.3. Rubber moulds filled with mortar.



Figure B.4. The three distinct armour units after demoulding and polishing.

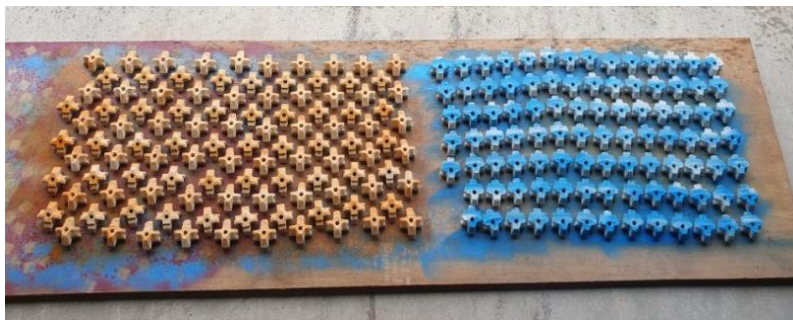


Figure B.5. Painting of the armour units in the predefined colours.

B.2. Mass, volume and density

Table B.1. Measured mass and submerged mass of XP-Base armour units with calculated volume and density.

Number	m_d (g)	m_s (g)	V (cm ³)	ρ (g/cm ³)
1	51.40	30.20	21.20	2.42
2	51.60	29.90	21.70	2.38
3	51.80	30.10	21.70	2.39
4	51.60	29.70	21.90	2.36
5	51.20	29.60	21.60	2.37
6	52.20	30.50	21.70	2.41
7	51.90	30.50	21.40	2.43
8	51.50	29.70	21.80	2.36
9	53.00	31.10	21.90	2.42
10	51.60	29.90	21.70	2.38
11	51.80	30.10	21.70	2.39
12	51.80	29.70	22.10	2.34
13	51.50	30.00	21.50	2.40
14	51.60	29.60	22.00	2.35
15	50.00	28.90	21.10	2.37
16	52.10	30.40	21.70	2.40
17	52.20	30.30	21.90	2.38
18	52.10	30.20	21.90	2.38
19	51.90	30.20	21.70	2.39
20	51.40	29.30	22.10	2.33
21	52.10	30.30	21.80	2.39
22	50.90	29.20	21.70	2.35
23	51.50	30.00	21.50	2.40
24	51.20	29.40	21.80	2.35
25	50.80	29.70	21.10	2.41
26	51.40	29.80	21.60	2.38
27	54.20	31.20	23.00	2.36
28	52.30	30.40	21.90	2.39
29	51.10	29.40	21.70	2.35
30	52.40	29.80	22.60	2.32
31	52.70	30.70	22.00	2.40
32	51.50	29.80	21.70	2.37
33	53.00	31.10	21.90	2.42
34	53.50	31.10	22.40	2.39
35	52.80	30.60	22.20	2.38
36	51.40	29.70	21.70	2.37
37	53.20	30.90	22.30	2.39

38	52.30	30.00	22.30	2.35
39	51.90	30.10	21.80	2.38
40	52.60	30.30	22.30	2.36
41	52.30	30.60	21.70	2.41
42	53.20	31.10	22.10	2.41
43	53.30	30.80	22.50	2.37
44	53.00	30.80	22.20	2.39
45	52.80	30.60	22.20	2.38
46	53.30	30.70	22.60	2.36
47	53.60	31.40	22.20	2.41
48	52.90	30.60	22.30	2.37
49	53.00	30.60	22.40	2.37
50	53.20	30.80	22.40	2.38

Table B.2. Measured mass and submerged mass of XP-Curve (version 2) armour units with calculated volume and density.

Number	m_d (g)	m_s (g)	V (cm³)	ρ (g/cm³)
1	56.90	32.90	24.00	2.37
2	56.90	33.30	23.60	2.41
3	56.40	32.80	23.60	2.39
4	56.10	32.40	23.70	2.37
5	57.10	33.30	23.80	2.40
6	56.90	33.20	23.70	2.40
7	55.90	32.20	23.70	2.36
8	56.50	33.20	23.30	2.42
9	56.70	33.10	23.60	2.40
10	56.80	32.70	24.10	2.36
11	56.90	32.90	24.00	2.37
12	57.70	33.80	23.90	2.41
13	56.40	32.80	23.60	2.39
14	56.30	32.90	23.40	2.41
15	56.20	32.50	23.70	2.37
16	56.30	32.60	23.70	2.38
17	56.20	32.60	23.60	2.38
18	56.40	32.70	23.70	2.38
19	56.40	32.80	23.60	2.39
20	57.50	33.40	24.10	2.39
21	56.40	32.70	23.70	2.38
22	55.30	32.00	23.30	2.37
23	57.10	32.80	24.30	2.35

24	56.00	32.30	23.70	2.36
25	57.70	33.30	24.40	2.36
26	58.60	34.10	24.50	2.39
27	57.30	32.70	24.60	2.33
28	55.80	32.20	23.60	2.36
29	55.60	32.40	23.20	2.40
30	57.50	33.30	24.20	2.38
31	57.80	33.50	24.30	2.38
32	55.80	32.40	23.40	2.38
33	57.10	33.00	24.10	2.37
34	58.10	33.60	24.50	2.37
35	58.50	33.80	24.70	2.37
36	56.00	32.50	23.50	2.38
37	58.40	33.80	24.60	2.37
38	57.40	33.60	23.80	2.41
39	57.90	34.00	23.90	2.42
40	57.30	33.10	24.20	2.37
41	58.20	33.80	24.40	2.39
42	57.20	33.00	24.20	2.36
43	57.00	33.30	23.70	2.41
44	57.40	33.10	24.30	2.36
45	58.00	33.70	24.30	2.39
46	57.50	33.20	24.30	2.37
47	57.30	33.20	24.10	2.38
48	57.30	33.00	24.30	2.36
49	58.00	33.50	24.50	2.37
50	57.10	33.00	24.10	2.37

Table B.3. Measured mass and submerged mass of XP-Curve (version 3) armour units with calculated volume and density.

Number	m_d (g)	m_s (g)	V (cm³)	ρ (g/cm³)
1	53.90	31.60	22.30	2.42
2	54.90	32.10	22.80	2.41
3	54.10	31.60	22.50	2.40
4	53.40	31.30	22.10	2.42
5	53.60	31.50	22.10	2.43
6	54.10	31.30	22.80	2.37
7	53.80	31.20	22.60	2.38
8	53.80	31.50	22.30	2.41
9	54.00	31.50	22.50	2.40

10	54.40	31.80	22.60	2.41
11	55.20	31.80	23.40	2.36
12	53.30	31.00	22.30	2.39
13	53.40	31.00	22.40	2.38
14	53.80	31.10	22.70	2.37
15	53.60	31.20	22.40	2.39
16	53.40	30.80	22.60	2.36
17	54.00	31.30	22.70	2.38
18	54.50	31.40	23.10	2.36
19	53.90	31.00	22.90	2.35
20	53.30	31.10	22.20	2.40
21	53.40	30.70	22.70	2.35
22	52.80	30.70	22.10	2.39
23	53.50	30.40	23.10	2.32
24	54.40	31.80	22.60	2.41
25	55.00	31.80	23.20	2.37
26	53.30	30.60	22.70	2.35
27	53.60	30.90	22.70	2.36
28	53.20	30.60	22.60	2.35
29	53.00	30.60	22.40	2.37
30	54.40	31.30	23.10	2.35
31	55.10	31.90	23.20	2.38
32	52.60	30.30	22.30	2.36
33	53.20	30.60	22.60	2.35
34	52.90	30.40	22.50	2.35
35	53.70	30.90	22.80	2.36
36	54.50	31.30	23.20	2.35
37	54.80	31.70	23.10	2.37
38	54.00	31.20	22.80	2.37
39	53.40	30.90	22.50	2.37
40	54.60	31.90	22.70	2.41
41	55.00	31.70	23.30	2.36
42	54.80	31.20	23.60	2.32
43	53.80	31.30	22.50	2.39
44	54.00	31.20	22.80	2.37
45	53.50	30.60	22.90	2.34
46	53.10	30.20	22.90	2.32
47	53.60	31.00	22.60	2.37
48	53.60	30.70	22.90	2.34
49	55.20	31.60	23.60	2.34
50	52.90	30.10	22.80	2.32

C. Wave climate

Table C.1. Wave climate during Series 0.1.

Run [H_{m0}]	Gauge 1		Gauges 2, 3, 4			Gauges 5, 6, 7		
	H_{m0} [cm]	T_p [s]	H_{m0} [cm]	H_{max} [cm]	T_p [s]	H_{m0} [cm]	H_{max} [cm]	T_p [s]
0.8	8.395	1.164	7.456	13.380	1.143	7.466	13.290	1.143
1.0	11.81	1.208	10.37	17.650	1.306	10.56	18.310	1.306
1.1	12.61	1.362	11.04	18.020	1.362	11.21	18.080	1.362
1.2	13.41	1.31	11.54	18.230	1.333	11.72	18.260	1.333
1.3	14.96	1.455	12.92	18.630	1.455	13.08	19.230	1.455

Table C.2. Wave climate during Series 1.1.

Run [H_{m0}]	Gauge 1		Gauges 2, 3, 4			Gauges 5, 6, 7		
	H_{m0} [cm]	T_p [s]	H_{m0} [cm]	H_{max} [cm]	T_p [s]	H_{m0} [cm]	H_{max} [cm]	T_p [s]
0.8	8.287	1.164	7.101	13.03	1.143	7.335	13.13	1.143
1.0	11.76	1.280	10.01	17.57	1.306	10.28	18.46	1.306
1.1	12.36	1.362	10.76	17.36	1.362	10.99	17.31	1.362
1.2	13.11	1.362	11.27	17.44	1.391	11.48	17.94	1.391
1.3	14.84	1.455	13.16	18.93	1.455	13.12	19.49	1.455
1.4	14.99	1.455	13.40	19.47	1.455	13.34	19.80	1.455
1.5	15.54	1.561	13.80	21.20	1.524	13.75	21.27	1.524
1.5	15.58	1.561	13.77	21.29	1.524	13.77	21.67	1.524

Table C.3. Wave climate during Series 1.2.1.

Run [H_{m0}]	Gauge 1		Gauges 2, 3, 4			Gauges 5, 6, 7		
	H_{m0} [cm]	T_p [s]	H_{m0} [cm]	H_{max} [cm]	T_p [s]	H_{m0} [cm]	H_{max} [cm]	T_p [s]
0.8	10.25	1.600	9.396	17.56	1.641	9.443	17.67	1.641
1.0	11.00	1.778	10.27	18.44	1.778	10.34	18.00	1.778
1.1	11.67	1.939	10.64	19.73	1.882	10.72	20.08	1.882
1.2	13.09	1.939	12.15	20.20	1.939	12.27	20.42	1.939
1.3	21.54	2.133	15.91	19.15	2.000	16.03	19.51	2.000

Table C.4. Wave climate during Series 1.2.2.

Run [H_{m0}]	Gauge 1		Gauges 2, 3, 4			Gauges 5, 6, 7		
	H_{m0} [cm]	T_p [s]	H_{m0} [cm]	H_{max} [cm]	T_p [s]	H_{m0} [cm]	H_{max} [cm]	T_p [s]
0.8	8.234	1.600	7.806	13.63	1.561	7.732	13.52	1.561
1.0	10.17	1.778	9.823	18.46	1.778	9.760	17.68	1.778
1.1	11.50	1.939	10.80	20.31	1.882	10.75	20.52	1.882
1.2	12.52	1.939	11.93	19.72	1.939	11.88	19.11	1.939

Table C.5. Wave climate during Series 1.3.

Run [H_{m0}]	Gauge 1		Gauges 2, 3, 4			Gauges 5, 6, 7		
	H_{m0} [cm]	T_p [s]	H_{m0} [cm]	H_{max} [cm]	T_p [s]	H_{m0} [cm]	H_{max} [cm]	T_p [s]
0.8	7.797	1.185	7.266	12.21	1.143	7.171	12.29	1.143
1.0	11.19	1.255	10.32	16.7	1.255	10.23	16.79	1.255
1.1	11.73	1.333	10.96	18.37	1.362	10.86	18.14	1.362
1.2	12.41	1.333	11.47	19.45	1.333	11.34	19.02	1.333
1.3	13.76	1.455	12.63	20.11	1.455	12.53	20.41	1.455
1.4	13.88	1.524	12.84	20.68	1.524	12.76	21.11	1.524
1.5	13.87	1.524	12.83	20.77	1.524	12.74	20.89	1.524

Table C.6. Wave climate during Series 1.4.1.

Run [H_{m0}]	Gauge 1		Gauges 2, 3, 4			Gauges 5, 6, 7		
	H_{m0} [cm]	T_p [s]	H_{m0} [cm]	H_{max} [cm]	T_p [s]	H_{m0} [cm]	H_{max} [cm]	T_p [s]
0.8	8.196	1.561	7.648	12.52	1.641	7.601	12.71	1.600
1.0	10.93	1.730	10.22	19.90	1.730	10.18	19.50	1.730
1.1	11.63	1.882	10.73	21.93	1.882	10.70	21.92	1.882
1.2	12.20	1.882	11.54	20.45	1.939	11.52	20.39	1.939
1.3	19.23	1.882	16.15	19.74	2.000	16.26	20.58	2.000

Table C.7. Wave climate during Series 1.4.2.

Run [H_{m0}]	Gauge 1		Gauges 2, 3, 4			Gauges 5, 6, 7		
	H_{m0} [cm]	T_p [s]	H_{m0} [cm]	H_{max} [cm]	T_p [s]	H_{m0} [cm]	H_{max} [cm]	T_p [s]
0.8	8.099	1.561	7.647	12.55	1.600	7.564	12.65	1.600
1.0	10.65	1.730	10.25	19.41	1.730	10.17	19.24	1.730
1.1	11.42	1.882	10.78	21.96	1.882	10.71	22.30	1.882
1.2	11.92	1.882	11.60	21.10	1.939	11.51	20.43	1.939
1.3	12.91	1.882	12.49	21.20	2.000	12.40	21.63	2.000

Table C.8. Wave climate during Series 2.1.

Run [H_{m0}]	Gauge 1		Gauges 2, 3, 4			Gauges 5, 6, 7		
	H_{m0} [cm]	T_p [s]	H_{m0} [cm]	H_{max} [cm]	T_p [s]	H_{m0} [cm]	H_{max} [cm]	T_p [s]
0.8	8.548	1.164	7.801	13.69	1.143	7.613	13.53	1.143
1.0	10.95	1.280	9.821	16.98	1.306	9.597	17.30	1.306
1.1	12.04	1.362	10.93	17.62	1.362	10.69	17.03	1.362
1.2	12.87	1.362	11.64	17.96	1.333	11.45	17.58	1.333
1.3	14.33	1.455	13.01	18.87	1.455	12.80	19.20	1.455
1.4	14.44	1.455	13.23	19.29	1.455	13.00	19.48	1.455

Table C.9. Wave climate during Series 2.2.

Run [H_{m0}]	Gauge 1		Gauges 2, 3, 4			Gauges 5, 6, 7		
	H_{m0} [cm]	T_p [s]	H_{m0} [cm]	H_{max} [cm]	T_p [s]	H_{m0} [cm]	H_{max} [cm]	T_p [s]
1.0	10.35	1.778	9.929	18.220	1.778	9.827	17.530	1.778
1.1	11.55	1.939	10.90	20.240	1.882	10.80	20.220	1.882
1.2	12.16	1.939	11.80	18.610	1.939	11.70	18.360	1.939

Table C.10. Wave climate during Series 2.3.

Run [H_{m0}]	Gauge 1		Gauges 2, 3, 4			Gauges 5, 6, 7		
	H_{m0} [cm]	T_p [s]	H_{m0} [cm]	H_{max} [cm]	T_p [s]	H_{m0} [cm]	H_{max} [cm]	T_p [s]
0.8	8.213	1.185	7.680	13.04	1.143	7.550	12.85	1.143
1.0	11.21	1.255	10.36	17.34	1.255	10.23	17.05	1.255
1.1	11.47	1.333	10.80	17.82	1.362	10.65	17.88	1.362
1.2	12.13	1.333	11.29	18.97	1.333	11.13	18.83	1.333
1.3	13.46	1.455	12.67	20.55	1.455	12.53	20.46	1.455
1.4	13.57	1.524	12.88	20.82	1.524	12.77	21.24	1.524

Table C.11. Wave climate during Series 2.4.

Run [H_{m0}]	Gauge 1		Gauges 2, 3, 4			Gauges 5, 6, 7		
	H_{m0} [cm]	T_p [s]	H_{m0} [cm]	H_{max} [cm]	T_p [s]	H_{m0} [cm]	H_{max} [cm]	T_p [s]
0.8	8.630	1.561	8.106	13.25	1.641	8.034	13.28	1.641
1.0	10.43	1.730	9.996	19.24	1.730	9.911	18.83	1.730
1.1	11.63	1.882	10.96	21.95	1.882	10.90	22.04	1.882
1.2	12.09	1.882	11.51	21.35	1.882	11.48	21.49	1.882

Table C.12. Wave climate during Series 3.1.

Run [H_{m0}]	Gauge 1		Gauges 2, 3, 4			Gauges 5, 6, 7		
	H_{m0} [cm]	T_p [s]	H_{m0} [cm]	H_{max} [cm]	T_p [s]	H_{m0} [cm]	H_{max} [cm]	T_p [s]
0.6	6.136	1.362	5.620	9.363	1.333	5.503	9.360	1.333
0.8	8.484	1.561	7.992	13.98	1.561	7.872	13.67	1.641
1.0	10.37	1.778	9.958	18.28	1.778	9.835	17.52	1.778
1.1	11.62	1.939	10.89	20.01	1.882	10.76	20.16	1.882
1.2	12.36	1.939	11.90	19.68	1.939	11.73	19.61	1.939

Table C.13. Wave climate during Series 3.2.

Run [H_{m0}]	Gauge 1		Gauges 2, 3, 4			Gauges 5, 6, 7		
	H_{m0} [cm]	T_p [s]	H_{m0} [cm]	H_{max} [cm]	T_p [s]	H_{m0} [cm]	H_{max} [cm]	T_p [s]
0.6	6.081	1.333	5.599	9.152	1.333	5.501	9.158	1.333
0.8	8.409	1.561	7.948	13.03	1.641	7.846	12.95	1.641
0.9	9.539	1.684	9.253	17.16	1.641	9.143	16.52	1.641
1.0	10.46	1.730	10.07	19.31	1.730	9.981	19.00	1.730
1.1	11.67	1.882	11.02	22.15	1.882	10.94	22.41	1.882
1.2	12.91	1.882	12.49	22.39	1.939	12.40	22.07	1.939
1.3	13.71	2.133	13.25	22.11	2.000	13.15	22.62	2.000
1.4	14.49	2.065	13.67	22.96	2.065	13.62	22.80	2.065

D. Visual documentation of test series

D.1. Model 0

D.1.1. Series 0.1



Figure D.1. Structure before 0.8 H_{m0} test run of Series 0.1.

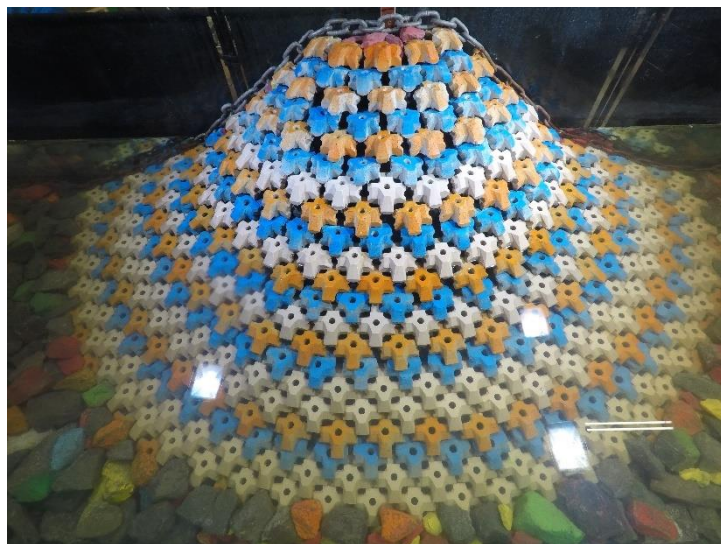


Figure D.2. Structure after 0.8 H_{m0} test run of Series 0.1 ($N_s = 1.89$).



Figure D.3. Structure after 1.0 H_{m0} test run of Series 0.1 ($N_s = 2.64$).



Figure D.4. Structure after 1.1 H_{m0} test run of Series 0.1 ($N_s = 2.81$).



Figure D.5. Structure after 1.2 H_{m0} test run of Series 0.1 ($N_s = 2.94$).



Figure D.6. Structure after $1.3 H_{m0}$ test run of Series 0.1 ($N_s = 3.28$).

D.2. Model 1

D.2.1. Series 1.1



Figure D.7. Structure before $0.8 H_{m0}$ test run of Series 1.1.



Figure D.8. Structure after 0.8 H_{m0} test run of Series 1.1 ($N_s = 1.82$).



Figure D.9. Structure after 1.0 H_{m0} test run of Series 1.1 ($N_s = 2.56$).

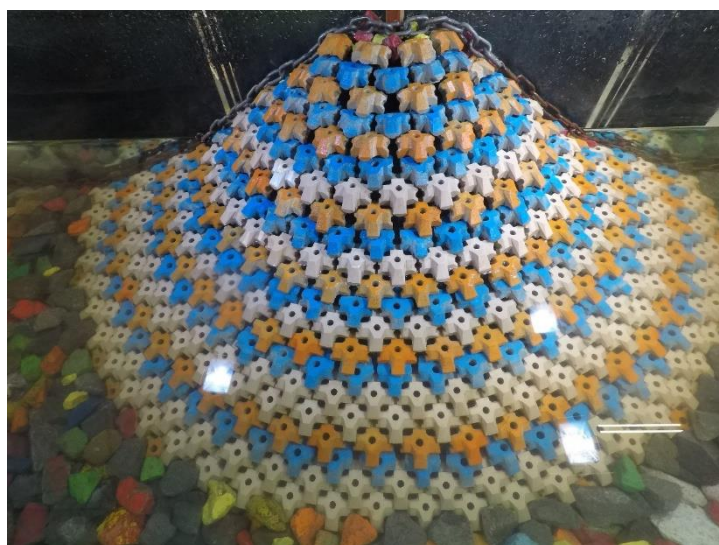


Figure D.10. Structure after 1.1 H_{m0} test run of Series 1.1 ($N_s = 2.75$).



Figure D.11. Structure after 1.2 H_{m0} test run of Series 1.1 ($N_s = 2.87$).

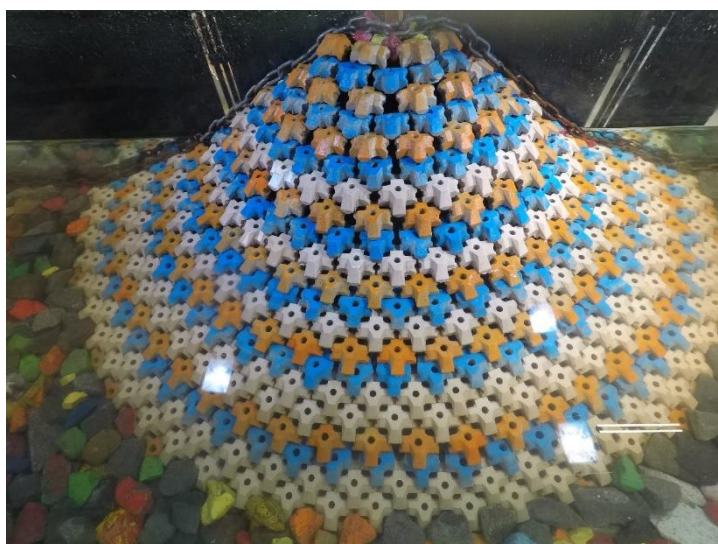


Figure D.12. Structure after 1.3 H_{m0} test run of Series 1.1 ($N_s = 3.32$).



Figure D.13. Structure after 1.4 H_{m0} test run of Series 1.1 ($N_s = 3.38$).

D.2.2. Series 1.2.1**Figure D.14.** Structure before 0.8 H_{m0} test run of Series 1.2.1.**Figure D.15.** Structure after 0.8 H_{m0} test run of Series 1.2.1 ($N_s = 2.38$).**Figure D.16.** Structure after 1.0 H_{m0} test run of Series 1.2.1 ($N_s = 2.60$).



Figure D.17. Structure after 1.1 H_{m0} test run of Series 1.2.1 ($N_s = 2.70$).



Figure D.18. Structure after 1.2 H_{m0} test run of Series 1.2.1 ($N_s = 3.09$).



Figure D.19. Structure after 1.3 H_{m0} test run of Series 1.2.1 ($N_s = 4.04$).

D.2.3. Series 1.2.2**Figure D.20.** Structure before 0.8 H_{m0} test run of Series 1.2.2.**Figure D.21.** Structure after 0.8 H_{m0} test run of Series 1.2.2 ($N_s = 1.96$).**Figure D.22.** Structure after 1.0 H_{m0} test run of Series 1.2.2 ($N_s = 2.47$).



Figure D.23. Structure after 1.1 H_{m0} test run of Series 1.2.2 ($N_s = 2.72$).



Figure D.24. Structure after 1.2 H_{m0} test run of Series 1.2.2 ($N_s = 3.01$).

D.2.4. Series 1.3



Figure D.25. Structure before 0.8 H_{m0} test run of Series 1.3.



Figure D.26. Structure after 0.8 H_{m0} test run of Series 1.3 ($N_s = 1.82$).



Figure D.27. Structure after 1.0 H_{m0} test run of Series 1.3 ($N_s = 2.60$).

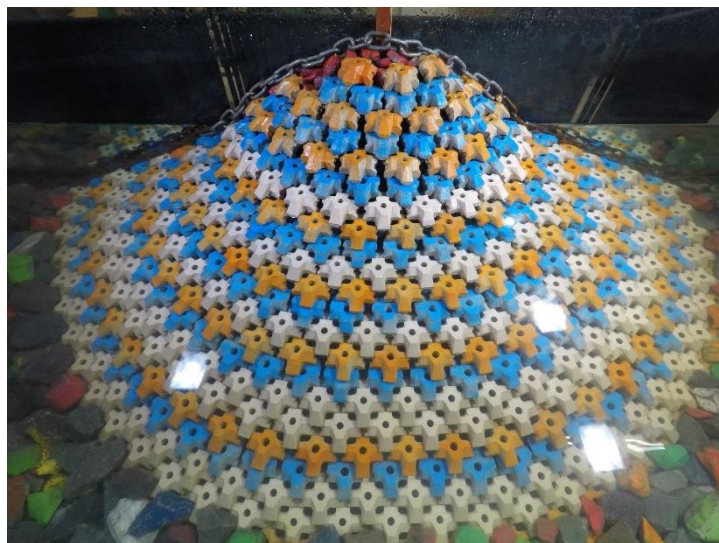


Figure D.28. Structure after 1.1 H_{m0} test run of Series 1.3 ($N_s = 2.76$).



Figure D.29. Structure after 1.2 H_{m0} test run of Series 1.3 ($N_s = 2.88$).

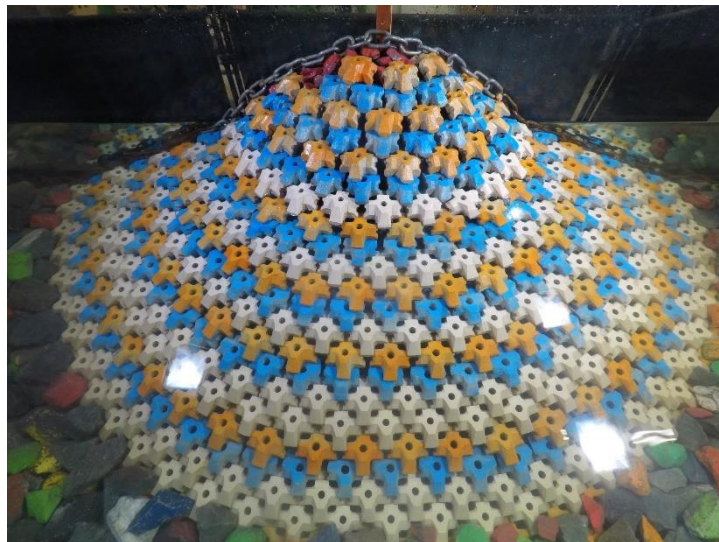


Figure D.30. Structure after 1.3 H_{m0} test run of Series 1.3 ($N_s = 3.18$).

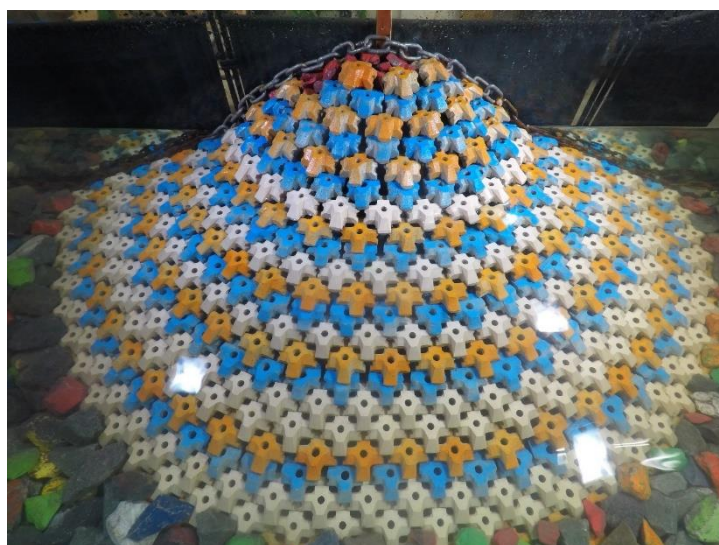


Figure D.31. Structure after 1.4 H_{m0} test run of Series 1.3 ($N_s = 3.23$).



Figure D.32. Structure after 1.5 H_{m0} test run of Series 1.3 ($N_s = 3.23$).

D.2.5. Series 1.4.1



Figure D.33. Structure before 0.8 H_{m0} test run of Series 1.4.1.



Figure D.34. Structure after 0.8 H_{m0} test run of Series 1.4.1 ($N_s = 1.93$).

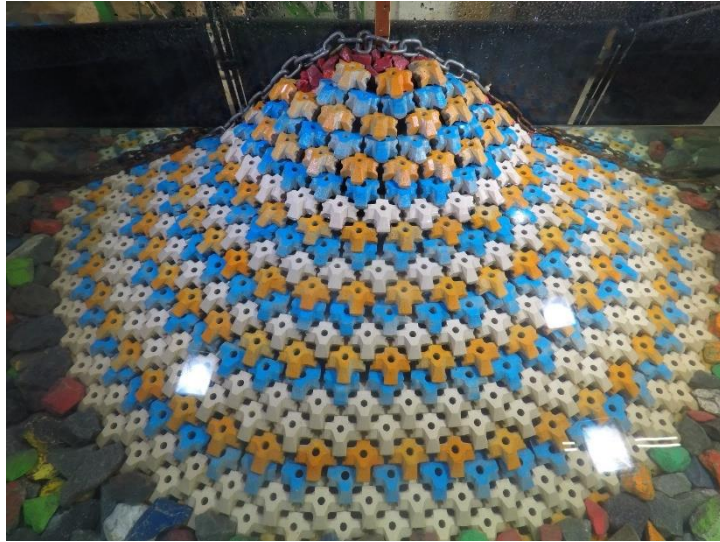


Figure D.35. Structure after 1.0 H_{m0} test run of Series 1.4.1 ($N_s = 2.58$).



Figure D.36. Structure after 1.1 H_{m0} test run of Series 1.4.1 ($N_s = 2.71$).



Figure D.37. Structure after 1.2 H_{m0} test run of Series 1.4.1 ($N_s = 2.91$).

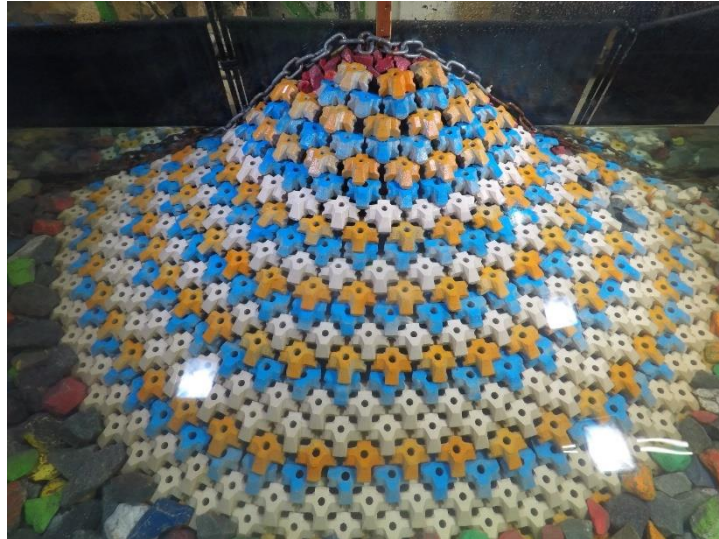


Figure D.38. Structure after 1.3 H_{m0} test run of Series 1.4.1 ($N_s = 4.09$).

D.2.6. Series 1.4.2



Figure D.39. Structure before 0.8 H_{m0} test run of Series 1.4.2.

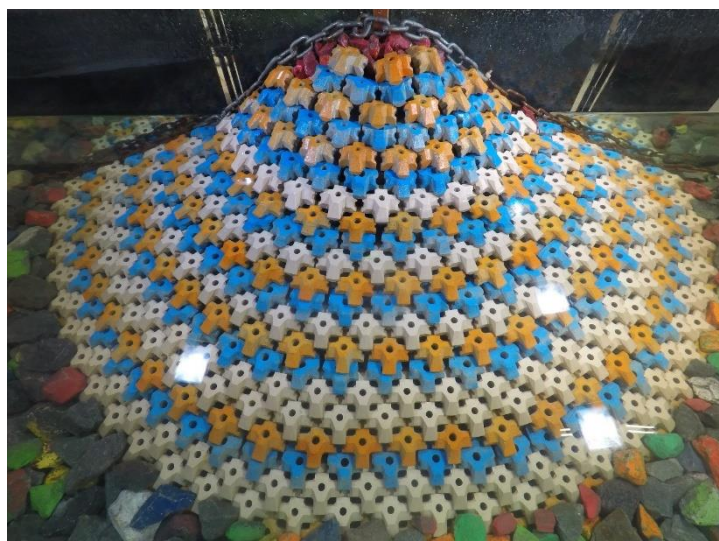


Figure D.40. Structure after 0.8 H_{m0} test run of Series 1.4.2 ($N_s = 1.92$).



Figure D.41. Structure after 1.0 H_{m0} test run of Series 1.4.2 ($N_s = 2.58$).



Figure D.42. Structure after 1.1 H_{m0} test run of Series 1.4.2 ($N_s = 2.72$).

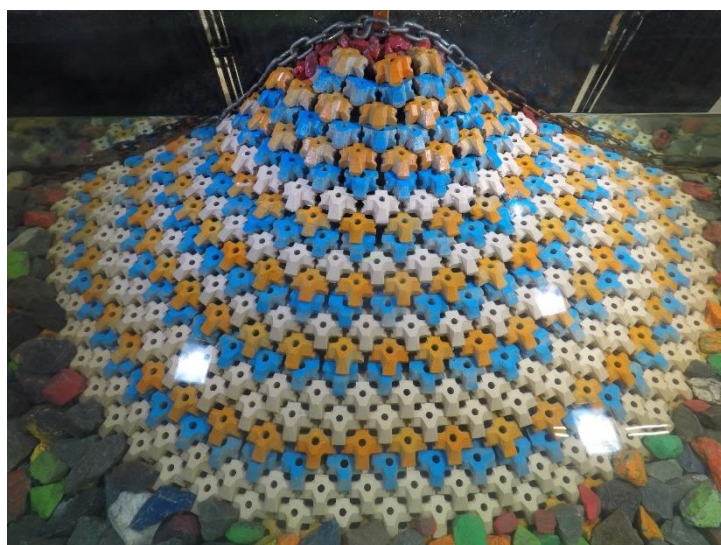


Figure D.43. Structure after 1.2 H_{m0} test run of Series 1.4.2 ($N_s = 2.92$).



Figure D.44. Structure after $1.3 H_{m0}$ test run of Series 1.4.2 ($N_s = 3.14$).

D.3. Model 2

D.3.1. Series 2.1



Figure D.45. Structure before $0.8 H_{m0}$ test run of Series 2.1.



Figure D.46. Structure after 0.8 H_{m0} test run of Series 2.1 ($N_s = 1.95$).



Figure D.47. Structure after 1.0 H_{m0} test run of Series 2.1 ($N_s = 2.45$).

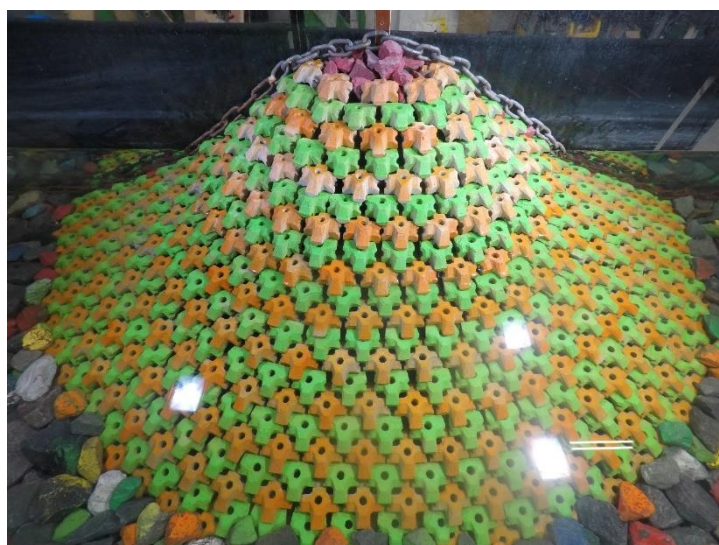


Figure D.48. Structure after 1.1 H_{m0} test run of Series 2.1 ($N_s = 2.73$).



Figure D.49. Structure after 1.2 H_{m0} test run of Series 2.1 ($N_s = 2.92$).



Figure D.50. Structure after 1.3 H_{m0} test run of Series 2.1 ($N_s = 3.26$).



Figure D.51. Structure after 1.4 H_{m0} test run of Series 2.1 ($N_s = 3.31$).

D.3.2. Series 2.2**Figure D.52.** Structure before 0.8 H_{m0} test run of Series 2.2.**Figure D.53.** Structure after 0.8 H_{m0} test run of Series 2.2 ($N_s \approx 1.96$).**Figure D.54.** Structure after 1.0 H_{m0} test run of Series 2.2 ($N_s = 2.50$).



Figure D.55. Structure after 1.1 H_{m0} test run of Series 2.2 ($N_s = 2.74$).



Figure D.56. Structure after 1.2 H_{m0} test run of Series 2.2 ($N_s = 2.97$).

D.3.3. Series 2.3



Figure D.57. Structure before 0.8 H_{m0} test run of Series 2.3.



Figure D.58. Structure after 0.8 H_{m0} test run of Series 2.3 ($N_s = 1.92$).



Figure D.59. Structure after 1.0 H_{m0} test run of Series 2.3 ($N_s = 2.60$).

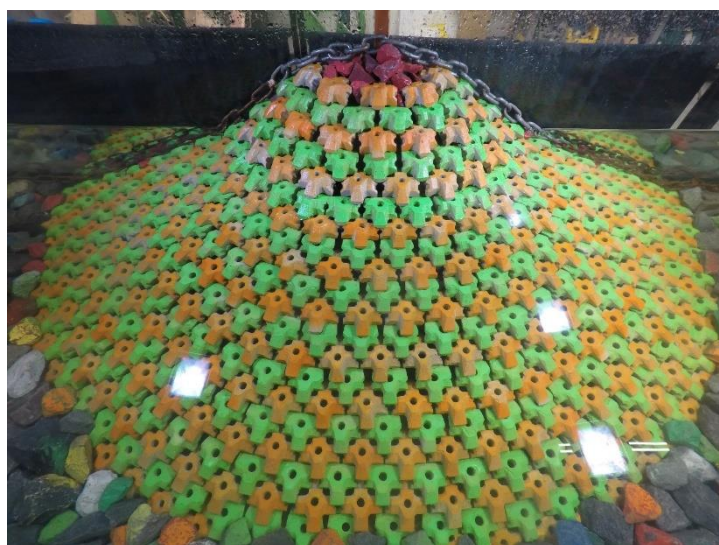


Figure D.60. Structure after 1.1 H_{m0} test run of Series 2.3 ($N_s = 2.71$).



Figure D.61. Structure after 1.2 H_{m0} test run of Series 2.3 ($N_s = 2.83$).



Figure D.62. Structure after 1.3 H_{m0} test run of Series 2.3 ($N_s = 3.18$).

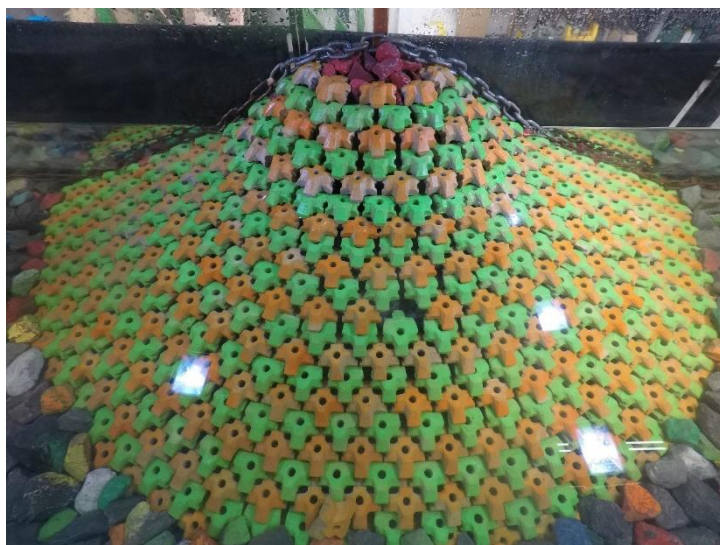
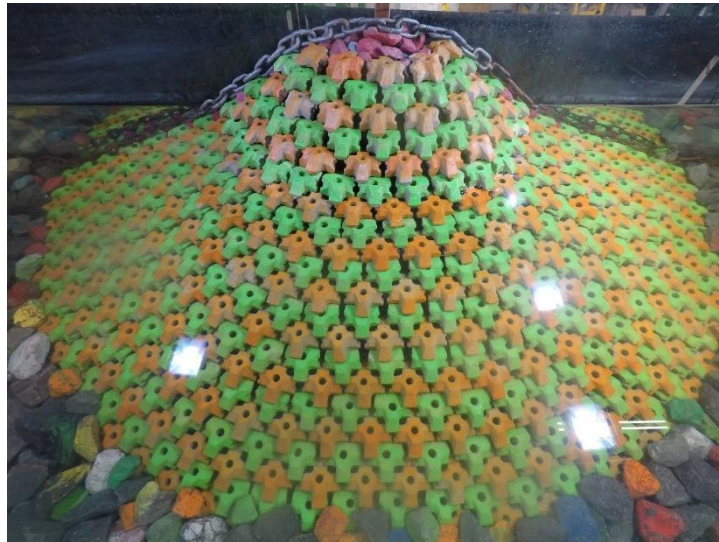


Figure D.63. Structure after 1.4 H_{m0} test run of Series 2.3 ($N_s = 3.24$).

D.3.4. Series 2.4**Figure D.64.** Structure before 0.8 H_{m0} test run of Series 2.4.**Figure D.65.** Structure after 0.8 H_{m0} test run of Series 2.4 ($N_s = 2.04$).**Figure D.66.** Structure after 1.0 H_{m0} test run of Series 2.4 ($N_s = 2.52$).

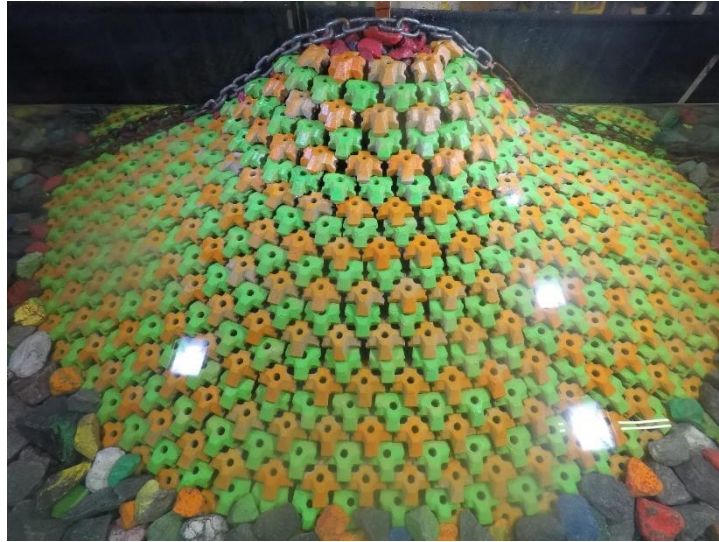


Figure D.67. Structure after 1.1 H_{m0} test run of Series 2.4 ($N_s = 2.76$).



Figure D.68. Structure after 1.2 H_{m0} test run of Series 2.4 ($N_s = 2.90$).

D.4. Xbloc

D.4.1. Series 3.1



Figure D.69. Structure before 0.6 H_{m0} test run of Series 3.1.



Figure D.70. Structure after 0.6 H_{m0} test run of Series 3.1 ($N_s = 1.41$).



Figure D.71. Structure after 0.8 H_{m0} test run of Series 3.1 ($N_s = 2.00$).



Figure D.72. Structure after 1.0 H_{m0} test run of Series 3.1 ($N_s = 2.50$).

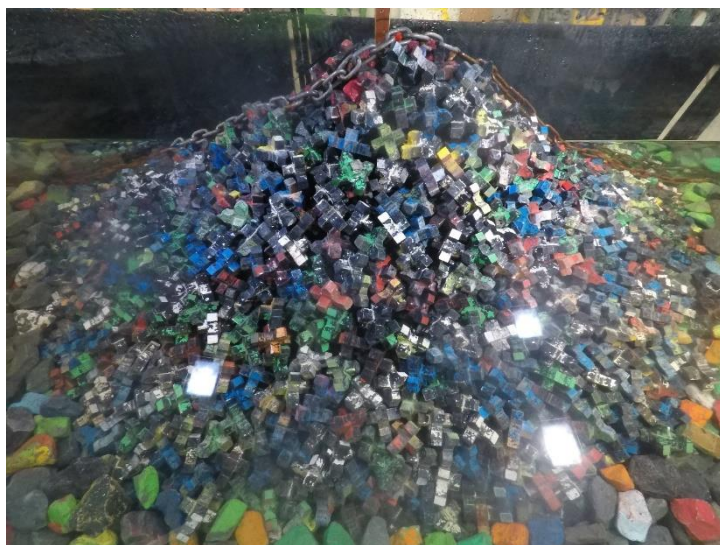


Figure D.73. Structure after 1.1 H_{m0} test run of Series 3.1 ($N_s = 2.74$).



Figure D.74. Structure after 1.2 H_{m0} test run of Series 3.1 ($N_s = 2.99$).

D.4.2. Series 3.2

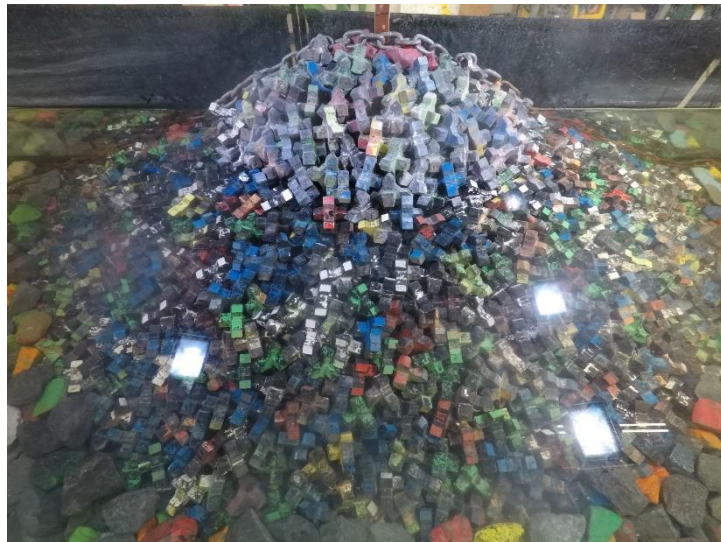


Figure D.75. Structure before 0.6 H_{m0} test run of Series 3.2.

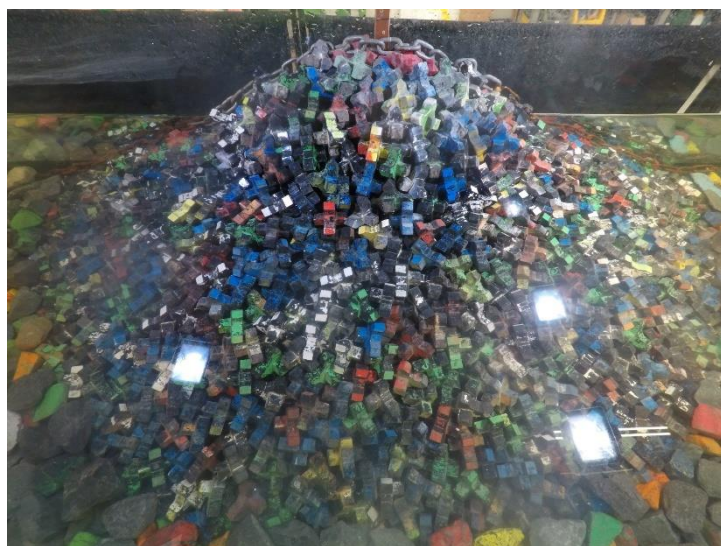


Figure D.76. Structure after 0.6 H_{m0} test run of Series 3.2 ($N_s = 1.40$).



Figure D.77. Structure after 0.8 H_{m0} test run of Series 3.2 ($N_s = 2.00$).



Figure D.78. Structure after 0.9 H_{m0} test run of Series 3.2 ($N_s = 2.32$).

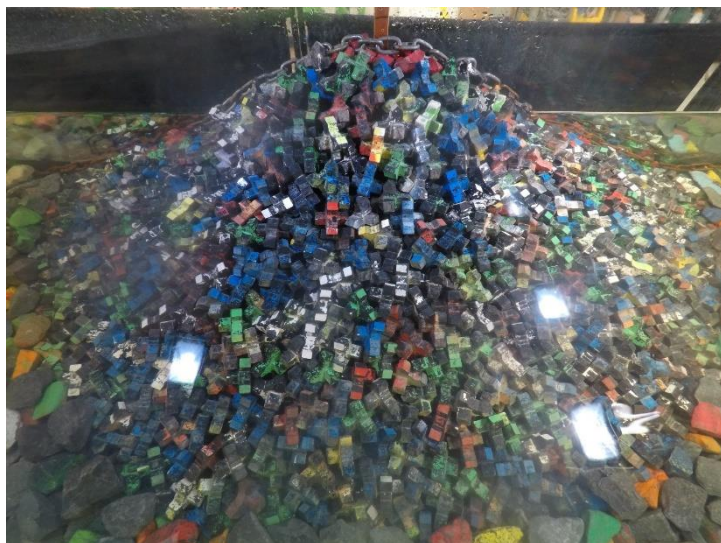


Figure D.79. Structure after 1.0 H_{m0} test run of Series 3.2 ($N_s = 2.53$).



Figure D.80. Structure after 1.1 H_{m0} test run of Series 3.2 ($N_s = 2.77$).



Figure D.81. Structure after 1.2 H_{m0} test run of Series 3.2 ($N_s = 3.14$).



Figure D.82. Structure after 1.3 H_{m0} test run of Series 3.2 ($N_s = 3.34$).



Figure D.83. Structure after $1.4 H_{m0}$ test run of Series 3.2 ($N_s = 3.45$).